

University Medical School of Naples  
“Federico II”



Department of Neuroscience, Reproductive Science, and Odontostomatology

*The effects of D2/D1R antagonists in an animal model of acute NMDAR  
hypofunction: translational inference from postsynaptic density Immediate-  
Early Gene-based network analyses*

PhD candidate: Dr. Annarita Barone

PhD Program in Neuroscience, XXXV Cycle

Tutor:  
Prof. Andrea de Bartolomeis

Coordinator:  
Prof. Maurizio Tagliatela

Academic year 2021/2022

## Contents

Abstract.....	4
1. Introduction.....	6
1.1. An overview of brain networks.....	6
1.2. Schizophrenia as a disorder of functional connectivity.....	9
1.3. Antipsychotic effects on functional connectivity.....	12
2. Aim of the study.....	16
3. Experiment n° 1.....	17
3.1. Material and methods.....	16
3.1.1. Animal treatment.....	16
3.1.2. In situ hybridization (ISH) procedures.....	16
3.1.3. Image analysis.....	18
3.1.4. Data processing.....	20
3.1.5. Statistical methods .....	21
3.1.5.1. Gene expression comparison.....	21
3.1.5.2. Comparison of correlation matrices.....	21
3.1.5.3. Descriptive analysis of networks.....	21
3.2. Results.....	23
3.2.1. Homer1a comparison.....	23
3.2.2. Comparison between correlation matrices.....	25
3.2.3. Descriptive analysis of networks.....	27
3.2.3.1. Network properties.....	27
3.2.3.2. Network topographical comparison.....	30
3.3. Discussion.....	40
4. Experiment n° 2.....	43
4.1. Material and methods.....	43
4.1.1. Animals.....	43
4.1.2. Animal treatment.....	43
4.1.3. ISH, image analysis, and data processing procedures.....	44
4.1.4. Statistical methods .....	44
4.1.5. Comparison of correlation matrices and generation of networks.....	45
4.2. Results.....	46
4.2.1. Gene expression comparisons.....	46

4.2.2. Construction and comparison of brain networks.....	51
5. Discussion.....	65
6. Limitations.....	68
7. References.....	69
8. Acknowledgements.....	77
9. Supplementary material.....	79

## Abstract

*Background:* Although extensively studied, the effect of antipsychotics has not been fully elucidated at the brain network level. We tested the hypothesis that acute administration of ketamine, haloperidol, and asenapine would modulate the functional connectivity of brain regions relevant to the pathophysiology of schizophrenia. To assess putative changes in brain network parameters and regional interactivity, we studied the transcript of Homer1a, an Immediate Early Gene that encodes a key molecule of the dendritic spine and that is involved in synaptic plasticity and metaplasticity, after typical and atypical antipsychotic administration.

*Methods:* We conducted two sets of experiments based on quantitative topographic imaging of Homer1a transcripts and analyzed the pattern of expression for each of them in a connectivity-based framework. In the first experiment, we analyzed Homer1 induction in different brain regions following the administration of haloperidol. Sprague-Dawley rats (n=26) were assigned to vehicle (VEH; NaCl 0.9%) or haloperidol (HAL; 0.8 mg/kg). In the second experiment, we analyzed gene expression after the administration of asenapine in rats pre-treated or not with ketamine, mimicking acute glutamatergic psychosis vs naturalistic conditions, respectively. Sprague-Dawley rats (n=20) were assigned to VEH or ketamine (KET; 30 mg/kg). Each pre-treatment group (n=10) was randomly split into two arms, receiving asenapine (ASE, 0.3 mg/kg), or saline (VEH). Homer1a mRNA levels were evaluated by *in situ hybridization*. Signal intensity analysis was performed in 33 Regions of Interest (ROIs) in the cortex, the caudate putamen, and the nucleus accumbens. We computed all possible pairwise Pearson correlations among signal intensity values in each ROI and generated a network for each treatment group in both experiments. We explored and compared network parameters (e.g., network topography, integration, segregation, small-world organization, and node attributes).

*Results:* Global efficiency and clustering coefficient of VEH and HAL networks were significantly different. The caudate putamen subdivisions and cortical and striatal regions displayed increased interactivity in the HAL network. On the other hand, it showed diminished associations between the caudate-putamen and nucleus accumbens, as well as the cingulate cortex and the anterior insula. Acute KET challenge was associated with negative correlations between Indusium griseum (Ig) and remaining ROIs, which were not detectable in other

treatment groups. KET/ASE group showed significantly higher inter-correlations between Ig and lateral putamen, the upper lip of the primary somatosensory cortex, septal area nuclei, and claustrum, in comparison to the KET/VEH network. ASE was able to modulate subcortical-cortical connectivity and increase the centrality of cingulate cortex and lateral septal nuclei.

*Conclusions:* These results confirm and extend the clinical evidence that antipsychotics may affect particular brain network features and the interaction of disease-related circuits.

# 1. Introduction

## 1.1. An overview of brain networks

The relevance of discrete functional patterns in neural circuits for brain high-level integration has been recognized for a long time (Fornito, 2016; White et al., 1986). Anatomical and functional connectivity is instrumental to enable neuronal computation, specificity of neuronal physiological responses, as well as integration of clusters of signals (Fornito, 2016). Sydney Brenner, the Nobel Prize in Physiology and Medicine, was the first to reconstruct the brain-wide map of neural connections of *Caenorhabditis elegans* by electron microscopy, laying the cornerstone of modern connectomics (White et al., 1986). In parallel and independently, Felleman and Van Essen conducted several neuroanatomical studies on primate brains in the attempt to delineate the hierarchical organization of cortical regions (Felleman and Van Essen, 1991). In particular, they were the first to reproduce the connectivity of the macaque visual cortex as a connection matrix, a compact description that takes the mathematical form of a directed graph, summarizing the constellation of neural inputs and outputs (Felleman and Van Essen, 1991). They highlighted the relevance of the anatomical organization of different areas and the connections between them (nodes and edges, in the graph theory language). These lines of investigations pointed to a complex connectivity architecture of the central nervous system, defined “connectome”. The term “connectome” indicates the comprehensive structural and functional description of the network elements and connections forming the human brain, but it has been defined also as “the knowledge of all the pre- and post- synaptic connections of a cell necessary to understand its role in a network” (Briggman and Denk, 2006), and “a connectivity map in which multiple or even all neuronal connections are rendered” (Livet et al., 2007).

The connectome is much more than an accumulation of a large number of empirical data. The operative novelty is that the connectome may provide a mechanistic basis and the theoretical rationale for understanding the functioning of the central nervous system. The functional or anatomical connections may represent electrical junctions, chemical synapses, or functional relationships (Sporns et al., 2005). In the presence of structural physical connections, we refer to structural connectivity, whereas in the presence of statistical correlations between measures of neuronal activity, we refer to functional connectivity.

However, links between nodes are characterised by a certain number of parameters, the number and density, location in space, length and trajectory. These parameters reflect various aspects of synapse morphology and functioning, the distribution of channels and receptors, and signal amplification by transduction cascades (Sporns et al., 2005). If data applied to generate

a connectome come from neurophysiological records, the nodes of the network correspond to individual neurons, while in neuroimaging studies the brain is usually divided into regions of interest (ROIs). Gene expression or proteomic values from different areas can also be used to construct a connectivity map and interrogate functional relationships between a large number of brain regions (Wheeler et al., 2014). Once nodes are defined, their mutual pairwise correlations can be determined and assembled in the form of a connection matrix, which, in turn, can be represented as a graph or network, offering a comprehensive set of information capturing either global (network-wide) or local (node- or edge-specific) aspects of interactivity. The basic characteristics of networks are summarized in Table 1.

<b>Attributes/Properties</b>	<b>Definition</b>
Node	A node is, together with edges, one of the two basic units of graphs. Nodes should reproduce discrete regions of interest with coherent patterns of extrinsic anatomical or functional connections.
Edge	An edge is, together with nodes, one of the two basic units of graphs. Edges may represent functional connections corresponding to magnitudes of correlations in activity and may occur between pairs of anatomically unconnected regions.
Path	Paths are sequences of distinct nodes and links. Paths in anatomical networks represent potential routes of information flow between pairs of brain regions. Lengths of paths estimate the potential for functional integration between brain regions, with shorter paths implying a stronger potential for integration.
Connected components	Within a network, all pairwise connected nodes form a connected component. The number of connected components indicates the connectivity of a network; a lower number of connected components suggests stronger connectivity.
Average distance	Average distance is the average shortest path of a graph, corresponding to the sum of all shortest paths between node pairs divided by the total number of node pairs. It is a simple and general parameter of graph compactness, i.e., the overall tendency of nodes to stay in proximity. A high average distance

	indicates that the nodes are dispersed, implying little graph compactness.
Average path length	The average path length is the expected distance between two connected nodes in a network.
Degree	The degree of a node is the number of edges linked to the node.
Density	The network density is a normalized version of the average number of neighbors, a parameter that indicates the average connectivity of a node in a network.
Clustering coefficient	The clustering coefficient of a node is a ratio that compares the number of edges between the neighbors of a node to the maximum number of edges that could possibly exist between the neighbors of that node. It is also known as <i>segregation</i> .
Global efficiency	Global efficiency is also defined as the average inverse shortest path length in the network and represents a measure of network <i>integration</i> .
Betweenness	The betweenness of a node is calculated considering couples of other nodes and counting the number of shortest paths linking them and passing through the node itself. Therefore, a high betweenness of a node means that it is crucial to maintain connections since it allows connecting network components that otherwise would be disjointed.
Eigenvector centrality	Measure of the influence of a node in a network, by assigning relative scores to each node based on their degree of connection, and may be defined as a sort of weighted degree, derived by structural topological properties of the underlying adjacent matrix (eigenvector).

**Table 1.** Definitions in graph theory: network, node and edge parameters

## **1.2. Schizophrenia as a disorder of functional connectivity**

Schizophrenia has been conceptualized as a neurodevelopmental disorder both of synaptic plasticity and functional connectivity (Stephan et al., 2006; Stephan et al., 2009). Altered synaptic morphology and function, potentially due to impairments in synaptic assembly, synaptic maturation, and neurotransmitters' signaling, which in turn might lead to aberrant connectivity, have been involved in the molecular pathogenesis of schizophrenia. Schizophrenia is therefore considered to belong to a group of disorders known as synaptopathies, including non-syndromic intellectual disabilities, autism spectrum disorders, schizophrenia, and Alzheimer's disease (Grabrucker et al., 2011). The "disconnection hypothesis" proposes that the core pathology of schizophrenia is an impaired control of synaptic plasticity, affecting the functional integration of neural systems, i.e., dysconnectivity (Sapienza et al., 2022). Anatomical dysconnectivity could arise from structural changes, i.e., "miswiring" of association fibers at the cellular level; functional dysconnectivity could arise from aberrant control of synaptic transmission and plasticity at the synaptic level (Stephan et al., 2006).

The hypothesis of schizophrenia as a dysconnectivity disorder has been validated by connectomic studies (Bullmore and Vértes, 2013; Cao et al., 2015). Neuroimaging data from the healthy population support the concept that the human brain may adopt a "small-world" organization, characterized by short node-to-node distance and the concomitant presence of highly clustered connectivity, ensuring the capability for specialized processing in local neighborhoods, as well as integrated processing throughout the entire central nervous system (Achard et al., 2006; van den Heuvel et al., 2008). These features may be significantly affected in subjects suffering from schizophrenia, and network parameters such as global efficiency and clustering coefficient, which respectively reflect measures of functional integration and segregation, have been found altered in functional magnetic resonance imaging (fMRI)-based studies (Bassett et al., 2012; Jiang et al., 2022; Lynall et al., 2010; van den Heuvel et al., 2013; Wang et al., 2012). The structural connectome in schizophrenia tends to follow a more segregated and less integrated network organization (Fornito and Bullmore, 2015; Narr and Leaver, 2015). However, brain functional organization may exhibit a "randomized tendency" in schizophrenia, e.g., increased global integration but decreased local segregation (Alexander-Bloch et al., 2010; Lo et al., 2015; Lynall et al., 2010).

Abnormalities in multiple neurotransmitters have been involved in schizophrenia pathophysiology and may lead to dysconnectivity or eventually be responsible for dysconnectivity amplification.

The strongest evidence points to abnormalities in dopamine, glutamate, and serotonin neurotransmission (Eggers, 2013; Park et al., 2022; Stahl, 2018). Signaling pathways activated by these neurotransmitters converge on postsynaptic density (PSD), an electron-dense thickening that includes hundreds of proteins localized at postsynaptic sites (de Bartolomeis and Fiore, 2004). PSD characterizes large excitatory glutamatergic synapses and is considered a structural-functional crossroad that may change synaptic strength in response to neural activity, thus contributing to information processing (Kennedy, 2000). Indeed, PSD has been involved in synaptic plasticity phenomena, since rearrangements in its structure and function are currently supposed to underlie synaptic plasticity-related events, such as long-term potentiation (LTP) and long-term depression (LTD)(Gold, 2012; Murakoshi and Yasuda, 2012). Recently, PSD has been associated in Genome-Wide Association Studies (GWAS) with serious psychiatric disorders including schizophrenia (Devlin et al., 2015).

Among PSD proteins, Homer proteins are multimodal postsynaptic adaptors that regulate PSD architecture (de Bartolomeis et al., 2022a). Homer genes encode a family of proteins including three isoforms in mammals (Homer1, Homer2, and Homer3), which are predominantly localized at the PSD, where they act as adaptors interacting with several PSD proteins (Fig. 1)(Shiraishi-Yamaguchi and Furuichi, 2007).

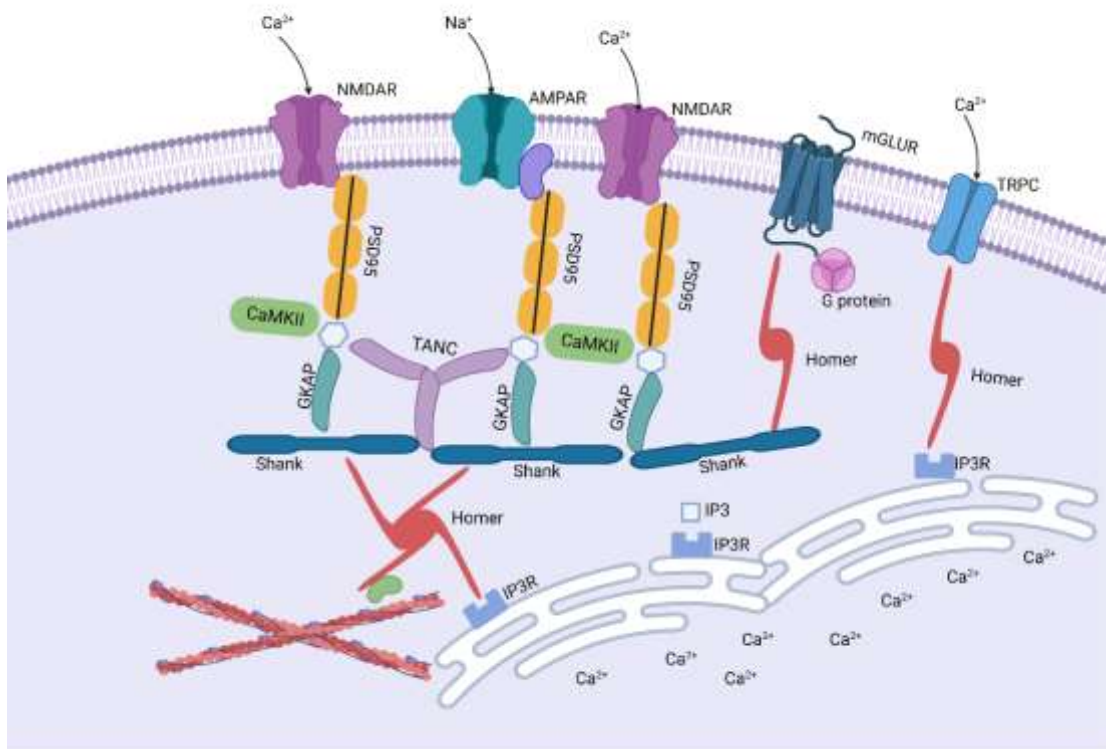


**Fig. 1.** Long Homers may bind several targets within the post-synaptic density, e.g., molecules involved in calcium dynamics, in cytoskeleton architecture, receptor trafficking, and

signal transduction. NMDAR = N-methyl-D-aspartate receptor; AMPAR =  $\alpha$ -amino-3-hydroxy-5-methyl-4-isoxazolepropionic acid; mGluR = metabotropic glutamate receptor; TRPC = transient receptor potential cation channels; PSD-95 = postsynaptic density protein 95; CAMKII = calcium/calmodulin kinase type II; GKAP = guanylate kinase-associated protein; IP3R = inositol-1,4,5-trisphosphate receptor. Created with Biorender.com.

Homer proteins are divided into: a) long isoforms, which are constitutively expressed (i.e., Homer1b/c, Homer 2, and Homer 3), equipped with a N-terminal Ena/VASP (EVH) domain allowing the binding to other PSD proteins and a C-terminal coiled-coil domain allowing self-assembly; b) short non-multimerizing splice variants of the Homer1 gene (Homer1a, Ania-3), expressed in an activity-dependent manner, which lack the C-terminal domain and are therefore able to interact with other PSD proteins but not to self-assemble (Shiraishi-Yamaguchi and Furuichi, 2007). Homer1a is an inducible Immediate Early Gene (IEG) expressed after neuronal stimulation and acts as an endogenous “dominant-negative” by disrupting long Homer protein–protein interactions, thus leading to rapid and transient rearrangements of long Homer clusters and, in turn, of synaptic architecture (de Bartolomeis et al., 2022a). Its expression may be affected by dopaminergic as well glutamatergic compounds (Buonaguro et al., 2017) including antipsychotics (Iasevoli et al., 2020; Iasevoli et al., 2010a; Iasevoli et al., 2010b) alone or in combination (Tomasetti et al., 2011).

Homer1a gene induction may lead to multiple intracellular signaling changes, including activation of group I metabotropic glutamate receptors (mGluRs) (Ango et al., 2001), and modulation of mGluR-induced intracellular calcium release (Bockaert et al., 2021). At the synaptic level, Homer1a may play a pivotal role in activity-induced remodeling of pre- and postsynaptic structures, being involved in glutamate-induced changes in the distribution of both presynaptic proteins (such as synaptotagmin, synaptophysin, and synapsin) and post-synaptic proteins (such as PSD-95, Homer1c, and Glur2 AMPA receptor subunits) (Inoue et al., 2007). A growing amount of evidence indicates that Homer family protein dysfunctions might be involved in the pathophysiology of neuropsychiatric disorders showing defects in synaptic plasticity, such as schizophrenia (Gilks et al., 2010; Spellmann et al., 2011; Szumlinski et al., 2006).

Noteworthy, the disruption of synaptic architecture may lead, in turn, to impaired interaction among neuronal populations and abnormal functional integration of neural systems, namely dysconnectivity and functional “miswiring” (Levitt et al., 2020).

### 1.3. Antipsychotic effects on functional connectivity

Antipsychotic medications are the cornerstone of pharmacological therapy for schizophrenia. Despite the well-established implications of dopamine D2 receptor (D2R) occupancy in the mechanism of action of antipsychotics, it has been suggested that the effects exerted on synaptic plasticity and metaplasticity may contribute to understanding the neurobiology underlying the clinical response to antipsychotics (de Bartolomeis et al., 2022b; Konradi and Heckers, 2001). In fact, several lines of evidence suggest that antipsychotics may act by modulating the expression and functions of PSD proteins (de Bartolomeis et al., 2019; de Bartolomeis et al., 2022b; de Bartolomeis et al., 2013; Tomasetti et al., 2017).

Preclinical studies have shown that Homer1a expression can be induced by acute administration of typical or atypical antipsychotics in brain regions relevant to the pathophysiology of schizophrenia, in a region-specific manner and potentially depending on the receptor occupancy profile (Iasevoli et al., 2020) (Fig. 2).

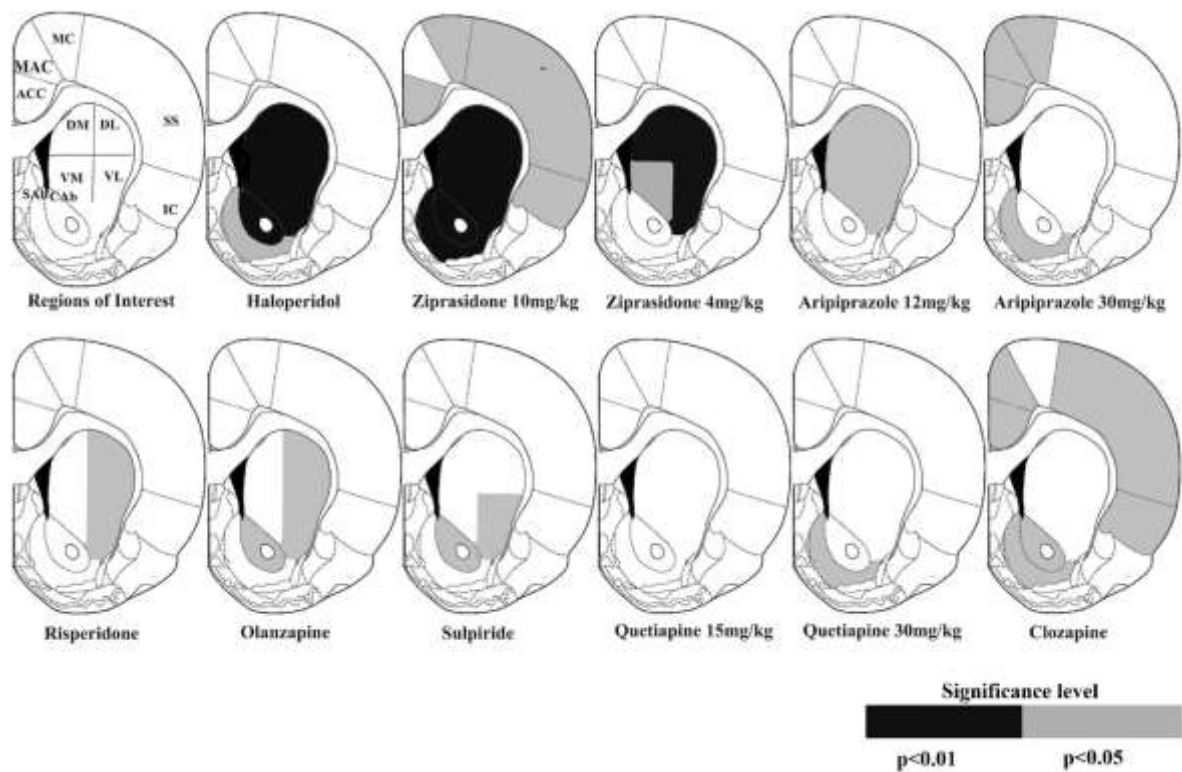


**Fig. 2.** Homer1a significant induction elicited by different acute antipsychotic treatments at different doses within regions of interest vs. vehicle. Black tones indicate high levels of significance. Grey tones indicate moderate levels of significance.

Moreover, antipsychotics may time-dependently disrupt the functional connectivity between the medial frontal cortex, the hippocampus, and the nucleus accumbens, as measured by H<sub>2</sub><sup>15</sup>O PET in patients with schizophrenia, with connectivity between the medial frontal cortex and the hippocampus acting as a predictor of treatment response (Bolding et al., 2012). Long-term treatment with antipsychotics has been shown to restore impaired functional connectivity within the default mode network (DMN) and the external attention system (EAS), as revealed by a longitudinal resting-state fMRI study (Deng et al., 2022). The DMN is a large-scale brain network known to have highly correlated activities, particularly active when the subject is in a state of conscious rest, such as daydreaming or mind-wandering, and deactivated in certain goal-oriented tasks involving the EAS (Christoff et al., 2009).

Other longitudinal fMRI studies explored the effects of antipsychotic exposure in drug-naïve patients, investigating changes in network connectivity and properties (Hadley et al., 2016). For instance, Hadley and colleagues demonstrated that 6-week risperidone treatment was able to modulate the pattern of faulty connectivity (e.g., altered functional integration and segregation) of brain networks but only in clinically responsive patients (Hadley et al., 2016). The same group showed that, after only one week of risperidone administration, the ventral tegmental area (VTA)/midbrain connectivity to bilateral regions of the thalamus was re-established (Hadley et al., 2014).

However, there are few studies in which the effects of antipsychotics on the functional connectivity of macroscale networks have been directly assessed, and antipsychotic treatment is rather considered a confounding variable. Indeed, it may be difficult to distinguish the structural and functional changes induced by antipsychotic drugs in the topography and connectivity of networks from those produced by the disease itself, apart from studies conducted in drug-naïve subjects. In this framework, preclinical research may allow us to address these limitations by assessing changes in functional connectivity following a pharmacological challenge in animals, controlling for potential confounding factors.

Given the involvement of Homer family protein in the dysconnectivity found in schizophrenia as well as in clinical response to antipsychotic administration, the expression of Homer1a may be properly used as an efficient tool for exploring antipsychotic-mediated neuronal activation, as well as a molecular sensor of synaptic plasticity rearrangements (de Bartolomeis et al., 2022a).

Based on these considerations, we decided to combine *in situ* hybridization (ISH) measurements of Homer1a expression with a graph theoretical approach, to develop a functional mapping of glutamatergic synaptic plasticity events evoked by antipsychotics. In the

present study we investigated the network effects elicited by two antipsychotic compounds exhibiting significantly different D2/D1 receptor ratios, namely haloperidol and asenapine (25:1 for haloperidol, and approximately 1:1 for asenapine) (Kusumi et al., 2015; Shahid et al., 2009).

Haloperidol is one of the most frequently used antipsychotics worldwide (Dold et al., 2015). Evidence exists that haloperidol administration may induce anatomical and molecular brain changes, especially in the striatum in terms of regional brain volume, synapse morphology, and synaptic protein levels (Benes et al., 1985; Konradi and Heckers, 2001; Park et al., 2019; Park et al., 2018; Wiedemann et al., 1992). In preclinical studies, haloperidol has been shown to induce Homer1a expression in the striatum, with prominent effect-size on the dorsal and lateral striatal regions and in the core and the shell of the nucleus accumbens (Ambesi-Impiombato, A. et al., 2007; Tomasetti et al., 2007). These effects have been suggested to determine acute and long-term changes in glutamatergic signaling, as well as in the dopamine-glutamate-serotonin interplay. The above-mentioned effects of haloperidol can potentially modify synaptic plasticity processes and dendritic spine morphology and, in turn, local and global connectivity properties (de Bartolomeis et al., 2013; de Bartolomeis et al., 2014).

Although functional brain connectivity has been found to be largely modulated by antipsychotics, the substantia nigra appears to be particularly affected; for instance, a single acute dose of haloperidol was found to induce focal changes in functional connectivity between this region and motor areas in rats, as revealed by a fMRI study (Gass et al., 2013). Decreased connectivity between substantia nigra and frontal regions may possibly relate to its therapeutic action. Moreover, Wheeler and colleagues evaluated the effects of chronic haloperidol exposure on functional brain networks properties in rats, by performing a network analysis of IEG expression pattern among 83 brain regions (Wheeler et al., 2014). They used *zif268* mRNA to map neural activation and demonstrated that haloperidol increased caudate putamen-thalamus interactivity in comparison to saline/vehicle (Wheeler et al., 2014). By evaluating and comparing the connectivity of the two generated networks, they found that chronic haloperidol administration resulted in altered correlated activity between the caudate-putamen and thalamus. Noteworthy, the caudate-putamen is the major input station of the basal ganglia projecting to the thalamus by inhibitory and GABAergic fibers. Following haloperidol therapy, Wheeler and colleagues found a significant inverse association between caudate-putamen and thalamic activity, which may be explained by a stronger inhibitory input from the basal ganglia to the thalamus (Wheeler et al., 2014).

Acute administration of antipsychotics has been associated with a reduction in locomotor behavior in animals (Irons et al., 2013; Wiley, 2008), as well as a fast-acting control of positive symptoms of schizophrenia in humans (Kapur et al., 2005), thus representing a well-recognized paradigm in preclinical research, allowing to make inference of relevant translational value.

Hence, in the first step of our study, we sought to determine the effects of a single acute dose of haloperidol on resting-state functional connectivity in the rat, by exploring brain network integration, segregation, and small-worldness measures, centrality metrics of network nodes, and disease-related circuit interactivity as compared to a vehicle-generated network.

Asenapine is an atypical antipsychotic, which, differently from haloperidol, exhibits a potent serotonergic activity and a peculiar action at D1 receptors (D1Rs) (Shahid et al., 2009). The action at D1R sites is even more attractive since D1R and N-methyl-D-aspartate receptor (NMDAR) couple at the postsynaptic site in dendritic spines, enhancing reciprocal activity through a positive feedback mechanism (Zhang et al., 2009). This compound has been found to significantly induce Homer1a in cortical and subcortical regions at medium and low doses (de Bartolomeis et al., 2015). Therefore, the choice of atypical antipsychotic asenapine is due to a larger NMDAR activation via post-synaptic D1Rs.

Therefore, as the second step in our study, we evaluated the administration of asenapine in rats pre-treated with ketamine. In fact, the acute administration of ketamine represents a validated animal model of schizophrenia (Neill et al., 2010). Ketamine acts as a NMDAR non-competitive antagonist, inducing delusions and hallucinations in healthy subjects, symptoms commonly observed in patients suffering from schizophrenia (Krystal et al., 1994). Unlike stimulants and amphetamines, non-competitive NMDAR antagonists are able to produce cognitive deficits characteristic of schizophrenia in addition to positive symptoms (Neill et al., 2010).

In summary, we combined ISH technique with a graph theoretical approach to develop a functional mapping of Homer1a-based synaptic plasticity events in rats pre-treated or not with ketamine, mimicking psychosis or naturalistic conditions, and subsequently exposed to antipsychotics. We tested the hypothesis that acute administration of the prototypical antipsychotic haloperidol and the atypical antipsychotic asenapine would significantly modulate the functional architecture of disease-related circuits as well as the characteristics of brain networks.

## **2. Aim of the study**

Here we tested the hypothesis that acute haloperidol and asenapine administration would modulate functional connectivity within the glutamatergic system among brain regions relevant to schizophrenia pathophysiology.

We took advantage of Homer1a expression, a marker of neural activity involved in glutamate transmission and synaptic plasticity, as a molecular tool to assess putative changes in brain regional interactivity after acute treatment.

### **3. Experiment n° 1**

#### **3.1. Material and methods**

##### **3.1.1. Animal treatment**

Twenty-six male Sprague-Dawley (average weight 250 g) were obtained from Charles-River Labs, Lecco. Animals were housed and let to adapt to human handling in a temperature and humidity-controlled colony room with a 12 h/12 h light/dark cycle and *ad libitum* access to food and water. All experimental procedures were conducted in agreement with the NIH Guide for Care and Use of Laboratory Animals (NIH publication no. 85-23, revised 1993) and were approved by local Animal Care and Use Committee. In order to minimize animal number and suffering, we gathered data from ISH signals obtained by film autoradiography of four previous experiments from our group (Ambesi-Impiombato, Alberto et al., 2007; de Bartolomeis et al., 2015; Iasevoli et al., 2010b; Tomasetti et al., 2007) in which rats were exposed to the same investigational conditions: same antipsychotic dosage, same route of administration, same timing of treatment and sacrifice, same equipment and same ISH procedures. Out of the total number of haloperidol-treated and vehicle-treated animals, we took into consideration for the analysis an equal number of cases and controls for which ISH was performed at the striatum level. We excluded animals for which we had not the possibility to complete a signal quantitation in all ROIs.

We included 26 animals assigned to receive vehicle (NaCl 0.9%, VEH, n = 13) or haloperidol 0.8 mg/kg (HAL, n = 13). Haloperidol injectable solution (Lusofarmaco, Italy) was dissolved in saline solution (NaCl 0.9%). Solutions were adjusted to physiological pH value and injected intraperitoneally at a final volume of 1 ml/kg. HAL was administered at behaviorally active doses (Tomasetti et al., 2007). Ninety minutes after treatment administration animals were sacrificed by decapitation.

##### **3.1.2. In situ hybridization (ISH) procedures**

Brains were quickly removed and frozen on powdered dry ice, and then kept at – 70 °C until sectioning. Serial coronal brain slices of 12 µm were cut on a cryostat using the Paxinos rat atlas as a reference (Paxinos et al., 1980) (approx. from bregma 1.20 mm to 1.00 mm). Care was taken to select identical anatomical levels of treated and control sections using thionin-stained reference slides. Sections were thaw-mounted onto gelatin-coated slides and stored at – 70 °C for further analysis.

The Homer1a probe used for radioactive ISH was an oligodeoxyribonucleotide complementary to bases 2527–2574 (GenBank accession number: #U92079; MWG Biotech, Firenze). The probe was designed from sequences available in the GenBank database. Confidence in the specificity of the probe was strengthened by a sequence search on Basic Local Alignment Search Tool (BLAST) database in order to avoid cross-hybridization. Radiolabeling and purification of oligonucleotide probes were conducted according to previously published protocols (Ambesi-Impiombato et al., 2003). A 50- $\mu$ l labeling reaction mix was prepared on ice using diethylpyrocarbonate-treated water, 1 $\times$  tailing buffer, 1.5 mM CoCl<sub>2</sub>, 7.5 pmol/ $\mu$ l of oligo, 125 units of TdT and 100  $\mu$ Ci 35S-dATP. The mix was incubated for 20 min at 37 °C. The unincorporated nucleotides were removed and separated from radiolabeled DNA using ProbeQuant G-50 microcolumns (Amersham Biosciences). Hybridized sections were dried and exposed to Kodak-Biomax MR Autoradiographic films (Sigma-Aldrich, Milano, Italy). A slide containing a scale of 16 known amounts of 14C standards (ARC-146C, American Radiolabeled Chemical, Inc., St. Louis, MO, USA) was co-exposed with the samples. Three adjacent animal brain sections were shown on each slide. The autoradiographic films were exposed in a time range of 10–45 days. The optimal time of exposure was chosen to maximize signal-to-noise ratio while preventing optical density from exceeding the saturation threshold.

### **3.1.3. Image analysis**

The quantitation of the autoradiographic signal was performed using a computerized image analysis system comprising a transparency film scanner (Microtek Europe B.V., Rotterdam, The Netherlands) and ImageJ software (v. 1.46v, <http://rsb.info.nih.gov/ij/>). The original features of the scanned images were preserved. Signal intensity analysis was conducted on digitized autoradiograms by measuring mean optical density within specific ROIs, and then quantitation was carried out by two independent investigators. For eliminating assessment bias, the investigators were blinded, i.e., not aware of the group allocation during quantitation procedures. Signal intensity was measured in 33 different ROIs, listed in Table 2, at the topographical level of the striatum (from Bregma +1.68 to +1.44), since it is believed to be one of the main sites of action of antipsychotic drugs (McCutcheon et al., 2019). However, at this topographical level, it was also possible to quantitate limbic and cortical ROIs. ROIs were outlined on digitized autoradiograms through the oval template tool of ImageJ software. Inter-rater reliability in quantitation was analyzed using Cohen's kappa ( $\kappa$ ) and the minimum acceptable was set at 0.8 (McHugh, 2012).

<b>Abbreviation</b>	<b>Brain region</b>
LSV	Lateral septal nucleus, ventral
Tu	Olfactory tubercle
LSD	Lateral septal nucleus, dorsal
LSI	Lateral septal nucleus, intermediate
Icj	Islands of Calleja
VP	Ventral pallidum
Shi	Septohippocampal nucleus
MS	Medial septum
VDB	Nucleus of the vertical limb of the diagonal band
IG	Indusium griseum
S1dz	Somatosensory 1, dysgranular zone
AIV	Agranular insular area, ventral
S1ULp	Upper lip of the primary somatosensory cortex
GI	Granular insular cortex
DI	Dysgranular insular cortex
Ac_sh	Accumbens nucleus, shell
Pir	Piriform cortex
AID	Agranular insular area, dorsal
LSS	Lateral stripe of striatum
Cg2	Cingulate cortex, area 2
CP_DL	Dorsolateral caudate putamen
CP_VL	Ventrolateral caudate putamen
CP_VM	Ventromedial caudate putamen
Cg1	Cingulate cortex, area 1

M2	Supplementary motor cortex
CP_DM	Dorsomedial caudate putamen
Den	Dorsal endopiriform nucleus
M1	Primary motor cortex
S1Fl	Somatosensory 1, forelimb region
Ac_co	Accumbens nucleus, core
Cl	Clastrum
S1j	Somatosensory 1, jaw region
S1jO	Primary somatosensory cortex, jaw region, oral surface

**Table 2.** Regions of interest (ROIs) quantitated and corresponding abbreviations.

### 3.1.4. Data processing

Measurements of mean optical density within ROIs were converted using a calibration curve based on the standard scale co-exposed with the sections. <sup>14</sup>C standard values from 4-12 were previously cross-calibrated to <sup>35</sup>S brain paste standards, in order to assign a disintegration per minute/milligrams (dpm/mg) tissue wet weight value to each optical density value through a calibration curve. A “best fit” 3rd degree polynomial was used to this aim. For each animal, measurements from three adjacent sections were averaged. In order to compare measurements from four different autoradiographic films, relative dpm mean values were normalized subtracting the background signal in order to remove the effects of different sheets of X-ray film used and adjusted dividing by the value of genu of corpus callosum (gcc).

### **3.1.5. Statistical methods**

#### **3.1.5.1. Gene expression comparison**

Data for each region were derived by averaging measurements from three adjacent sections of single animals. The Shapiro-Wilk test was used to check if relative dpm values followed a normal distribution. The Student's *t*-test was used to compare VEH and HAL values in each ROI. The significance level for comparisons was set at 0.05. We applied Bonferroni correction for multiple testing (adjusted *p*-value = 0.0015). JMP software version 9.0.1–SAS Institute Inc. and IBM SPSS 25 software were used for statistical analysis.

#### **3.1.5.2. Comparison of correlation matrices**

Using the Homer1a signals as dependent variables, we calculated the Pearson's *r* for all possible pairwise correlations between the 33 ROIs in each treatment group (i.e., VEH and HAL) and two correlation matrices were generated. We used the permutation test based on Fisher's *z* transformation to compare correlation coefficients between groups (Sakaori, 2002) and detect statistically significant differences (*p*-value < 0.05).

#### **3.1.5.3. Descriptive analysis of networks**

The correlation matrices were used to generate two networks showing the functional connections among ROIs, separately for each treatment group. The connections between regions were given by the Pearson's correlation coefficients. We computed different network statistics across several thresholds defined by the percentile of the observed correlation coefficients distribution of each treatment group. We analyzed the connection density, defined as the ratio of observed edges to the number of possible edges for a given network (Hu, 2018).

We evaluated also the global efficiency and clustering coefficient, measures of functional integration and segregation, respectively (Cai et al., 2020). Global efficiency was defined as the average inverse shortest path length in the network, while clustering coefficient was defined as the global transitivity index and computed as the ratio of the triangles and the connected triples in the graph. Network small-worldness was assessed by computing the small world index, obtained by comparing clustering and path length of a given network to an equivalent random network with the same degree on average that combines the clustering coefficients and the global efficiency information.

To ascertain whether the properties of the networks differed considerably between the experimental and random control networks, 100 simulated networks were randomly generated by permuting the values of the original networks for each threshold value from 0.05 to 0.95. The statistics distribution generated under the random network hypothesis were depicted as box plots. Moreover, we assessed basic centrality attributes of nodes such as degree, betweenness, and eigenvector centrality at fixed thresholds of 80th, 90th and 95th percentiles of the correlation distribution observed in each network. The degree of a node was defined as the number of neighbours of the node, a very high degree of a node indicating a putative network hub, namely a central node facilitating flow over a network (Power et al., 2013).

The betweenness centrality of a node is calculated considering couples of other nodes and counting the number of shortest paths connecting them and passing through the node itself. This metric is used to detect the amount of influence a node has over the flow of information in a graph (Scardoni and Laudanna, 2012). Hence, a high betweenness of a node means that it is essential to maintain connections among network components that would be otherwise disconnected.

Eigenvector centrality measures the transitive influence of a node in a network, by assigning relative scores to each node based on their degree. This metric may be considered as a sort of weighted degree, derived by structural topological properties of the underlying adjacent matrix (eigenvector) (Joyce et al., 2010).

## 3.2. Results

### 3.2.1. Homer1a comparison

The 33 ROIs selected for the network analysis were compared for their levels of Homer1a mRNA expression. Both raw and normalized gene expression data were assessed (Supplementary Table 1). Gene expression values were compared both as raw and normalized data (Table 3). Only the dorsolateral and ventrolateral caudate putamen showed significant differences between VEH and HAL treatment when analyzing non-normalized data, with a trend toward significance in both the dorsomedial ( $p = 0.08$ ) and ventromedial ( $p = 0.06$ ) caudate putamen. After normalization, HAL group showed a significant increase in the expression of Homer1a mRNA in all caudate-putamen and accumbens regions as well as in the nucleus of the vertical limb of the diagonal band, in comparison to VEH. Significant differences in the lateral caudate putamen survived after the Bonferroni correction.

These outcomes were in line with earlier studies from our group (Ambesi-Impiombato, A. et al., 2007; de Bartolomeis et al., 2015; Iasevoli et al., 2010b). Representative autoradiographic images of the VEH and HAL groups are shown in Fig. 3.

Brain region	p-value (raw data)	p-value (normalized data)
Lateral septal nucleus, ventral	ns	ns
Olfactory tubercle	ns	ns
Lateral septal nucleus, dorsal	ns	ns
Lateral septal nucleus, intermediate	ns	ns
Islands of Calleja	ns	ns
Ventral pallidum	ns	ns
Septohippocampal nucleus	ns	0.069
Medial septum	ns	ns
Nucleus of the vertical limb of the diagonal band	ns	<b>0.048</b>
Indusium griseum	ns	ns
Somatosensory 1, dysgranular zone	ns	ns

Agranular insular area, ventral	ns	ns
Upper lip of the primary somatosensory cortex	ns	ns
Granular insular cortex	ns	ns
Dysgranular insular cortex	ns	ns
Accumbens nucleus, shell	ns	<b>0.006</b>
Piriform cortex	ns	ns
Agranular insular area, dorsal	ns	ns
Lateral stripe of striatum	ns	ns
Cingulate cortex, area 2	ns	ns
Dorsolateral caudate putamen	<b>0.004</b>	<b>0.001</b>
Ventrolateral caudate putamen	<b>0.006</b>	<b>&lt;0.0001</b>
Ventromedial caudate putamen	<i>0.06</i>	<b>0.004</b>
Cingulate cortex, area 1	ns	ns
Supplementary motor cortex	ns	ns
Dorsomedial caudate putamen	<i>0.08</i>	<b>0.004</b>
Dorsal endopiriform nucleus	ns	ns
Primary motor cortex	ns	ns
Somatosensory 1, forelimb region	ns	ns
Accumbens nucleus, core	ns	<b>0.003</b>
Clastrum	ns	ns
Somatosensory 1, jaw region	ns	ns
Primary somatosensory cortex, jaw region, oral surface	ns	ns

**Table 3.** Results of Student's *t* test comparing HAL vs. VEH groups throughout the 33 regions of interest. Comparisons were independently run with raw and normalized data.

Significant values were outlined in bold. Significant p-values after Bonferroni correction were given in red. Trends toward significance were given in italics. ns: not significant.

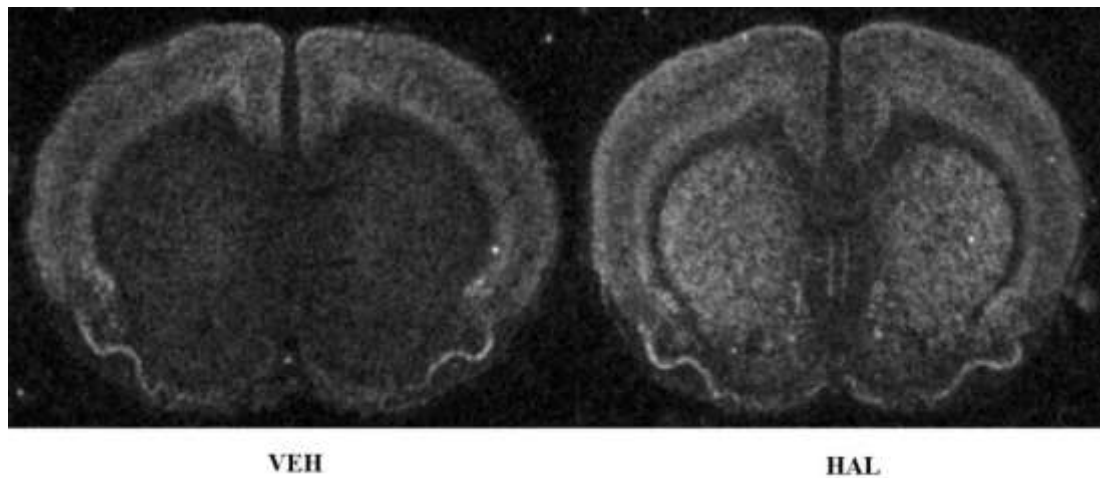


**Fig. 3.** Representative autoradiographic film images of Homer1a induction after acute treatment with VEH and HAL. As can be easily observed, Homer1a was significantly induced by HAL administration in striatal subregions. VEH= vehicle; HAL= haloperidol.

### **3.2.2. Comparison between correlation matrices**

The two Pearson correlation matrices are reported in Fig. 4. Noteworthy, the correlations between the basal nuclei (i.e., septal nuclei, ventral pallidum, caudate putamen) and the Indusium griseum became negative in HAL network. Additionally, the HAL network showed stronger positive correlations among the caudate putamen subdivisions than the VEH network. The two matrices were compared using the permutation test, and significant differences are graphically displayed in Fig. 5. In 36 pairwise correlations, the Pearson's  $r$  was significantly different. It should be noted that the correlation coefficients in the HAL matrix were significantly higher than those in the VEH in the following pairs: M2 and CP\_DM, M2 and CP\_VL, and S1j and Ac\_co (Fig. 5).

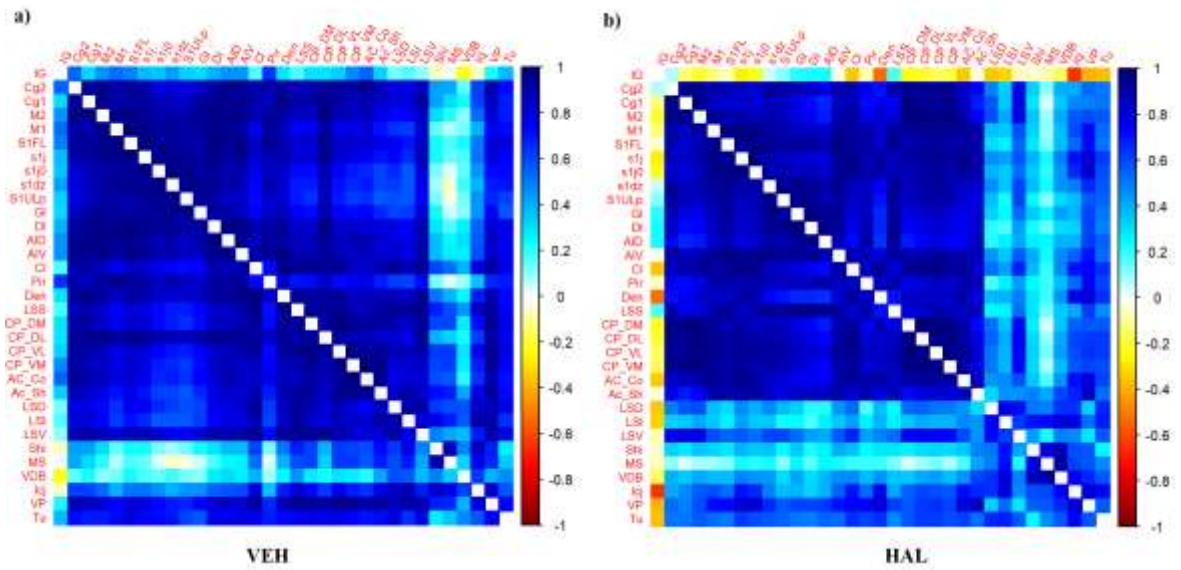


**Fig. 4.** Correlation Matrix for VEH (panel a) and HAL (panel b) groups. Variables are grouped according to hierarchical clustering. According to the colour scale on the right of the matrix, positive correlations are reported in blue, negative ones in red. VEH= vehicle; HAL= haloperidol.

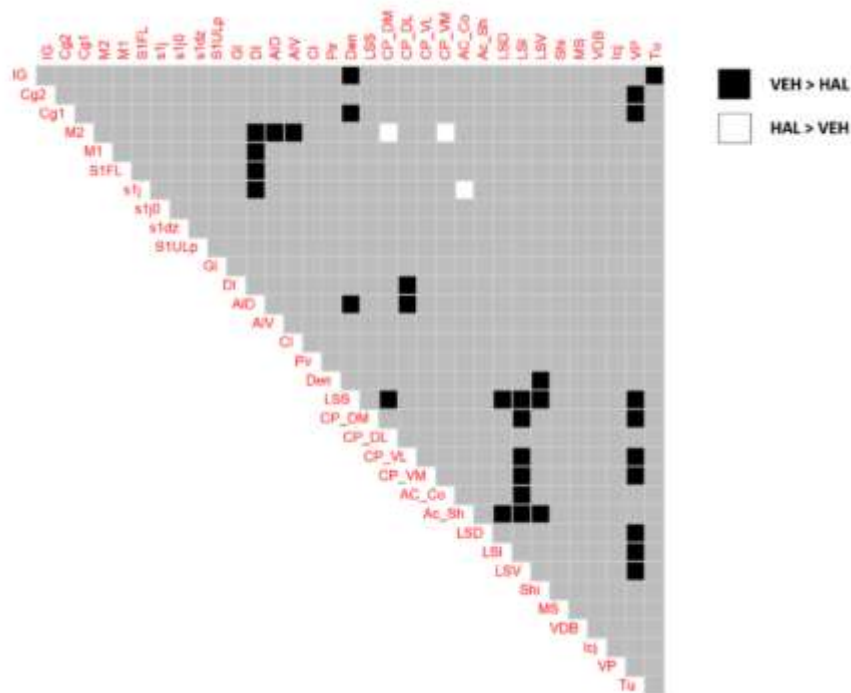


**Fig. 5.** Differences between HAL and VEH correlation matrices. White squares indicate couples of correlations in which HAL Pearson's  $r$  is significantly higher than in VEH. On the contrary, black squares indicate couples of correlations in which VEH Pearson's  $r$  is significantly higher than HAL. VEH= vehicle; HAL= haloperidol.

### 3.2.3. Descriptive analysis of networks

#### 3.2.3.1. Network properties

We observed that the connection density of HAL-treated and in VEH-treated networks was comparable (Fig. 6). By looking at the graph (Fig. 6), we observed that for extreme threshold values, the global efficiency was higher in the HAL network than VEH network. However, compared to both treatment networks, randomly generated networks showed greater global efficiency values (Fig. 7).

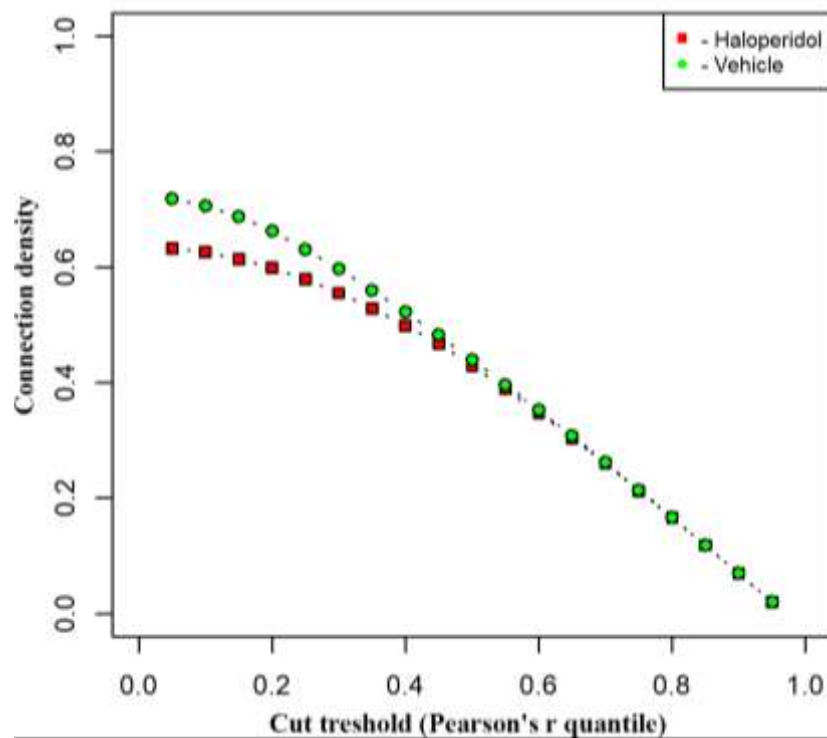


**Fig. 6.** Connection density of VEH (given as green circles), and HAL (given as red squares) networks across thresholds. VEH= vehicle; HAL=haloperidol.

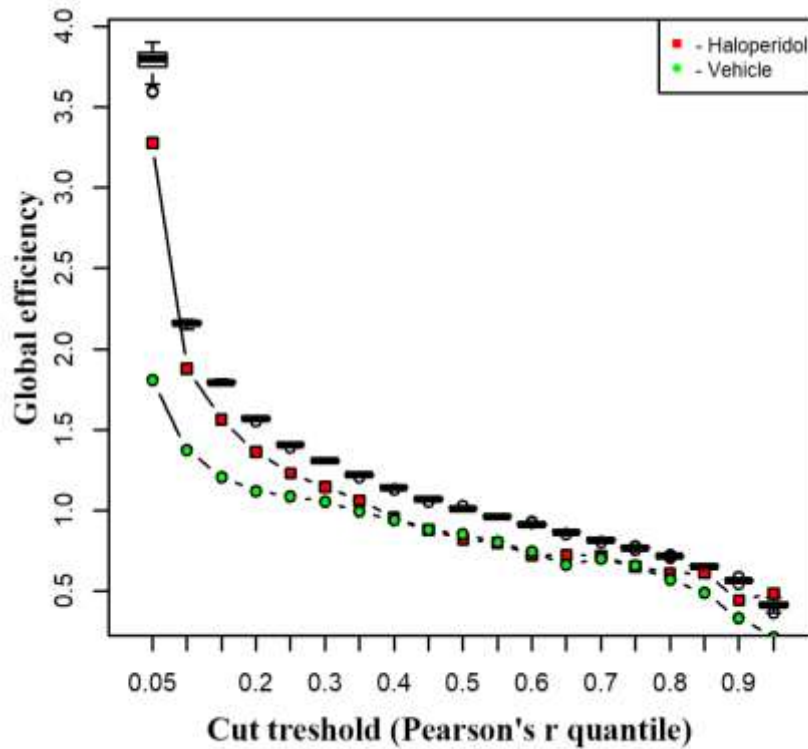


**Fig. 7.** Global efficiency values of VEH (green circles) and HAL (red squares) network across the thresholds. Randomly generated networks (black box plots) exhibited higher global efficiency compared to VEH and HAL networks. VEH= vehicle; HAL=haloperidol

At visual examination, the clustering coefficient was higher in the HAL network than in the VEH network and random-generated networks (Fig. 8), with a sharp increase for very low density (note that the r quantile = 0.95, retains a density of 0.02).

Small-world Index was higher for the HAL network than for the VEH network for threshold values above r quantile= 0.60 (Fig. 9), with marked differences for lower network density. These findings suggest that antipsychotics treatment enhanced the small-worldness of the brain network, which was significantly structured and exhibited increased efficiency after HAL administration.

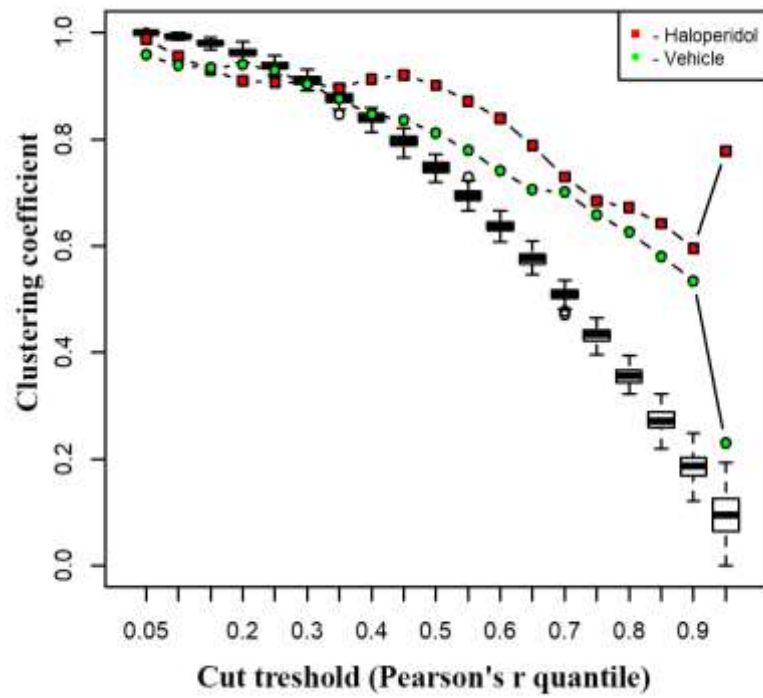


**Fig. 8.** Clustering coefficient values in VEH (green circles) and HAL (red squares) network across the r quantile thresholds. Randomly generated networks (black box plots) exhibited a lower clustering coefficient compared to VEH and HAL networks. VEH= vehicle; HAL= haloperidol.

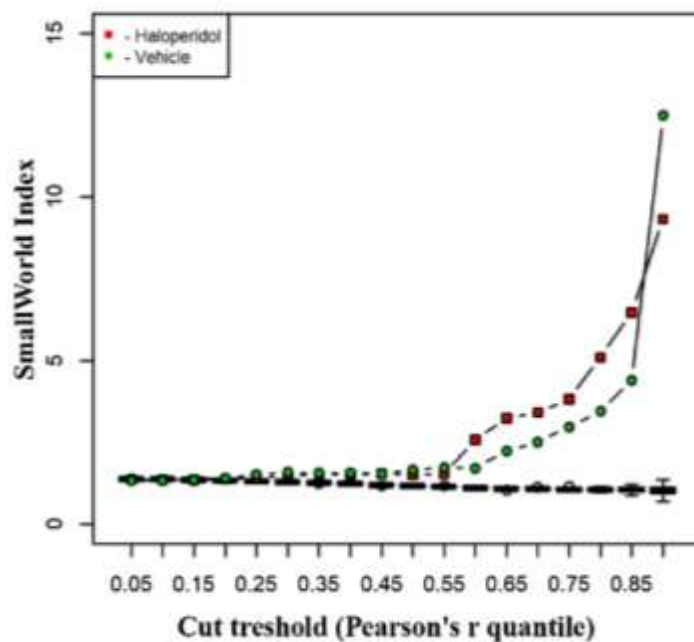


**Fig. 9.** Small-world index values in VEH (green circles) and HAL (red squares) network across the  $r$  quantile thresholds. Randomly generated networks (black box plots) exhibited a lower small-world index compared to VEH and HAL networks

### **3.2.3.2. Network topographical comparison**

In order to provide a more in-depth insight into brain network topography, we focused on a few threshold values of interest. We considered three cut-offs: 80%, 90% and 95%. As illustrated in Fig. 10, the functional networks HAL and VEH were structured differently and displayed distinct topographical differences, particularly with regard to the inter-correlations between cortical and striatal areas. In fact, the cingulate cortex, the primary and supplementary motor cortex (Cg1, Cg2, M1 and M2), and anterior insular cortex (AIV and AID) has stronger functional relations within the VEH network in comparison to HAL network. By retaining the top 10% strongest correlations, we observed that these connections were lost in the HAL-treated group, whereas Cg1, M1, and M2 exhibited a high degree of inter-correlations with caudate-putamen (CP\_DM, CP\_DL, CP\_VL, and CP\_VM). Additionally, the four subdivisions of caudate-putamen (ventrolateral, ventromedial, posterolateral, and posteromedial subdivisions) appeared to be highly connected to each other in the HAL network, but not in the VEH network. Furthermore, strong inter-correlations between caudate-putamen and the core and shell of nucleus accumbens were detectable in the VEH network but were not in the HAL network.

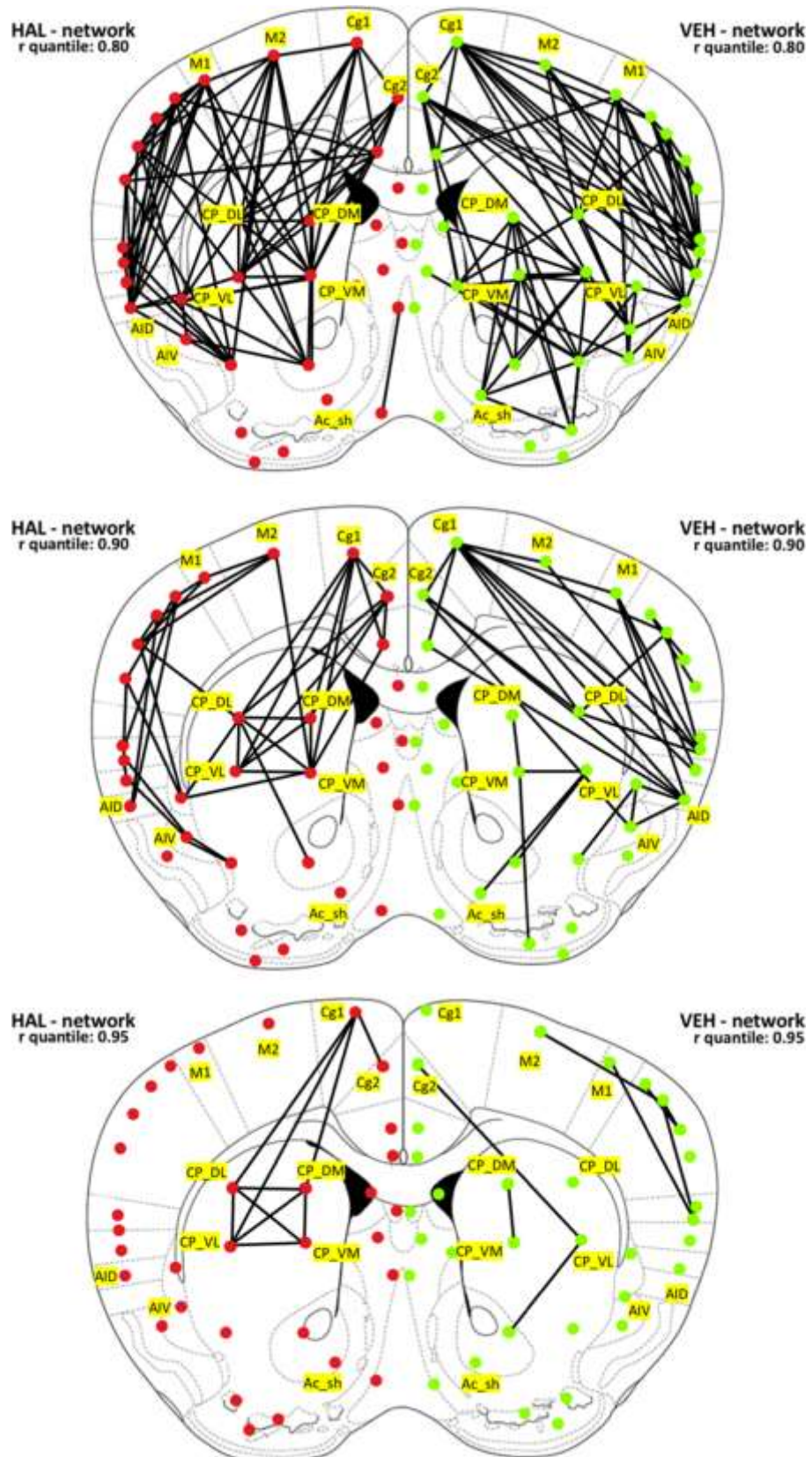


**Fig. 10.** HAL and VEH networks were generated by retaining the 5%, 10%, and 20% of the strongest correlations, respectively.

### 3.2.3.3. Nodes attributes

After acute HAL administration, centrality metrics of discrete nodes of the network were found to be steadily increasing with decreasing connection density values. In particular, the degree and eigenvector centrality of CP\_VL, CP\_VM, CP\_DM, CP\_DL, and M2 were higher for rare networks (tables 4 and 5). The betweenness centrality increased in AIV, S1dz, CP\_VM, CP\_DL, CP\_DM, GI, DI, S1j, and s1j0 for less dense networks (table 6).

On the other hand, the degree of S1FL, S1j, DI, and CP\_VM was higher in VEH network (table 7), while eigenvector centrality and betweenness increased in S1FL, s1j, s1j0, and DI for less dense networks (tables 8 and 9).

Therefore, centrality metrics were extensively modulated by HAL, particularly in the caudate-putamen, insula, supplementary motor cortex, and somatosensory cortex, suggesting that antipsychotic treatment may affect the organization of functional hubs.

<b>ROI</b>	<b>Degree 80%</b>	<b>Degree 90%</b>	<b>Degree 95%</b>
CP_VL	0.076	0.092	0.136
M1	0.07	0.052	0
S1FL	0.065	0.052	0
Cl	0.06	0.052	0
CP_DL	0.06	0.079	0.182
CP_VM	0.06	0.067	0.182
AIV	0.059	0.026	0
s1j	0.049	0.066	0.046
s1dz	0.049	0.04	0
CP_DM	0.049	0.067	0.182
AC_Co	0.048	0.013	0
M2	0.044	0.079	0.182
Cg2	0.043	0.039	0
LSS	0.043	0.026	0
s1j0	0.038	0.052	0.046
S1ULp	0.038	0.026	0
GI	0.038	0.039	0
DI	0.038	0.039	0
Cg1	0.033	0.066	0.045
AID	0.016	0.026	0
Den	0.011	0	0
MS	0.005	0	0
VDB	0.005	0	0
IG	0	0	0

Pir	0	0	0
Ac_Sh	0	0	0
LSD	0	0	0
LSI	0	0	0
LSV	0	0	0
Shi	0	0	0
Icj	0	0	0
VP	0	0	0
Tu	0	0	0

**Table 4.** Degree values for each node of the HAL network at different thresholds (80, 90 and 95%). Regions of interest given in red are those exhibiting increasing degree of connections despite the lower density of the network.

<b>ROI</b>	<b>Eigenvector Centrality 80%</b>	<b>Eigenvector Centrality 90%</b>	<b>Eigenvector Centrality 95%</b>
<b>CP_VL</b>	<b>0.08</b>	<b>0.13</b>	<b>0.165</b>
M1	0.075	0.039	0
<b>CP_VM</b>	<b>0.067</b>	<b>0.121</b>	<b>0.203</b>
<b>CP_DL</b>	<b>0.067</b>	<b>0.13</b>	<b>0.203</b>
CI	0.064	0.06	0
S1FL	0.062	0.019	0
s1j	0.059	0.029	0
<b>CP_DM</b>	<b>0.056</b>	<b>0.121</b>	<b>0.203</b>
AIV	0.056	0.004	0
AC_Co	0.053	0.006	0
<b>M2</b>	<b>0.051</b>	<b>0.132</b>	<b>0.178</b>
s1j0	0.046	0.028	0
s1dz	0.044	0.001	0
Cg2	0.044	0.07	0
Cg1	0.038	0.11	0.048
LSS	0.033	0	0
S1ULp	0.03	0	0
GI	0.027	0	0
DI	0.026	0	0

Den	0.012	0	0
AID	0.009	0	0
VP	0	0	0
VDB	0	0	0
Tu	0	0	0
Shi	0	0	0
Pir	0	0	0
MS	0	0	0
LSV	0	0	0
LSI	0	0	0
LSD	0	0	0
IG	0	0	0
Icj	0	0	0
Ac_Sh	0	0	0

**Table 5.** Eigenvector centrality values for each node of the HAL network at different thresholds (80, 90 and 95%). ROIs given in red are those displaying increasing eigenvector centrality despite the lower density of the network.

ROI	Betweenness 80%	Betweenness 90%	Betweenness 95%
S1FL	0.159	0.166	0
M1	0.132	0.108	0
CP_VL	0.107	0.117	0
Cl	0.1	0.045	0
<b>AIV</b>	<b>0.096</b>	<b>0.154</b>	<b>0</b>
LSS	0.071	0	0
Cg2	0.051	0.003	0
<b>sldz</b>	<b>0.048</b>	<b>0.139</b>	<b>0</b>
AC_Co	0.043	0	0
<b>CP_VM</b>	<b>0.042</b>	<b>0.003</b>	<b>0.111</b>
<b>CP_DL</b>	<b>0.038</b>	<b>0.024</b>	<b>0.111</b>
<b>GI</b>	<b>0.025</b>	<b>0.095</b>	<b>0</b>

DI	0.025	0.067	0
S1ULp	0.022	0	0
CP_DM	0.014	0.003	0.111
s1j	0.012	0.052	0
M2	0.007	0.005	0.667
s1j0	0.007	0.016	0
IG	0	0	0
Cg1	0	0.002	0
AID	0	0	0
Pir	0	0	0
Den	0	0	0
Ac_Sh	0	0	0
LSD	0	0	0
LSI	0	0	0
LSV	0	0	0
Shi	0	0	0
MS	0	0	0
VDB	0	0	0
Icj	0	0	0
VP	0	0	0
Tu	0	0	0

**Table 6.** Betweenness centrality values for each node of the HAL network at different thresholds (80, 90 and 95%). ROIs given in red are those exhibiting increasing betweenness centrality despite the lower density of the network.

ROI	Degree 80%	Degree 90%	Degree 95%
M2	0.06	0.118	0
S1FL	0.06	0.079	0.137
DI	0.06	0.093	0.182
AIV	0.06	0.079	0.045
s1j	0.055	0.079	0.136
M1	0.049	0.053	0.045

CP_DL	0.049	0.052	0.045
Cg1	0.044	0.053	0.045
AID	0.044	0.066	0.045
Den	0.043	0.039	0
LSS	0.043	0.013	0
s1j0	0.038	0.04	0.091
s1dz	0.038	0.026	0.046
CP_DM	0.038	0.013	0.046
CP_VL	0.038	0.039	0.046
Cl	0.033	0.026	0
Cg2	0.032	0.026	0
Ac_Sh	0.032	0.013	0
LSV	0.032	0	0
GI	0.027	0	0
CP_VM	0.027	0.04	0.046
VP	0.027	0.013	0
S1ULp	0.022	0.026	0
AC_Co	0.022	0.013	0.046
Pir	0.016	0	0
LSD	0.005	0	0
LSI	0.005	0	0
IG	0	0	0
Shi	0	0	0
MS	0	0	0
VDB	0	0	0
Icj	0	0	0
Tu	0	0	0

**Table 7.** Degree values for nodes of the VEH network at different cut thresholds (80, 90 and 95%). ROIs given in red are those displaying increasing degree of connections despite the lower density of the network.

ROI	Eigenvector Centrality 80%	Eigenvector Centrality 90%	Eigenvector Centrality 95%
DI	0.084	0.126	0.224
M2	0.081	0.141	0
S1FL	0.08	0.115	0.196
AIV	0.08	0.097	0.087
s1j	0.071	0.1	0.2
CP_DL	0.069	0.075	0
M1	0.068	0.085	0.077
AID	0.066	0.096	0.087
Cg1	0.058	0.06	0
Den	0.048	0.029	0
s1j0	0.046	0.019	0.092
s1dz	0.046	0.004	0.036
Cg2	0.043	0.042	0
GI	0.031	0	0
Pir	0.026	0	0
LSV	0.024	0	0
S1ULp	0.023	0.004	0
LSS	0.012	0.001	0
Cl	0.011	0.005	0
CP_DM	0.007	0	0
CP_VL	0.006	0	0
AC_Co	0.006	0	0
Ac_Sh	0.004	0	0
VP	0.004	0	0
CP_VM	0.003	0	0
LSD	0.001	0	0
LSI	0.001	0	0
IG	0	0	0
Shi	0	0	0
MS	0	0	0
VDB	0	0	0

Icj	0	0	0
Tu	0	0	0

**Table 8.** Eigenvector centrality values for each node of the VEH network at different cut thresholds (80, 90 and 95%). ROIs given in red are those exhibiting increasing eigenvector centrality despite the lower density of the network.

ROI	Betweenness 80%	Betweenness 90%	Betweenness 95%
Den	0.172	0.134	0
LSS	0.118	0	0
Cg2	0.081	0	0
Cl	0.068	0.071	0
<b>DI</b>	<b>0.067</b>	<b>0.041</b>	<b>0.333</b>
M2	0.066	0.121	0
AC_Co	0.063	0	0
LSV	0.058	0	0
AIV	0.057	0.117	0
CP_DL	0.048	0.024	0
<b>S1FL</b>	<b>0.047</b>	<b>0.033</b>	<b>0.182</b>
<b>s1j</b>	<b>0.039</b>	<b>0.187</b>	<b>0.303</b>
CP_DM	0.023	0	0
Cg1	0.022	0.061	0
CP_VL	0.019	0.036	0
M1	0.011	0	0
<b>s1j0</b>	<b>0.009</b>	<b>0.133</b>	<b>0.182</b>
s1dz	0.009	0	0
Ac_Sh	0.008	0	0
AID	0.006	0.006	0
GI	0.005	0	0
CP_VM	0.003	0.036	0
VP	0.002	0	0
IG	0	0	0
S1ULp	0	0	0

Pir	0	0	0
LSD	0	0	0
LSI	0	0	0
Shi	0	0	0
MS	0	0	0
VDB	0	0	0
Icj	0	0	0
Tu	0	0	0

**Table 9.** Betweenness centrality values for each node of the VEH network at different cut thresholds (80, 90 and 95%). ROIs given in red display increasing eigenvector centrality despite the lower density of the network.

### 3.3. Discussion

The present study was aimed at exploring the changes induced by antipsychotics, in topological properties of brain networks, by mapping the expression of the IEG Homer1a.

In order to achieve this objective, we focused on investigating:

1) the shifting balance between functional integration and segregation of the brain network after HAL administration compared to VEH, hypothesising that it may be finely tuned by antipsychotics;

2) differences in functional links connecting ROIs which are relevant to schizophrenia pathophysiology in the two treatment groups;

3) changes in functional hubs.

To assess differences between HAL and VEH networks we computed measures of connection density, global efficiency, clustering coefficient, and small-world index. Then, we obtained measures of centrality of each node. As major results of the study, we observed that:

1) Antipsychotic medication enhanced the network's small-worldness, raised functional integration and segregation.

2) The topographical differences between networks were remarkable. HAL induced higher intercorrelations between the four subdivisions of the caudate-putamen, and between dorsal striatum and accumbens, whereas it decreased intercorrelations between areas belonging to the salience circuit;

3) Caudate-putamen, insula, supplementary motor cortex, and somatosensory cortex gained centrality after antipsychotic administration.

The global efficiency of HAL-treated network was found to be higher than that of the VEH, and this could have important implications for treating schizophrenia symptoms. Global efficiency, which measures how effectively information is transferred across long distances in a network, appears to be a good indicator of human cognitive functioning (Stanley et al., 2015).

Therefore, by improving global efficiency, antipsychotics may assure a greater functional integration, which may enhance higher-order brain activities. Of interest, Hadley and colleagues showed that unmedicated patients with schizophrenia had lower global efficacy at the baseline, but this parameter increased after six weeks of antipsychotic treatment only in those patients who responded adequately (Hadley et al., 2016).

It is therefore possible that modifications to network characteristics could be an epiphenomenon of a successful dopamine manipulation exerted by antipsychotics, pointing to increases in network integration as a function of therapeutic response.

Moreover, the clustering coefficient, a measure of functional segregation showing the degree to which a network is divided into sub-specialized regions, was found to be higher in the HAL network vs vehicle network. This may be a result of various network segments becoming more functionally specialized. The ability of antipsychotic treatment to dynamically reorganize the network structure and optimize a fine balance between segregation and integration of specialized brain areas, which is characteristic of a small-world organization, may underlie its clinical action.

Furthermore, the network's topological structure has been found to be sensitive to HAL exposure. In particular, the inter-correlations between cingulate cortex and anterior insular cortex have been found to be disrupted by HAL administration. Of interest, anterior insular cortex and cingulate cortex compose the salience network, a large-scale brain network of the human brain (Seeley et al., 2007), recently recognized also in rats (Tsai et al., 2020). The salience network is believed to participate in a variety of functions including communication, social behavior, and self-awareness through the integration of sensory, emotional, and cognitive information (Craig, 2009; Gogolla et al., 2014; Menon and Uddin, 2010) and has been shown to be strongly involved in the ability to discriminate between self-generated and external information (Wylie and Tregellas, 2010).

The conceptualization of psychotic disorders as the result of assignment of abnormal salience to neutral stimuli goes along with the hypothesis that hyperconnectivity in salience network may explain positive symptoms of schizophrenia (i.e., hallucinations and delusions) (Corlett et al., 2016). Haloperidol ability to modulate these specific interconnections, which are particularly pronounced in psychotic patients (Fornito et al., 2013), is consistent with a potential antipsychotics' effects on positive symptoms related to aberrant assignment of salience (Kapur et al., 2006).

Moreover, we found that the cingulate cortex shared a higher degree of intercorrelations with caudate-putamen in HAL network than in VEH network. Of interest, it has been reported that subjects with at-risk mental state (AMRS) and patients with first-episode-psychosis (FEP) display reduced functional connectivity between prefrontal cortex and dorsal caudate in fMRI studies (Dandash et al., 2014; Fornito et al., 2013). Hence, dopamine manipulation might influence functional dysconnectivity by targeting specific disease-related circuits, such as salience and fronto-striatal circuits which are reorganized in schizophrenia.

Furthermore, the four subdivisions of caudate-putamen (ventrolateral, ventromedial, posterolateral, and posteromedial) appear highly connected to each other in HAL network but not in the VEH network. These findings agree with the results of Wheeler and colleagues, which

found increased inter-connectivity in caudate-putamen after chronic haloperidol exposure (Wheeler et al., 2014). These striatal effects exerted by HAL may account for the onset of extrapyramidal symptoms.

Finally, we analyzed centrality metrics in both networks, and identified several nodes with increasing centrality over decreasing connection density values. These nodes became central regardless of the progressive rarefaction of the network. Thus, antipsychotics may affect functional hubs, regions projecting with abundant, strategic, and long-range connections to other specialized areas, which are relevant for integration processes. For instance, it is known that patients affected by schizophrenia exhibit reduced centrality of crucial frontal hubs such as superior frontal and anterior cingulate regions (van den Heuvel, M. P. et al., 2010), as well as parietal, limbic, and insular hubs (Rubinov and Bullmore, 2013). The betweenness centrality of these nodes classified individuals suffering from schizophrenia from healthy controls with a high level of accuracy (Achard et al., 2006). Our results show that the prototypical typical antipsychotic haloperidol impacts the centrality of dorsal striatum, somatosensorial, insular, and supplementary motor cortex areas. These findings suggest that antipsychotics could affect relevant nodes attributes and modulate the organization of functional hubs.

In summary, the modifications induced by acute HAL administration, point to a multimodal adaptation in the functional organization of brain network. Antipsychotic medications may effectively modulate brain network topology, network properties, node attributes, and interactivity within specific disease-related circuits.

## **4. Experiment n° 2**

### **4.1. Material and methods**

#### **4.1.1. Animals**

Twenty male Sprague-Dawley rats (n=20) with an average weight of 250 g (Charles-River Labs, Lecco) were housed and adapted to human handling in a temperature and humidity-controlled colony room, under a 12:12-h light:dark photocycle with unrestricted access to food and water. The experimental procedures and animal handling techniques were conducted in agreement with the NIH Guide for Care and Use of Laboratory Animals (NIH publication no. 85-23, revised 1996) and approved by local Animal Care and Use Committee. All feasible measures have been taken to reduce animal suffering.

#### **4.1.2. Animal treatment**

Animals were randomly assigned to two groups (n=10 for each pre-treatment group), receiving saline (VEH; NaCl 0.9%) or KET (30 mg/kg), in order to measure Home1a transcript levels either under physiological conditions or after challenge of the glutamatergic system by a NMDAR antagonist. In fact, among tested preclinical models, acute KET injection at a sub-anesthetic and sub-convulsant dose was selected to replicate the behavioural and neurochemical characteristics of schizophrenia (Lipska and Weinberger, 2000; Chatterjee et al., 2012).

Subsequently, the antipsychotic asenapine (ASE, 0.3 mg/kg), or saline (VEH), was given to each pre-treatment group after being randomly divided into two arms (n=5 for each treatment group). Thirty minutes after pre-treatment, the second compound was injected intraperitoneally. KET (Sigma-Aldrich, St. Louis, MS, USA) and ASE (Lundbeck A/S, Copenhagen, Denmark) were supplied as a powder and dissolved in saline solution (NaCl 0.9%), adjusted to physiological pH, and injected intraperitoneally at the final volume of 1 mL/kg. According to previously reported experimental methods, ASE was given at behaviourally active dosages that are known to promote gene expression (Majercikova and Kiss, 2016; Ohyama et al., 2016). Therefore, the following four treatment groups were obtained: a) VEH+VEH; b) VEH+ASE; c) KET+ASE d) KET+VEH (please see Fig. 11). Ninety minutes after the second injection, animals were sacrificed by decapitation.

### 4.1.3. ISH, image analysis, and data processing procedures

The ISH, image analysis, and data processing protocols were the same as in the first experiment (please refer to section 3.1.2, 3.1.3, and 3.1.4).

### 4.1.4. Statistical methods

By averaging measurements from three adjacent sections of each animal brain, we calculated gene expression values in each region. The Shapiro-Wilk test was used to determine if the relative dpm values were distributed normally. Repeated measures analysis of variance (ANOVA) was used to determine the individual contribution of each of the categorization factors on the outcome of the dependent variable (i.e., Homer1a gene expression). In particular, we analyzed the effect of the between-subjects variable (treatment) as well as the within-subject variable (ROI) effects and their interaction.

Moreover, we used the Student's *t* test to compare the transcript values of Homer1a in:

i) VEH/VEH vs KET/VEH groups, in order to evaluate Homer1a expression in the presence or absence of a challenge of the glutamatergic system.

ii) VEH/VEH vs VEH/ASE groups, in order to understand the effect of the antipsychotic on gene expression in baseline conditions.

iii) KET/VEH vs KET/ASE groups, to assess the effects of ASE on Homer1a transcript levels in an animal model of schizophrenia. The comparisons were performed using the Student's *t*-test. The threshold for comparisons' significance was set at 0.05. Multiple testing error was managed by using Bonferroni correction (adjusted p-value = 0.0015). For statistical analysis, SAS Institute Inc.'s JMP software version 9.0.1 and IBM SPSS 25 were adopted.

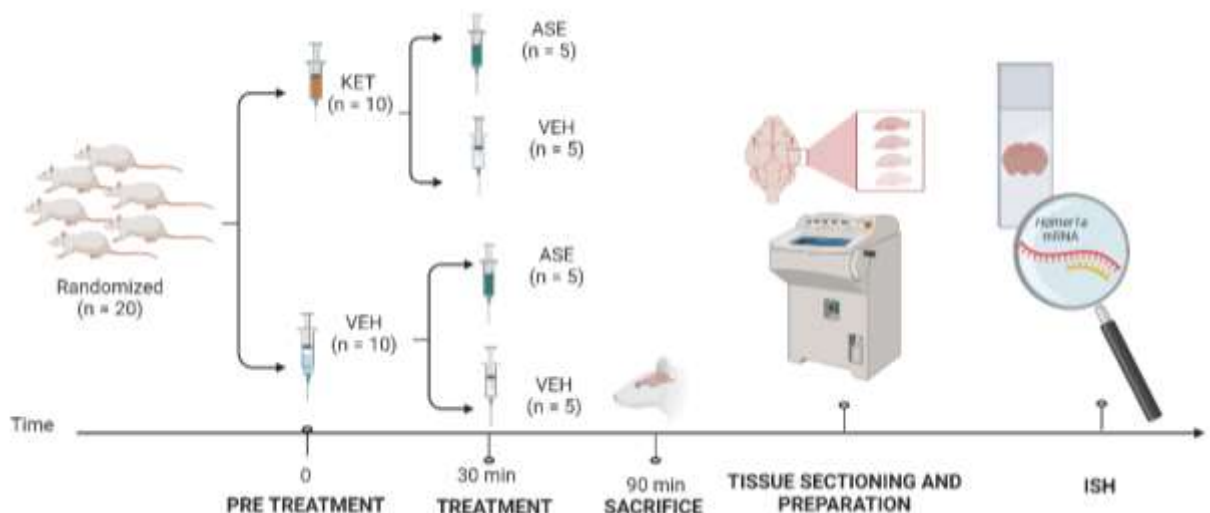


**Fig. 11.** Graphical abstract summarizing the study protocol

#### **4.1.5. Comparison of correlation matrices and generation of networks**

Using the Homer1a signal intensity measures in each ROI as dependent variables, we calculated the Pearson's  $r$  for all possible pairwise correlations in each treatment group (i.e., VEH/VEH, VEH/ASE, KET/VEH, and KET/ASE) and four correlation matrices were generated. The statistical analyses and graphical outputs were obtained using the software R.4.2.1 with the "hmisc", "corrplot", and "dnt" packages (<http://www.r-project.org/>), as well as Cytoscape software 3.8.2 (<http://www.cytoscape.org/>). We used a function providing a permutation-based frame for comparing networks and calculated significant differences between paired edges. We calculated network properties, such as characteristic path length, clustering coefficients, network density, and connected components. We compared global strength of the networks and basic centrality properties of nodes such as degree and betweenness centrality.

Networks consisting of 33 nodes (as many as the ROIs investigated) were graphically generated; each network was summarized by its weighted adjacency matrix, where the edge weights between two nodes refer to the corresponding  $r$  correlation coefficient value, ranging from -1 to +1, indicating the magnitude or strength of an edge.

Graphical outputs were obtained by styling the edges based on their weights, and nodes based on the degree. In the effort to retain only relevant edges and avoid spurious ones, we filtered significant correlations with a minimum p-value  $<0.01$  in order to achieve a trade-off between sensitivity and specificity.

## **4.2. Results**

### **4.2.1. Gene expression comparison**

The dependent variable was normally distributed for each combination of the levels of the between- and within-subjects factors, as revealed by Shapiro-Wilk test, which did not give significant results. Mauchly's test of sphericity indicated that the assumption of sphericity was violated, then we applied the Huynh-Feldt correction for degrees of freedom. There was a statistically significant two-way interaction between treatment and ROI,  $F(21.56, 115) = 2.096$ ,  $p=0.002$ , partial  $\eta^2 = 0.308$ .

Homer1a mRNA expression levels were compared in the 33 ROIs of VEH/VEH and KET/VEH groups. Homer1a expression was significant lower in KET/VEH group compared to

VEH/VEH group in the cingulate cortex (cg2 and cg1) (95% CI, -0.47 to -0.09,  $t(8)=-3.48$ ,  $p=0.008$ ; 95% CI, -0.64 to -0.20,  $t(8)=-4.43$ ,  $p=0.002$ , respectively), in primary and supplementary motor cortex (95% CI, -0.51 to -0.10,  $t(8)=-3.47$ ,  $p=0.008$ ; 95% CI, -0.59 to -0.12,  $t(8)=-3.56$ ,  $p=0.007$ , respectively), in the forelimb, jaw region, and dysgranular zone of the somatosensory cortex (CI, -0.44 to -0.07;  $t(8)=-3.22$ ,  $p=0.012$ ; CI, -0.38 to -0.02,  $t(8)=-2.59$ ,  $p=0.032$ ; CI, -0.37 to 0.00,  $t(8)=-2.28$ ,  $p=0.05$ , respectively), in all striatal subregions (in CPDM, CI, -0.55 to -0.05,  $t(4.96)=-3.14$ ;  $p=0.026$ ; CPDL, CI, -0.57 to -0.11,  $t(5.81)=-3.63$ ;  $p=0.012$ ; CPVL, CI, -0.57 to -0.03,  $t(4.65)=-2.93$ ,  $p=0.036$ ; CPVM, CI, -0.69 to -0.15,  $t(4.72)=-4.09$ ,  $p=0.011$ ), in the nucleus accumbens (the core, CI, -0.51 to -0.00,  $t(4.43)=-2.73$ ,  $p=0.047$ ; the shell CI, -0.58 to 0.00,  $t(5.32)=-2.44$ ,  $p=0.05$ ), the ventral region of the lateral septal nuclei (CI, -0.27 to -0.01,  $t(8)=-2.59$ ,  $p=0.033$ ), the Calleja's islands (CI, -0.24 to -0.05,  $t(8)=-3.55$ ,  $p=0.007$ ), the ventral pallidum (CI, -0.32 to 0.10,  $t(8)=-4.21$ ,  $p=0.003$ ), and olfactory tubercle (CI, -0.36 to -0.03,  $t(8)=-2.67$ ,  $p=0.028$ ). Nonetheless, significant values did not survive after Bonferroni correction.

As revealed by VEH/VEH and VEH/ASE comparisons, ASE administration resulted in higher Homer1a transcript levels in the area 2 of the cingulate cortex (CI, -0.36 to -0.01,  $t(8)=-2.43$ ,  $p=0.041$ ), whereas Homer1a expression was lower in the ventral pallidum (CI, -0.023 to -0.02,  $t(8)=-2.67$ ,  $p=0.028$ ). Significant values did not survive after Bonferroni correction.

Noteworthy, the administration of asenapine in an animal model of schizophrenia obtained by acute ketamine exposure was able to restore the original Homer1a expression almost in all the regions considered. In particular, when comparing Homer1a transcript levels in KET/VEH vs KET/ASE, we found an increase in Homer1a expression in all subregions (please see table 10) except for Indusium griseum, the oral surface of the jaw region of the somatosensory cortex, the nucleus of the vertical limb of the diagonal band, and the olfactory tubercle.

When multiple testing was taken into account using Bonferroni's correction, significant differences survived in dorsolateral, dorsomedial, and ventral-lateral caudate-putamen, as well as in the medial septum ( $p<0.001$ ).

ROIs	<i>t</i>	Degree of freedom	<i>p</i> -value	Confidence interval	
				Inferior	Superior
Ig	-1,17	8	0,275	-0,16	0,05
cg2	-3,00	8	<b>0,017</b>	-0,40	-0,05
cg1	-2,59	8	<b>0,032</b>	-0,49	-0,03

M2	-2,89	8	<b>0,020</b>	-0,52	-0,06
M1	-2,60	8	<b>0,032</b>	-0,51	-0,03
S1FL	-3,19	8	<b>0,013</b>	-0,55	-0,09
S1j	-2,32	8	<b>0,049</b>	-0,53	0,00
S1jO	-1,73	8	0,121	-0,69	0,10
S1DZ	-2,50	8	<b>0,037</b>	-0,53	-0,02
S1ULp	-2,30	8	<b>0,051</b>	-0,55	0,00
GI	-2,52	8	<b>0,036</b>	-0,61	-0,03
DI	-3,21	8	<b>0,012</b>	-0,66	-0,11
AID	-3,42	8	<b>0,009</b>	-0,63	-0,12
AIV	-2,83	8	<b>0,022</b>	-0,54	-0,05
CI	-2,94	8	<b>0,019</b>	-0,55	-0,07
Pir	-2,66	8	<b>0,029</b>	-0,50	-0,03
Den	-2,91	8	<b>0,02</b>	-0,36	-0,04
LSS	-3,28	8	<b>0,011</b>	-0,58	-0,10
CPDM	-5,41	8	<b>0,001</b>	-0,52	-0,21
CPDL	-6,24	8	<b>&lt;0,001</b>	-0,7	-0,32
CPVL	-6,93	8	<b>&lt;0,001</b>	-0,84	-0,42
CPVM	-4,32	8	<b>0,003</b>	-0,71	-0,21
AcCo	-3,36	8	<b>0,01</b>	-0,58	-0,11
AcSh	-3,49	8	<b>0,008</b>	-0,63	-0,13
LSD	-3,13	8	<b>0,014</b>	-0,46	-0,07
LSI	-2,90	8	<b>0,02</b>	-0,26	-0,03
LSV	-3,14	8	<b>0,014</b>	-0,38	-0,06
Shi	-3,58	8	<b>0,007</b>	-0,36	-0,08
MS	-4,84	8	<b>0,001</b>	-0,29	-0,1
VDB	-2,61	8	0,06	-0,37	0,01
Icj	-2,71	8	<b>0,027</b>	-0,47	-0,04
VP	-2,70	8	<b>0,027</b>	-0,48	-0,04
Tu	-1,95	8	0,086	-0,44	0,04

**Table 10.** Results of Student's *t* test comparing KET/VEH vs KET/ASE groups throughout the 33 regions of interest. Significant values were outlined in bold. Significant adjusted p-values after Bonferroni correction were given in red. ns: not significant.

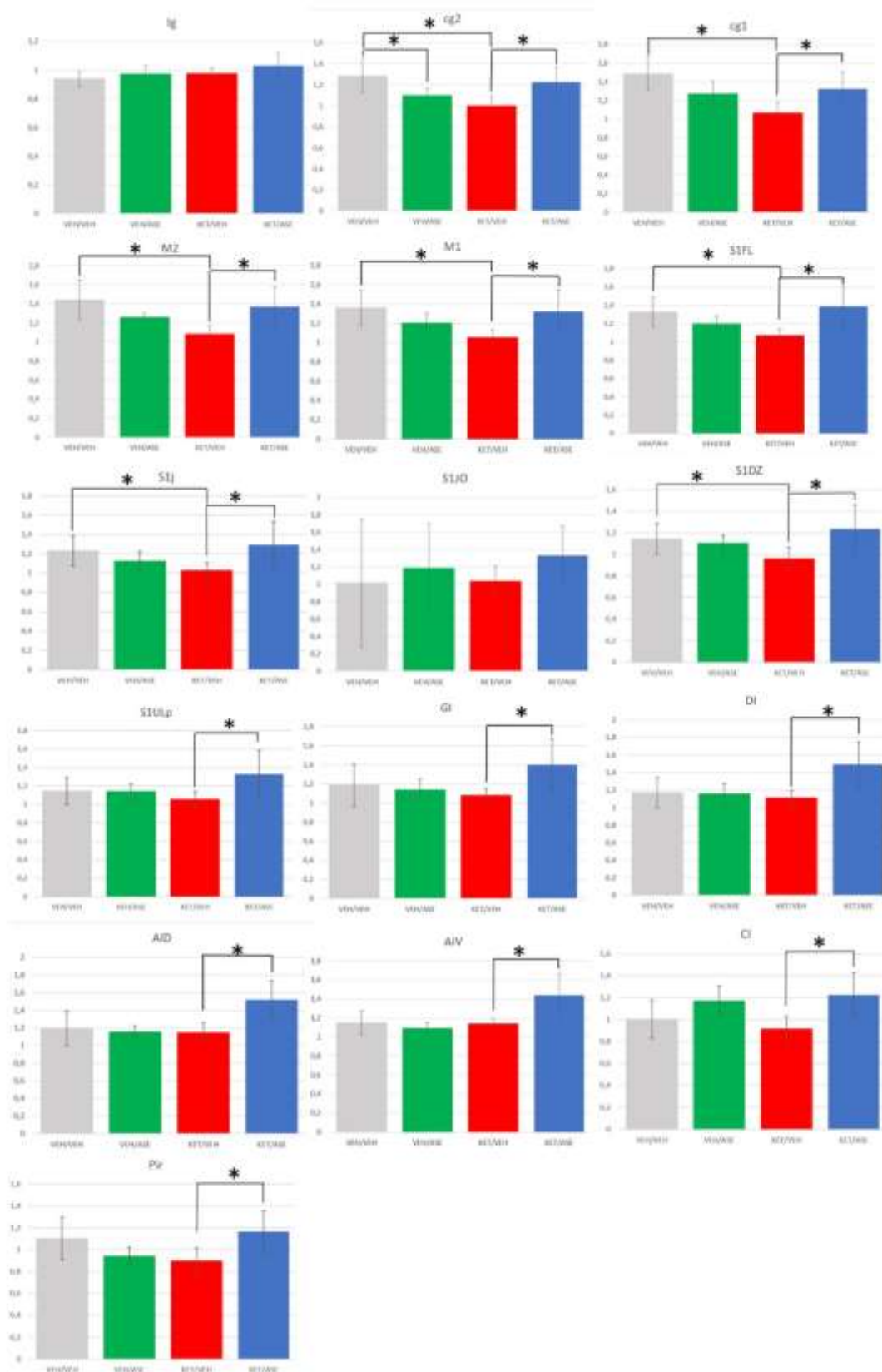


**Fig. 12.** Illustrative histograms of Homer1a expression in different treatment groups throughout cortical subregions.

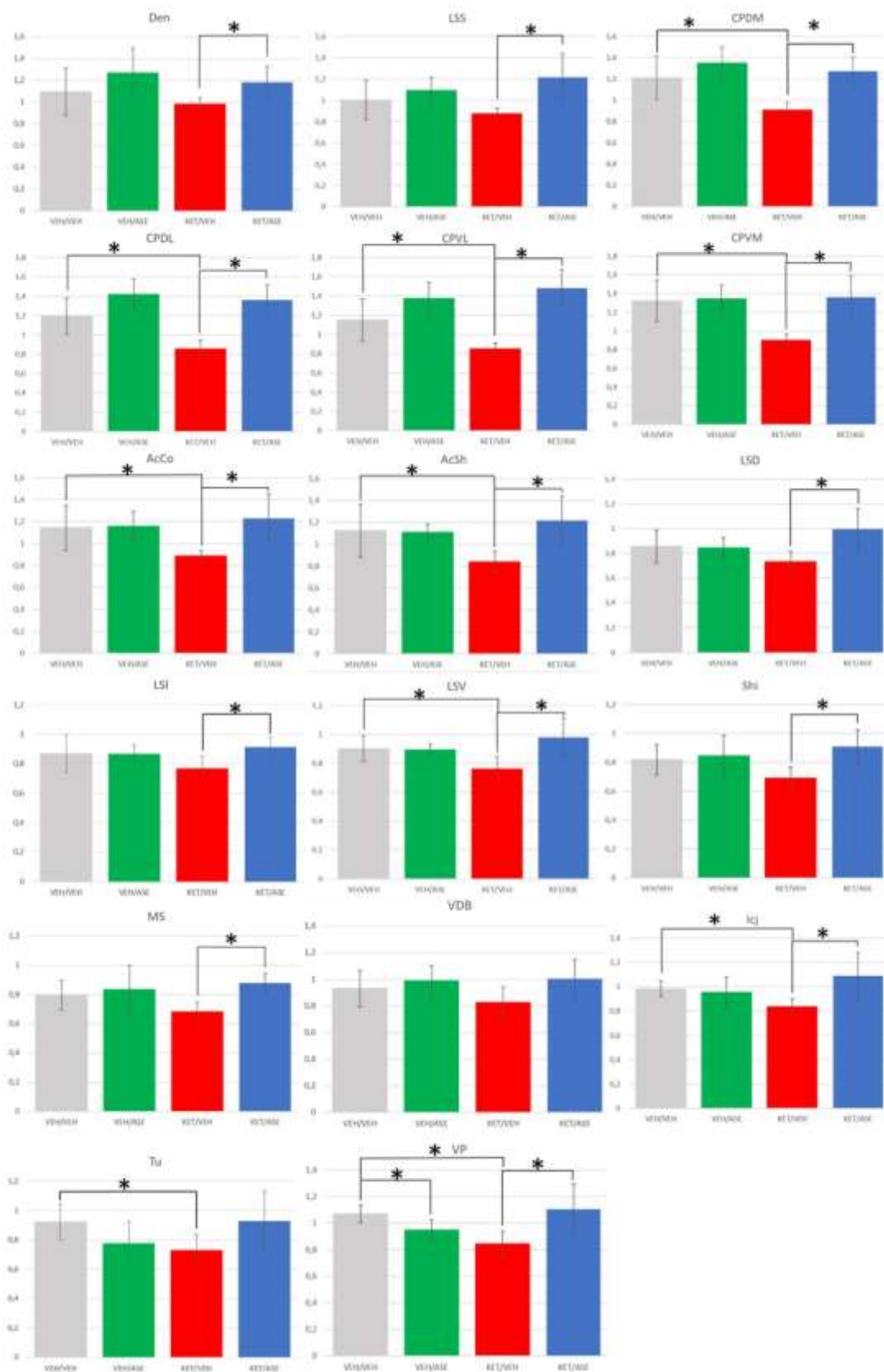


**Fig. 13.** Illustrative histograms of Homer1a expression in different treatment groups throughout striatal subregions.

### 4.2.1. Generation and comparison of correlation matrices

We calculated all pairwise correlations in each treatment group (please see Supplementary Table 1, 2, and 3 for Pearson's and p-values) and generated four correlation matrices (please see Fig. 14-17).

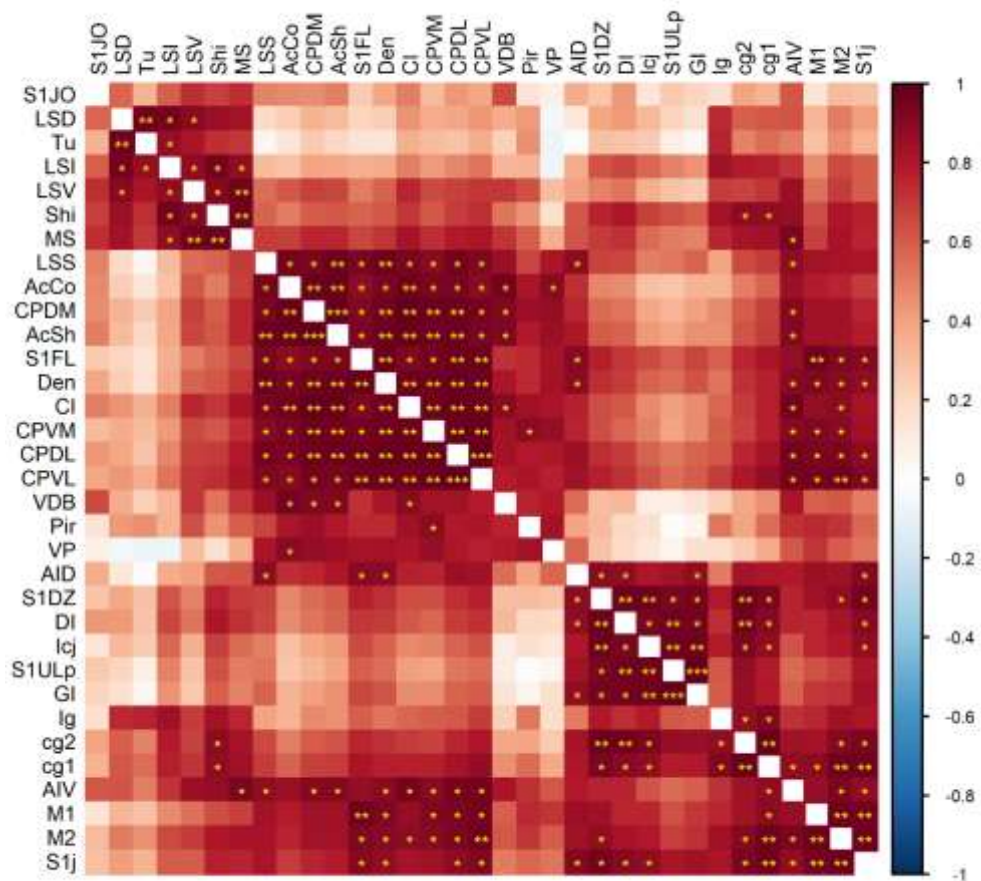


**Fig. 14.** Correlation matrix for the VEH/VEH group. Variables are grouped according to hierarchical clustering. According to the colour scale on the right of the matrix, positive correlations are reported in red, negative ones in blue. Asterisks represent significance levels, accordingly: p-values <0.05 are indicated with an asterisk, p-values <0.01 with two asterisks, p-values <0.001 with three asterisks. VEH= vehicle.

It is noteworthy that the administration of ASE is associated with the appearance of many negative correlations between ROIs in the VEH/ASE matrix. It should be noted that methods for comparing brain networks largely ignore negative correlations (Schwarz and McGonigle, 2011) even if negative edges may be neurobiologically relevant and their significance is yet to be clarified (Zhan et al., 2017). In this case, the inter-correlation between accumbens, cingulate cortex, motor cortex ROIs and striatal subregions became negative.

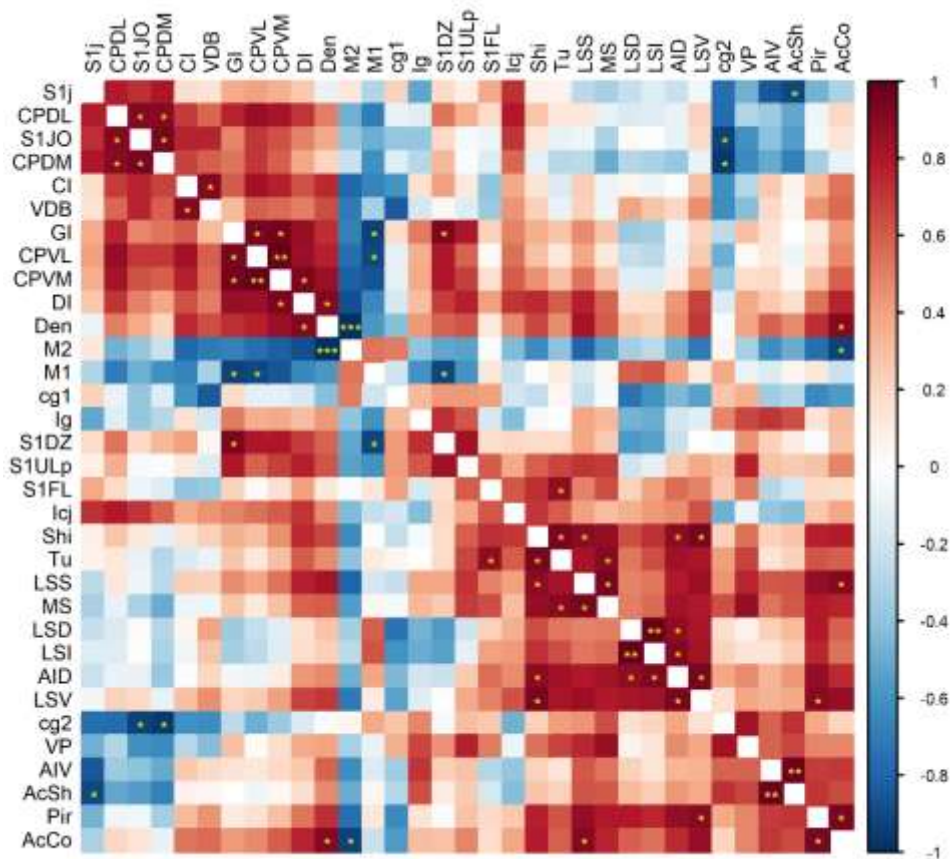


**Fig. 15.** Correlation matrix for VEH/ASE group. Variables are grouped according to hierarchical clustering. According to the colour scale on the right of the matrix, positive correlations are reported in red, negative ones in blue. Asterisks represent significance levels, accordingly: p-values <0.05 are reported with an asterisk; p-values <0.01 with two asterisks, p-values <0.001 with three asterisks. VEH= vehicle; ASE= asenapine.

Acute KET challenge is associated with the appearance of negative correlations between Ig and all remaining ROIs. Since the indusium griseum receive dense dopamine afferents and contains dopaminergic neurons, this region has been described as a common neuronal target of psychostimulant action (Carmena et al., 2014; Fuzik et al., 2019). Given the effects of ketamine on dopamine functions (Kokkinou et al., 2018), it is conceivable that ketamine has similar effects to amphetamines on this specific brain region, which is classically considered as a part or a remnant of the hippocampus.

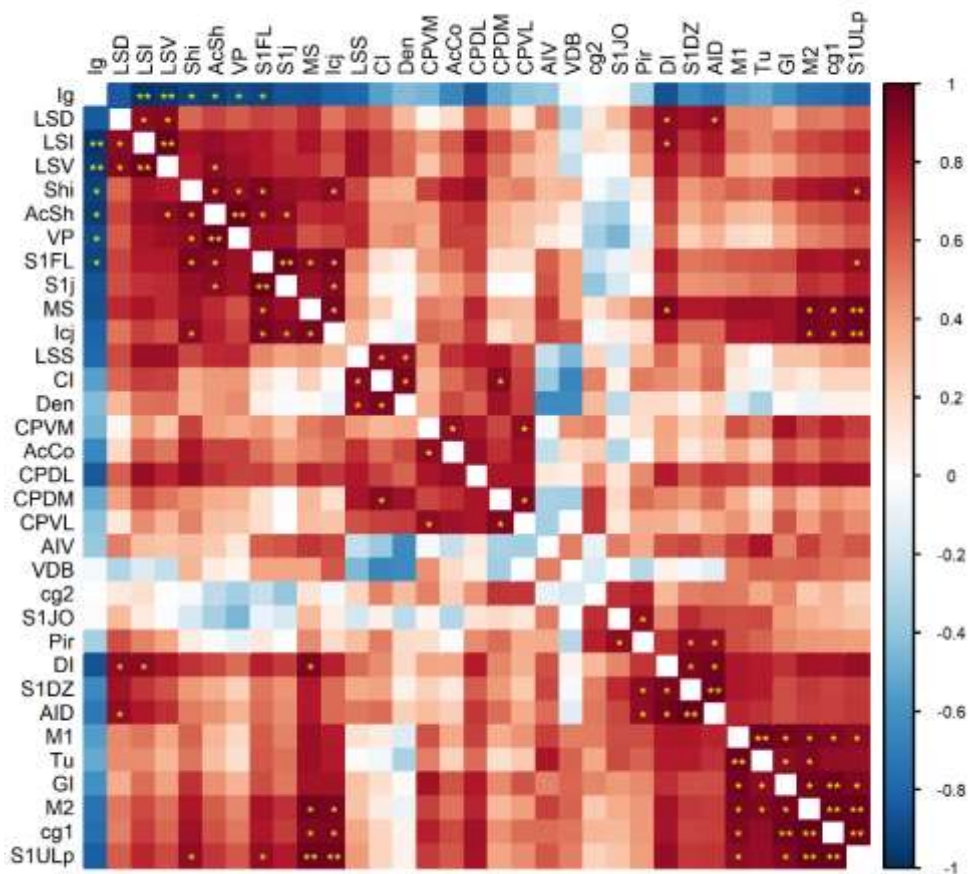


**Fig. 16.** Correlation matrix for KET/VEH group. Variables are grouped according to hierarchical clustering. According to the colour scale on the right of the matrix, positive correlations are reported in red, negative ones in blue. Asterisks represent significance levels, accordingly: p-values <0.05 are indicated with an asterisk, p-values <0.01 are reported with two asterisks, p-values <0.001 are summarized with three asterisks. KET= ketamine; VEH= vehicle.

The KET/ASE matrix is characterized by a pattern of stronger and positive connections, a large portion of which are significant or highly significant. The connections between caudate-putamen subdivisions as well as between insular portions appear strong and positive, similarly to what also occurs in the VEH/VEH matrix.

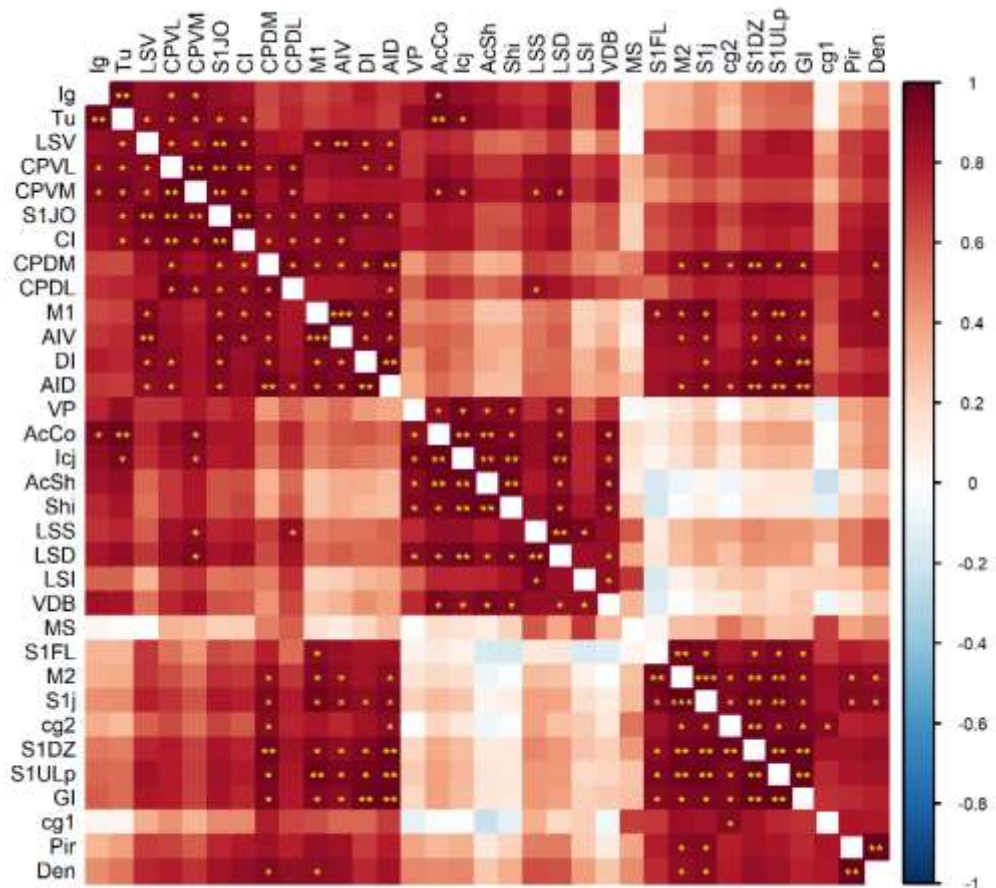


**Fig. 17.** Correlation matrix for KET/ASE group. Variables are grouped according to hierarchical clustering. According to the colour scale on the right of the matrix, positive correlations are reported in red, negative ones in blue. Asterisks represent significance levels, accordingly: p-values <0.05 are indicated with an asterisk, p-values <0.01 with two asterisks, p-values <0.001 with three asterisks. KET= ketamine; ASE= asenapine.

By using the permutation test we compared the edge weight of pairs of matrices (VEH/VEH vs VEH/ASE; VEH/VEH vs KET/VEH, and KET/VEH vs KET/ASE). Significant differences are graphically displayed in Fig. 18-20.

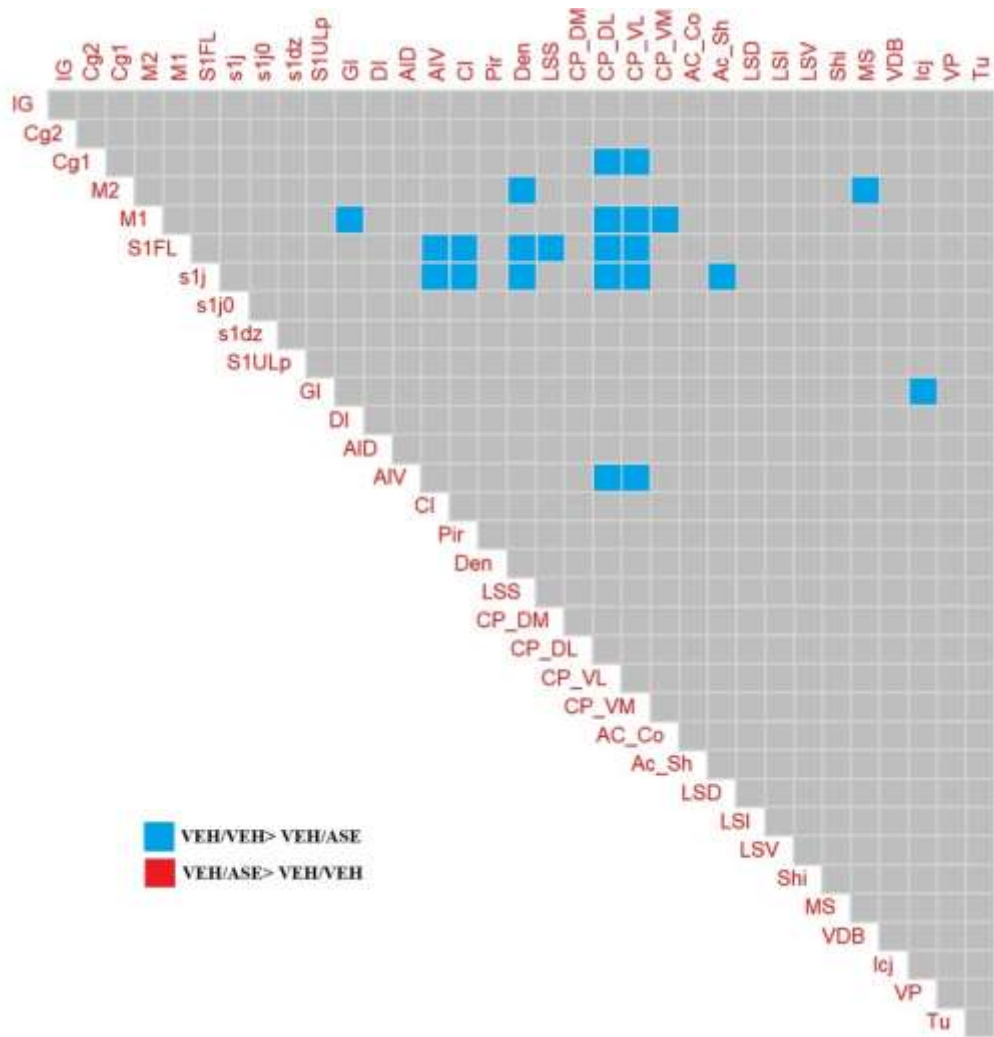


**Fig. 18.** Differences between VEH/VEH and VEH/ASE correlation matrices. Blue squares indicate pairs of correlations in which VEH/VEH Pearson's  $r$  is significantly higher than in VEH/ASE. On the contrary, red squares indicate couples of correlations in which VEH/ASE Pearson's  $r$  is significantly higher than VEH/VEH. VEH= Vehicle; ASE= Asenapine.

Ketamine challenge resulted in a reduction of Pearson's  $r$  coefficient in multiple pairs of correlation between insular ROIs and several cortical and subcortical regions.

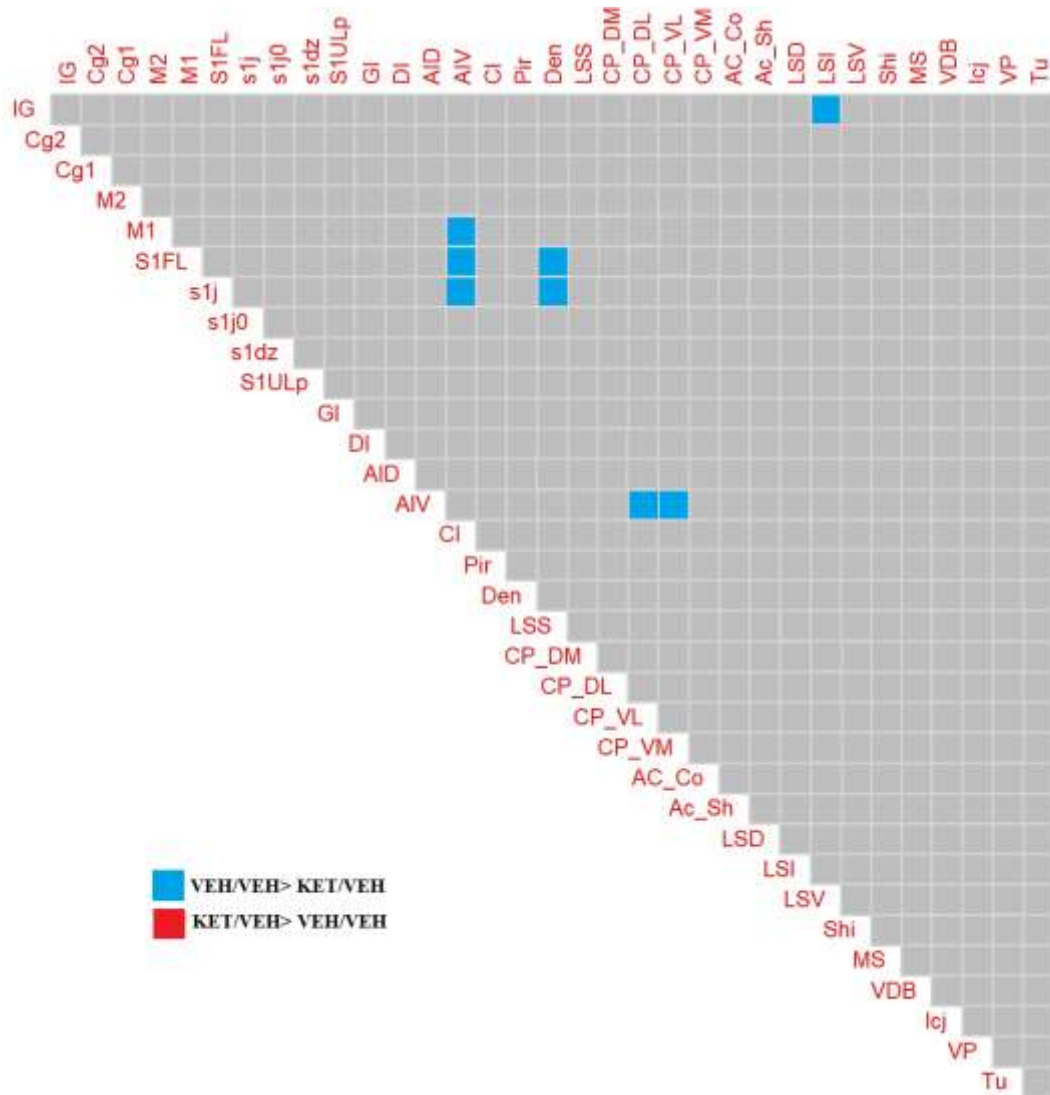


**Fig. 19.** Differences between VEH/VEH and KET/VEH correlation matrices. Blue squares indicate pairs of correlations in which VEH/VEH Pearson's  $r$  is significantly higher than in KET/VEH. On the contrary, red squares indicate couples of correlations in which KET/VEH Pearson's  $r$  is significantly higher than VEH/VEH. VEH= Vehicle; KET= ketamine.

The administration of the antipsychotic asenapine after acute ketamine challenge inverted the Pearson's  $r$  coefficient in multiple correlations between indusium griseum and several basal nuclei (Fig. 30).

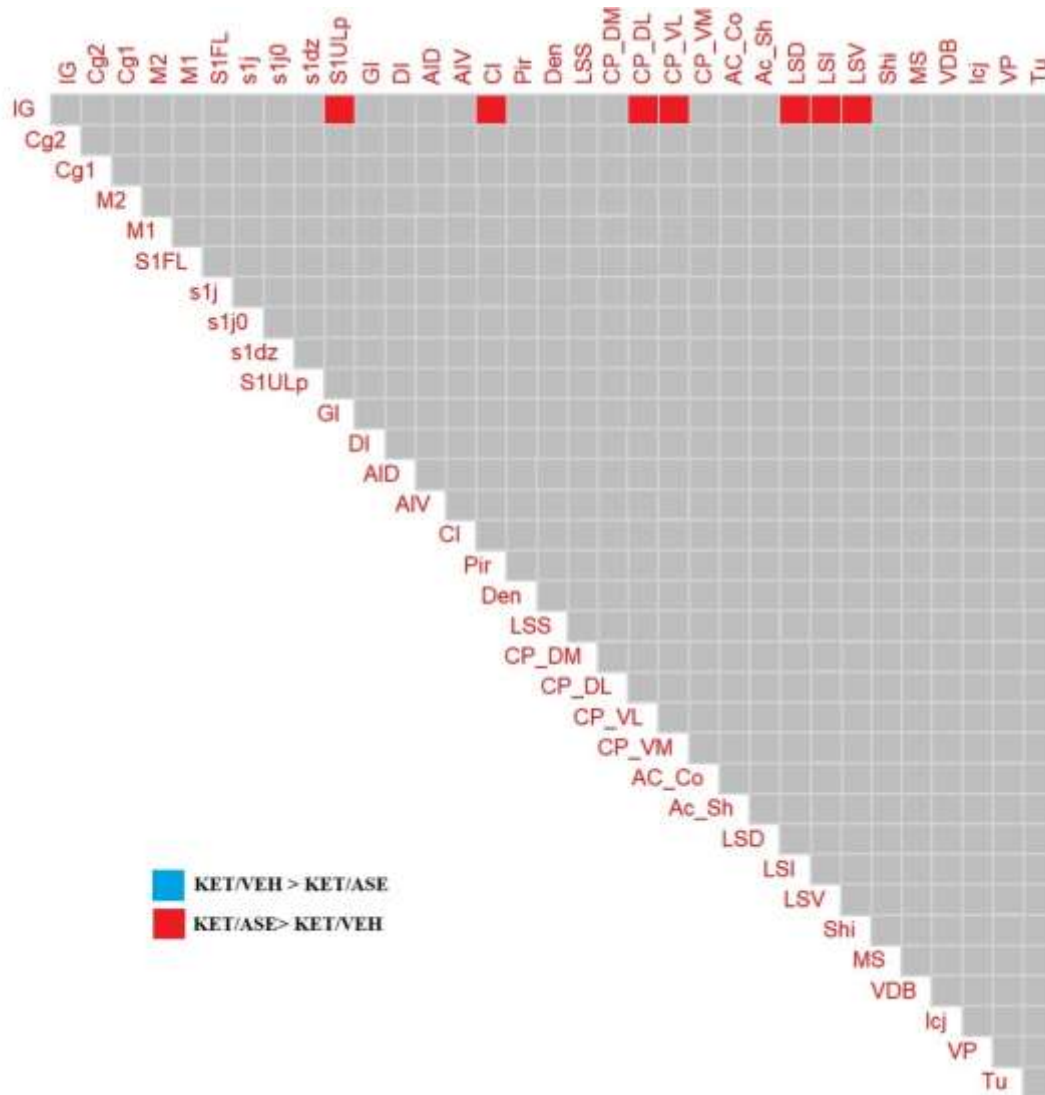


**Fig. 30.** Differences between KET/VEH and KET/ASE correlation matrices. Blue squares indicate pairs of correlations in which KET/VEH Pearson's  $r$  is significantly higher than in KET/ASE. On the contrary, red squares indicate couples of correlations in which KET/ASE Pearson's  $r$  is significantly higher than KET/VEH. VEH= Vehicle; KET= ketamine; ASE= asenapine.

### 4.2.2. Construction and comparison of brain networks

Networks were drawn as indirect graphs, with edges indicating a two-way relationship. We retained only significant correlations with  $p$ -value  $<0.01$  in order to achieve a trade-off between sensitivity and specificity. Networks were styled with a force-directed layout, which allows us to visually outline clusters, cliques, and bridges (please see Fig. 31-34). The colour of nodes was assigned depending on the degree. To facilitate interpretation, we have positioned the network nodes on the corresponding ROIs (please see Fig 35).

We calculated a series of parameters for each network, i.e., number of nodes, number of edges, network density, centralization, characteristic path length, clustering coefficients, and connected components (please see table 11).

	VEH/VEH	VEH/ASE	KET/VEH	KET/ASE
Number of nodes	28	17	30	30
Number of edges	64	10	69	47
Network density	0.255	0.667	0.159	0.122
Network centralization	0.242	1	0.200	0.148
Characteristic path length	2.935	1.33	3.830	4.489
Connected components	2	7	1	2
Clustering coefficient	0.648	0	0.507	0.366

**Table 11.** Discrete parameters are reported for each network

When comparing networks in terms of global strength, the VEH/VEH network did not significantly differ from KET/VEH ( $p=0.547$ ), nor KET/VEH differed from KET/ASE ( $p=0.45$ ), whereas VEH/ASE exhibited a significantly reduced global strength compared to VEH/VEH ( $p= 0.049$ ).

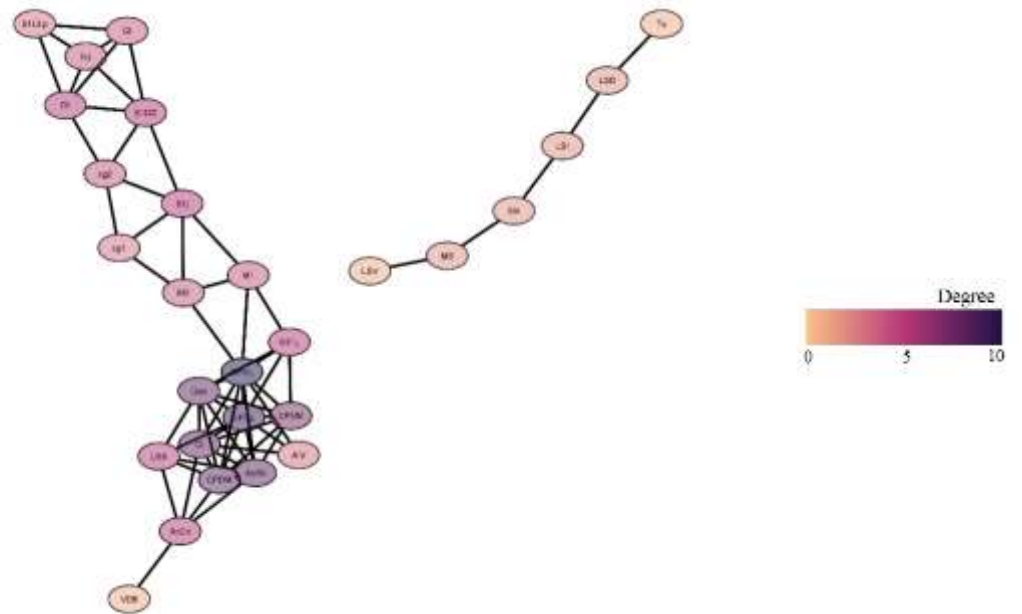


**Fig. 31.** VEH/VEH network. Nodes in the networks represent ROIs and edges reflect super threshold correlations ( $\alpha= 0.01$ ). The degree is reflected by the colour of the node, as reported in the legend.

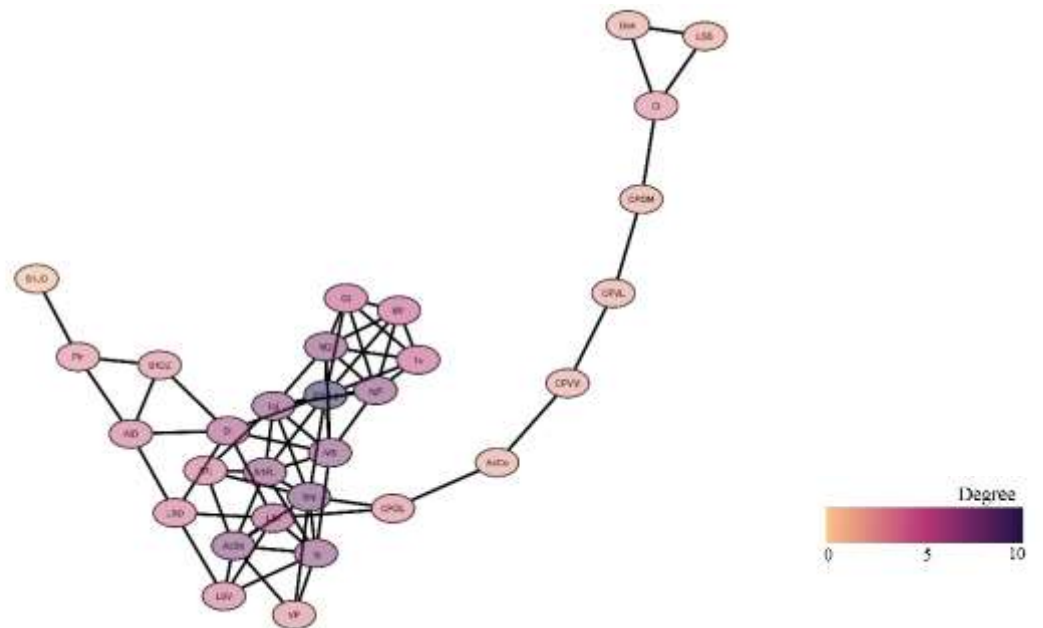


**Fig. 32.** KET/VEH network. Nodes in the networks represent ROIs and edges reflect super threshold correlations ( $\alpha= 0.01$ ). The degree is reflected by the colour of the node, as reported in the legend

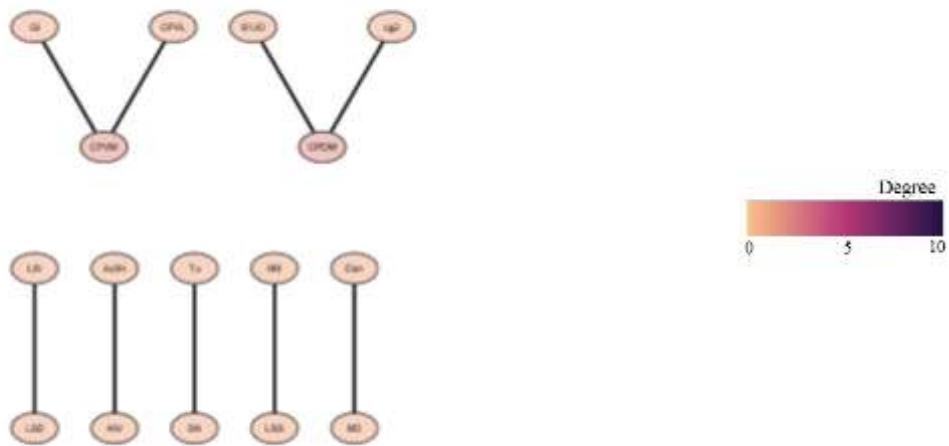


**Fig. 33.** VEH/ASE network. Nodes in the networks represent ROIs and edges reflect super threshold correlations ( $\alpha= 0.01$ ). The degree is reflected by the colour of the node, as reported in the legend.

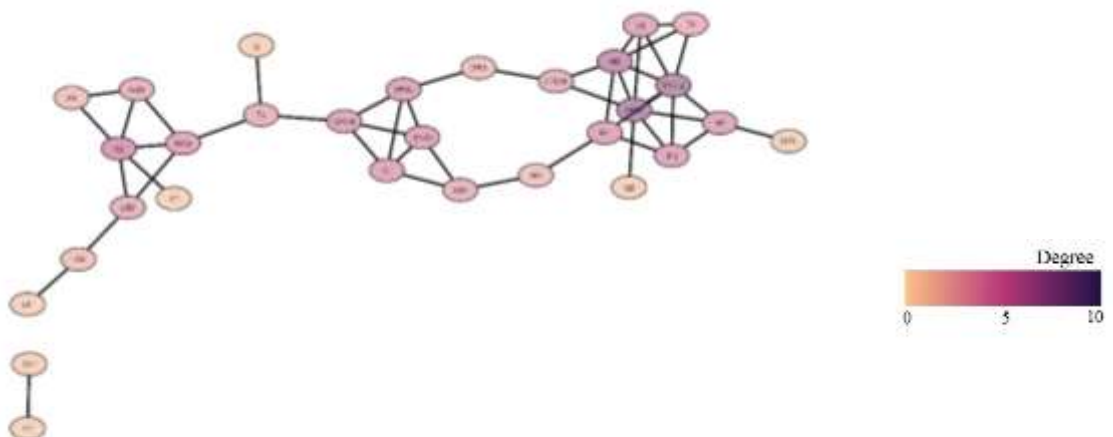


**Fig. 34.** KET/ASE network. Nodes in the networks represent ROIs and edges reflect super threshold correlations ( $\alpha= 0.01$ ). The degree is reflected by the colour of the node, as reported in the legend

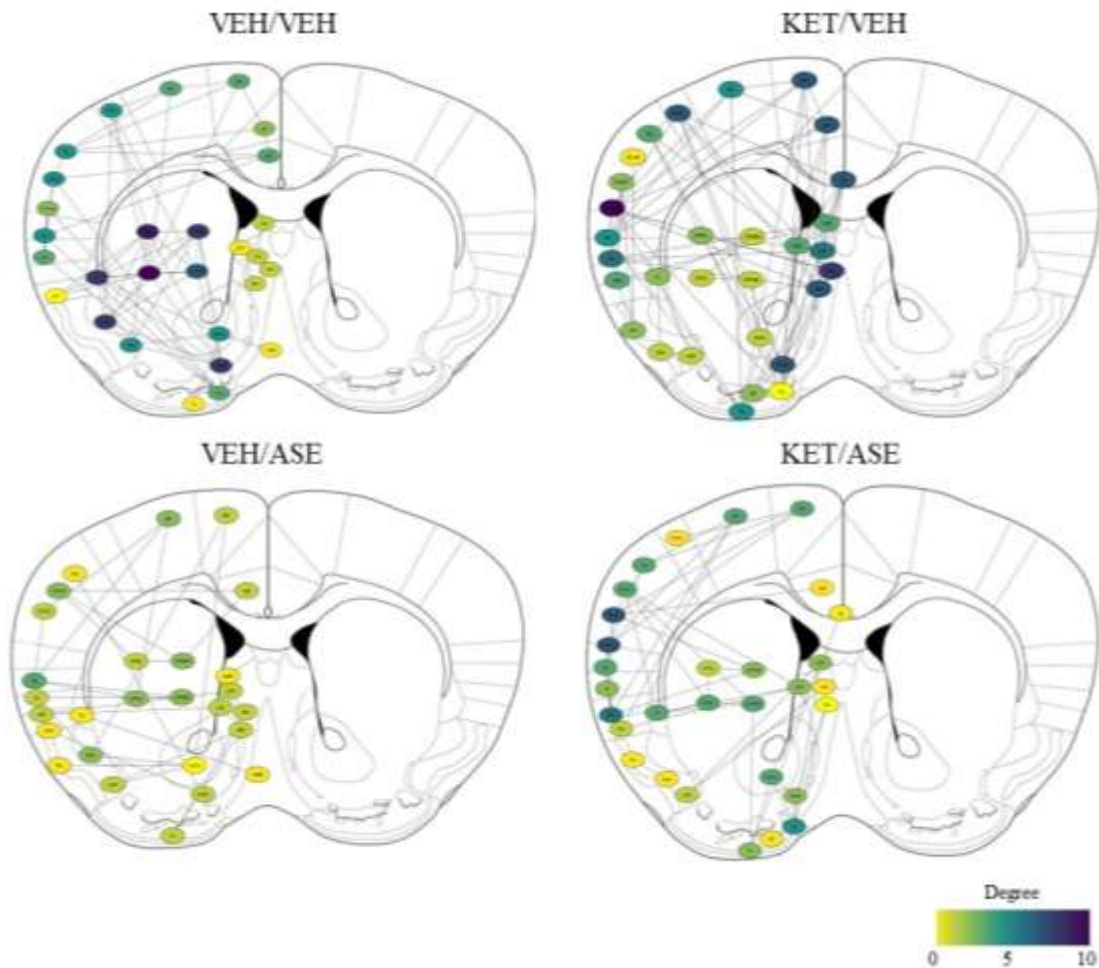


**Fig. 35.** Network construction and comparison. Nodes in the networks represent ROIs and edges reflect super threshold correlations ( $\alpha= 0.01$ ). The degree is reflected by the colour of the node, as reported in the legend.

When comparing the node centrality metrics between VEH/VEH and VEH/ASE networks, the degree was significantly different in Cl, CPDL, CPDM, CPVL, S1FL, Den, AIV, AcSh, while the betweenness differed only in cg2 and LSV. In particular, asenapine administration was associated with an increase in the betweenness of the cingulate cortex in this paradigm.

When comparing VEH/VEH and KET/VEH networks, the degree was not different among nodes, while betweenness was significantly lower in M2 and MS after acute ketamine challenge.

Finally, the betweenness of S1DZ, CPDM, LSV, Ig, Shi, Pir, and cg1 was significantly different between KET/VEH and KET/ASE networks, while no difference in degree was observed. In particular, the betweenness of cg1 and LSV was higher in KET/ASE network, while the betweenness of S1DZ, CPDM, Ig, Shi, and Pir was higher in KET/VEH network. Betweenness centrality of nodes is represented in Fig. 36, whereas comparisons are displayed in table 12.

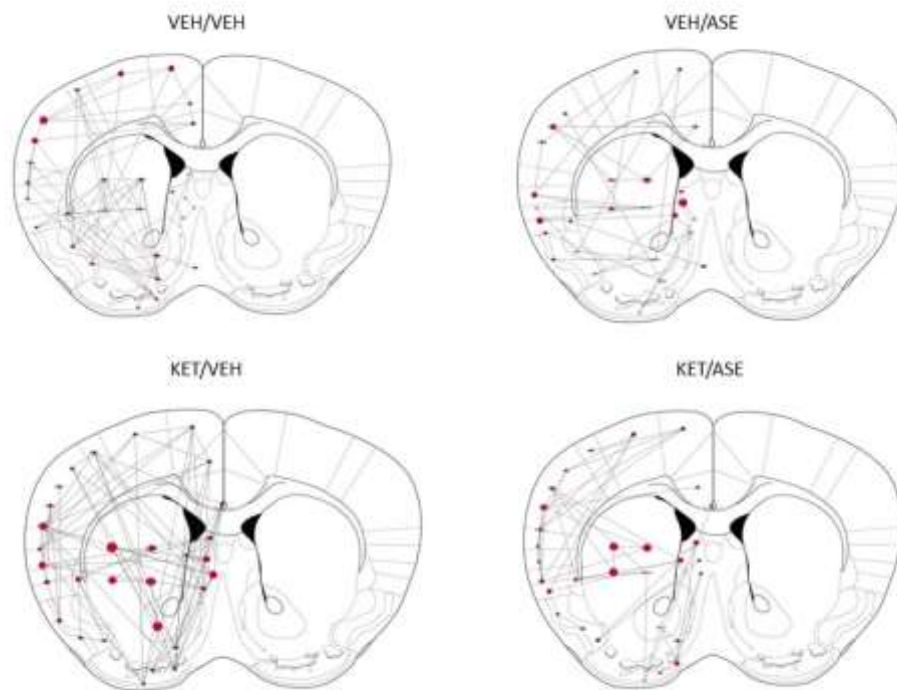


**Fig. 36.** The size of each node represents the measure of betweenness centrality in super threshold correlations ( $\alpha= 0.01$ ).

ROI	Betweenness		p- valu e	Betweenness		p- valu e	Betweenness		p- valu e
	VEH/VE H	VEH/AS E		VEH/VE H	KET/VE H		KET/VE H	KET/AS E	
Ig	16	6	1	16	6	0,07 4	6	0	<b>0,03 2</b>
cg2	6	12	<b>0,01 7</b>	6	6	0,11 8	6	0	0,71 2
cg1	4	4	0,08 8	4	6	0,15 4	6	10	<b>0,04 5</b>
M2	10	18	0,08 8	10	4	<b>0,02 2</b>	4	0	0,80 9
M1	6	28	0,81 2	6	24	0,18 8	24	0	0,82 3
S1FL	8	0	0,64	8	0	0,14 8	0	0	0,91 5
S1j	6	4	0,63 1	6	4	0,37	4	0	0,45 7
S1JO	0	6	0,08 6	0	2	1	2	22	0,25 5
S1DZ	0	10	1	0	8	0,47 4	8	0	<b>0,00 9</b>
S1UL p	0	34	0,93 8	0	0	0,13 8	0	0	0,09 9
Gl	0	2	0,61 7	0	6	1	6	0	0,47 9
DI	0	40	0,19 6	0	20	0,18 8	20	8	0,17 3
AID	10	0	1	10	16	0,24 1	16	0	0,41 4
AIV	28	10	0,69 2	28	10	0,24 5	10	4	0,83 8
CI	6	10	0,29 3	6	16	0,45 7	16	34	0,16 8
Pir	2	36	0,66 8	2	6	0,09 9	6	0	<b>0,04</b>
Den	2	18	0,58 2	2	10	0,26 2	10	0	0,37 8
LSS	0	14	0,34 4	0	12	0,86	12	8	0,42 7
CPD M	0	12	0,40 7	0	12	0,39	12	10	<b>0,00 9</b>
CPDL	0	26	0,08 9	0	82	0,15 9	82	74	0,05 6
CPVL	10	14	0,31 1	10	6	0,29	6	36	0,32 5
CPV M	0	2	0,45 9	0	0	0,19 6	0	32	0,41 4

AcCo	0	16	0,34 7	0	4	0,56 1	4	0	0,45 5
AcSh	0	12	0,49 7	0	0	0,62 9	0	0	0,54 5
LSD	0	6	0,38 6	0	0	0,35 4	0	0	0,10 2
LSI	0	10	0,19 2	0	18	0,78 4	18	12	0,06 7
LSV	20	16	<b>0,03</b> <b>1</b>	20	2	0,27 1	2	6	<b>0,01</b> <b>7</b>
Shi	22	12	0,66	22	6	0,73 3	6	0	<b>0,03</b> <b>5</b>
MS	40	28	0,45 5	40	14	<b>0,04</b> <b>2</b>	14	2	1
VDB	4	16	0,58 5	4	0	0,46 3	0	0	0,52 5
Icj	0	30	0,33 8	0	12	1	12	0	0,70 7
VP	0	22	0,59 6	0	2	0,47 3	2	0	0,36 7
Tu	0	0	0,62	0	12	1	12	0	0,5

**Table 12.** Comparisons between networks in terms of betweenness centrality.

## 5. Discussion

In the present experiment, we evaluated whether the expression of the IEG *Homer1a* in multiple cortical and subcortical ROIs was affected by the treatment with the second-generation antipsychotic ASE, administered alone in naïve (i.e., VEH-pre-treated) rats or KET-pre-treated rats. Based on previously published papers, acute KET administration is regarded as a valuable and heuristic preclinical model of psychosis (Buonaguro et al., 2017). It has been documented that KET treatment in humans (at dose levels comparable to those utilized in our investigation) causes behavioral and neurochemical effects mimicking psychosis, including the multifaceted symptom presentation (Iasevoli et al., 2014; Krystal et al., 1994).

In the current work, we did not observe a significant induction of *Homer1a* by acute KET administration. After normalization of data on values of *gcc*, a region that should not deliver signal intensity, *Homer1a* expression values in the KET/VEH group were even lower than in the control group, although the significance did not survive Bonferroni correction. These results differ from a previous report from our group, which instead found a dose-dependent increase in *Homer1a* levels after ketamine administration (Iasevoli et al., 2007). However, the inconsistency in findings could be attributable to the subsequent administration of saline after KET challenge and the wait of additional thirty minutes before animal sacrifice. Hence, it is possible that, after acute ketamine exposure, *Homer1a* transcript levels increased for 90 minutes and returned to approximately baseline values in 120 minutes. We may therefore have captured different moments of the *Homer1a* expression curve following the challenge with a NMDAR antagonist. In a previous work by Buonaguro et al., exploring the effects at a post-synaptic level of antipsychotics and minocycline both in a naturalistic context and after ketamine challenge, the Authors did not perform gene expression comparisons between groups receiving different pre-treatments, and comparisons were separately carried out between VEH pre-treated groups on one hand and KET pre-treated groups on the other (Buonaguro et al., 2017).

ASE administration in VEH-pretreated animals produced a region-specific pattern, inducing *Homer1a* only to a limited extent and never reaching significance. Again, after normalization, *Homer1a* values were higher in the *cg2* and *vp* in the control group than in the VEH/ASE group, although significance did not survive Bonferroni correction.

Lastly, the administration of ASE in an animal model of acute NMDAR dysfunction obtained by acute KET challenge was able to upregulate *Homer1a* almost in all the regions considered. In particular, significant differences survived in the medial septum, dorsolateral, dorsomedial, and ventrolateral caudate-putamen when multiple testing correction was taken into account. These findings are consistent with previous reports showing that asenapine only

mildly impacts cortical gene expression (de Bartolomeis et al., 2015). Asenapine relevant action in ketamine pre-treated rats, paralleled by the failure to detect an increase in Homer1a transcript levels in vehicle pre-treated rats, may indicate that antipsychotics preferentially deliver their effects in a context of altered glutamatergic functions much more than under physiological conditions.

It has been argued that the extent of Homer1a induction may be secondary to the degree of dopamine receptor blockade and the specific subtype (Iasevoli et al., 2009). Given the peculiar synergism of D1Rs and NMDARs, asenapine effects on Homer1a may depend on its action at D1R sites (Wirkner et al., 2004). Homer1a induction may also be triggered by 5-HT<sub>2A</sub> receptor antagonism, which positively affects glutamatergic transmission (Yuen et al., 2008). However, repeated asenapine exposure in animal models has been associated with 5-HT<sub>2A</sub> binding in the medial prefrontal cortex and dorsolateral frontal cortex but not in other brain regions (Tarazi et al., 2010). Moreover, striatal density of D1 receptors is high whereas that of 5-HT<sub>2A</sub> receptors is low, thus asenapine-induced striatal gene expression could be mainly driven by the action at D1R sites (Hall et al., 1994).

As it can be inferred from the observation of the correlation matrices, the topographical organization of the four functional networks (i.e., VEH/VEH, VEH/ASE, KET/VEH, KET/ASE) varied widely, with special attention paid to the link between the cortex and striatum. In the present experiment, we observed that the VEH/VEH network was characterized by stronger functional connections between the ventral insular cortex (AIV) and lateral caudate-putamen (CP\_VL and CP\_DL) compared to VEH/ASE network. Ventral caudate-putamen and insular regions has been involved in the assignment of emotional value and reward magnitude expectation (Duarte et al., 2020). The links between the somatosensory areas (S1FL and S1j) and AIV, Cl, and Den (the latter two ROIs belonging to the amygdala complex (Smith et al., 2019) are reduced in the VEH/ASE network. As well known, the insula receives sensory inputs from the somatosensory cortices relevant to pain sensitivity (Wylie and Tregellas, 2010). Antipsychotic ability to target discrete insular connections with striatal and somatosensorial regions might account for their effects on perception, motivation, and salience assignment.

Acute KET challenge in the KET/VEH group is associated with negative correlations between Indusium griseum (Ig) and remaining ROIs, which are not observed in other treatment groups. It is noteworthy that Ig has been described as a vestigial structure in humans and a remnant of the former part of the hippocampus in animals. Hippocampus is central in the neurobiology of psychotic disorders and the perturbation of functional connectivity within the hippocampus as well as its extrinsic connections have been deemed crucial for explaining

neuropsychological deficits of schizophrenia much more than psychotic symptoms (Harrison, 2004). However, only Ig correlation with LSI (part of the septal area, the anterior portion of the limbic system) was significantly weakened in the comparison between VEH/VEH and KET/VEH.

On the other hand, it should be noted that the KET/ASE group showed significantly higher inter-correlations between Ig and lateral putamen, the upper lip of the primary somatosensory cortex, septal area nuclei, and claustrum, in comparison to the KET/VEH group. Since brain sections were quantitated at the topographical level of the striatum, we were unable to directly investigate the connectivity of hippocampal regions. However, Ig behaves as a single functional and neuroanatomical unit together with the anterior continuation of the hippocampus (Laplante et al., 2013), a candidate region in the study of schizophrenia and a functional hub for multiple brain networks (Edmiston et al., 2020). Altered hippocampal-striatal coupling has been reported to be involved in deficits in associative learning tasks (Edmiston et al., 2020). In this context, it is noteworthy that ASE administration in KET-pretreated rats appears to reverse Pearson's  $r$  coefficient in Ig-caudate correlations.

Finally, we analyzed global strength and indices of centrality in each network and identified discrete nodes with enhanced centrality metrics. Although ASE does not directly recruit these regions by inducing Homer1a expression, it was able to increase the centrality of the cingulate cortex ROIs. The cingulate cortex has been reported to exert a pivotal role in regulating cognitive, sensorimotor, affective, and visceral functions (Margulies et al., 2007). The centrality of several brain regions, including olfactory, medial, and superior frontal regions, anterior cingulate, medial temporal pole, and superior occipital regions has been found reduced in functional connectomic studies conducted on schizophrenia patients (van den Heuvel, Martijn P. et al., 2010). We may therefore conceive that ASE ability to enhance the betweenness of Cg1 both in VEH- and KET-pretreated rats may contribute to its antipsychotic action.

KET/ASE group exhibited increased betweenness of the LSV compared to KET/VEH. Since lateral septal nuclei have been recently identified as critical hubs linking hippocampal and prefrontal activity with subcortical areas, participating in cognitive functions and motivated behaviors, this action may account for the beneficial impact on negative symptoms in psychosis (Besnard and Leroy, 2022).

In conclusion, we detected significant differences in nodes and edges measures across groups exposed to different treatments, highlighting asenapine capability to finely regulate brain connectivity by shaping synaptic architecture and restoring a functional pattern of interregional co-activation.

## **6. Limitations**

The major limitation of this study is the heterogeneity of the statistical methods applied for network analysis in the two experiments. However, network analysis is a recently introduced paradigm of exploration of functional connectivity, and the temporal distance between the two experiments allowed us to assess the suitability of the type of test to be conducted. While in the first experiment, which was published in the journal of Behavioral Brain Research, the analysis had a more qualitative nature, in the second experiment we preferred to adopt a quantitative analytic approach.

## 7. References

- Achard, S., Salvador, R., Whitcher, B., Suckling, J., Bullmore, E., 2006. A resilient, low-frequency, small-world human brain functional network with highly connected association cortical hubs. *The Journal of neuroscience : the official journal of the Society for Neuroscience* 26(1), 63-72. <https://doi.org/10.1523/jneurosci.3874-05.2006>
- Alexander-Bloch, A.F., Gogtay, N., Meunier, D., Birn, R., Clasen, L., Lalonde, F., Lenroot, R., Giedd, J., Bullmore, E.T., 2010. Disrupted modularity and local connectivity of brain functional networks in childhood-onset schizophrenia. *Frontiers in systems neuroscience* 4, 147. <https://doi.org/10.3389/fnsys.2010.00147>
- Ambesi-Impiombato, A., D'Urso, G., Muscettola, G., de Bartolomeis, A., 2003. Method for quantitative in situ hybridization histochemistry and image analysis applied for Homer1a gene expression in rat brain. *Brain research. Brain research protocols* 11(3), 189-196. [https://doi.org/10.1016/s1385-299x\(03\)00056-4](https://doi.org/10.1016/s1385-299x(03)00056-4)
- Ambesi-Impiombato, A., Panariello, F., Dell'aversano, C., Tomasetti, C., Muscettola, G., de Bartolomeis, A., 2007. Differential expression of Homer 1 gene by acute and chronic administration of antipsychotics and dopamine transporter inhibitors in the rat forebrain. *Synapse (New York, N.Y.)* 61(6), 429-439. <https://doi.org/10.1002/syn.20385>
- Ambesi-Impiombato, A., Panariello, F., Dell'aversano, C., Tomasetti, C., Muscettola, G., de Bartolomeis, A., 2007. Differential expression of Homer 1 gene by acute and chronic administration of antipsychotics and dopamine transporter inhibitors in the rat forebrain. *Synapse (New York, N.Y.)* 61(6), 429-439. <https://doi.org/https://doi.org/10.1002/syn.20385>
- Ango, F., Prézeau, L., Muller, T., Tu, J.C., Xiao, B., Worley, P.F., Pin, J.P., Bockaert, J., Fagni, L., 2001. Agonist-independent activation of metabotropic glutamate receptors by the intracellular protein Homer. *Nature* 411(6840), 962-965. <https://doi.org/10.1038/35082096>
- Bassett, D.S., Nelson, B.G., Mueller, B.A., Camchong, J., Lim, K.O., 2012. Altered resting state complexity in schizophrenia. *NeuroImage* 59(3), 2196-2207. <https://doi.org/10.1016/j.neuroimage.2011.10.002>
- Benes, F.M., Paskevich, P.A., Davidson, J., Domesick, V.B., 1985. The effects of haloperidol on synaptic patterns in the rat striatum. *Brain research* 329(1-2), 265-273. [https://doi.org/10.1016/0006-8993\(85\)90532-3](https://doi.org/10.1016/0006-8993(85)90532-3)
- Besnard, A., Leroy, F., 2022. Top-down regulation of motivated behaviors via lateral septum sub-circuits. *Molecular psychiatry*. <https://doi.org/10.1038/s41380-022-01599-3>
- Bockaert, J., Perroy, J., Ango, F., 2021. The Complex Formed by Group I Metabotropic Glutamate Receptor (mGluR) and Homer1a Plays a Central Role in Metaplasticity and Homeostatic Synaptic Scaling. *The Journal of neuroscience : the official journal of the Society for Neuroscience* 41(26), 5567-5578. <https://doi.org/10.1523/jneurosci.0026-21.2021>
- Bolding, M.S., White, D.M., Hadley, J.A., Weiler, M., Holcomb, H.H., Lahti, A.C., 2012. Antipsychotic Drugs Alter Functional Connectivity between the Medial Frontal Cortex, Hippocampus, and Nucleus Accumbens as Measured by H215O PET. *Frontiers in psychiatry* 3, 105. <https://doi.org/10.3389/fpsy.2012.00105>
- Briggman, K., Denk, W., 2006. Briggman, K. L. & Denk, W. Towards neural circuit reconstruction with volume electron microscopy techniques. *Curr. Opin. Neurobiol.* 16, 562-570. *Current opinion in neurobiology* 16, 562-570. <https://doi.org/10.1016/j.conb.2006.08.010>
- Bullmore, E., Vértes, P., 2013. From Lichtheim to Rich Club: Brain Networks and Psychiatry. *JAMA Psychiatry* 70(8), 780-782. <https://doi.org/10.1001/jamapsychiatry.2013.212> %J JAMA Psychiatry
- Buonaguro, E.F., Tomasetti, C., Chiodini, P., Marmo, F., Latte, G., Rossi, R., Avvisati, L., Iasevoli, F., de Bartolomeis, A., 2017. Postsynaptic density protein transcripts are differentially modulated by minocycline alone or in add-on to haloperidol: Implications for treatment

resistant schizophrenia. *Journal of psychopharmacology* (Oxford, England) 31(4), 406-417. <https://doi.org/10.1177/0269881116658987>

Cai, L., Wei, X., Liu, J., Zhu, L., Wang, J., Deng, B., Yu, H., Wang, R., 2020. Functional Integration and Segregation in Multiplex Brain Networks for Alzheimer's Disease. 14. <https://doi.org/10.3389/fnins.2020.00051>

Cao, M., Wang, Z., He, Y., 2015. Connectomics in psychiatric research: advances and applications. *Neuropsychiatric disease and treatment* 11, 2801-2810. <https://doi.org/10.2147/ndt.S63470>

Carmena, A., Granado, N., Ares Santos, S., Alberquilla, S., Tizabi, Y., Moratalla, R., 2014. Methamphetamine-Induced Toxicity in Indusium Griseum of Mice is Associated with Astro- and Microgliosis. *Neurotoxicity research* 27. <https://doi.org/10.1007/s12640-014-9505-9>

Chatterjee, M., Verma, R., Ganguly, S., Palit, G., 2012. Neurochemical and molecular characterization of ketamine-induced experimental psychosis model in mice. *Neuropharmacology* 63(6), 1161-1171. <https://doi.org/10.1016/j.neuropharm.2012.05.041>

Christoff, K., Gordon, A.M., Smallwood, J., Smith, R., Schooler, J.W., 2009. Experience sampling during fMRI reveals default network and executive system contributions to mind wandering. *Proceedings of the National Academy of Sciences* 106(21), 8719-8724. <https://doi.org/10.1073/pnas.0900234106>

Corlett, P.R., Honey, G.D., Fletcher, P.C., 2016. Prediction error, ketamine and psychosis: An updated model. *Journal of psychopharmacology* (Oxford, England) 30(11), 1145-1155. <https://doi.org/10.1177/0269881116650087>

Craig, A.D., 2009. How do you feel--now? The anterior insula and human awareness. *Nature reviews. Neuroscience* 10(1), 59-70. <https://doi.org/10.1038/nrn2555>

Dandash, O., Fornito, A., Lee, J., Keefe, R.S., Chee, M.W., Adcock, R.A., Pantelis, C., Wood, S.J., Harrison, B.J., 2014. Altered striatal functional connectivity in subjects with an at-risk mental state for psychosis. *Schizophrenia bulletin* 40(4), 904-913. <https://doi.org/10.1093/schbul/sbt093>

de Bartolomeis, A., Avagliano, C., Vellucci, L., D'Ambrosio, L., Manchia, M., D'Urso, G., Buonaguro, E.F., Iasevoli, F., 2019. Translating preclinical findings in clinically relevant new antipsychotic targets: focus on the glutamatergic postsynaptic density. Implications for treatment resistant schizophrenia. *Neuroscience and biobehavioral reviews* 107, 795-827. <https://doi.org/10.1016/j.neubiorev.2019.08.019>

de Bartolomeis, A., Barone, A., Buonaguro, E.F., Tomasetti, C., Vellucci, L., Iasevoli, F., 2022a. The Homer1 family of proteins at the crossroad of dopamine-glutamate signaling: An emerging molecular "Lego" in the pathophysiology of psychiatric disorders. A systematic review and translational insight. *Neuroscience and biobehavioral reviews* 136, 104596. <https://doi.org/10.1016/j.neubiorev.2022.104596>

de Bartolomeis, A., Barone, A., Vellucci, L., Mazza, B., Austin, M.C., Iasevoli, F., Ciccarelli, M., 2022b. Linking Inflammation, Aberrant Glutamate-Dopamine Interaction, and Post-synaptic Changes: Translational Relevance for Schizophrenia and Antipsychotic Treatment: a Systematic Review. *Molecular neurobiology*. <https://doi.org/10.1007/s12035-022-02976-3>

de Bartolomeis, A., Buonaguro, E.F., Iasevoli, F., 2013. Serotonin-glutamate and serotonin-dopamine reciprocal interactions as putative molecular targets for novel antipsychotic treatments: from receptor heterodimers to postsynaptic scaffolding and effector proteins. *Psychopharmacology* 225(1), 1-19. <https://doi.org/10.1007/s00213-012-2921-8>

de Bartolomeis, A., Fiore, G., 2004. Postsynaptic density scaffolding proteins at excitatory synapse and disorders of synaptic plasticity: implications for human behavior pathologies. *International review of neurobiology* 59, 221-254. [https://doi.org/10.1016/s0074-7742\(04\)59009-8](https://doi.org/10.1016/s0074-7742(04)59009-8)

de Bartolomeis, A., Iasevoli, F., Marmo, F., Buonaguro, E.F., Eramo, A., Rossi, R., Avvisati, L., Latte, G., Tomasetti, C., 2015. Progressive recruitment of cortical and striatal regions by

inducible postsynaptic density transcripts after increasing doses of antipsychotics with different receptor profiles: insights for psychosis treatment. *European neuropsychopharmacology : the journal of the European College of Neuropsychopharmacology* 25(4), 566-582. <https://doi.org/10.1016/j.euroneuro.2015.01.003>

de Bartolomeis, A., Latte, G., Tomasetti, C., Iasevoli, F., 2014. Glutamatergic postsynaptic density protein dysfunctions in synaptic plasticity and dendritic spines morphology: relevance to schizophrenia and other behavioral disorders pathophysiology, and implications for novel therapeutic approaches. *Molecular neurobiology* 49(1), 484-511. <https://doi.org/10.1007/s12035-013-8534-3>

Deng, M., Liu, Z., Shen, Y., Cao, H., Zhang, M., Xi, C., Zhang, W., Tan, W., Zhang, J., Chen, E., Lee, E., Pu, W., 2022. Treatment Effect of Long-Term Antipsychotics on Default-Mode Network Dysfunction in Drug-Naïve Patients With First-Episode Schizophrenia: A Longitudinal Study. *Frontiers in pharmacology* 13, 833518. <https://doi.org/10.3389/fphar.2022.833518>

Devlin, B., Kelsoe, J.R., Sklar, P., Daly, M.J., O'Donovan, M.C., Craddock, N., Kendler, K.S., A Weiss, L., Wray, N.R.J.N.n., 2015. Psychiatric genome-wide association study analyses implicate neuronal, immune and histone pathways. 18(2), 199-209.

Dold, M., Samara, M.T., Li, C., Tardy, M., Leucht, S., 2015. Haloperidol versus first-generation antipsychotics for the treatment of schizophrenia and other psychotic disorders. *The Cochrane database of systematic reviews* 1, Cd009831. <https://doi.org/10.1002/14651858.CD009831.pub2>

Duarte, I.C., Coelho, G., Brito-Costa, S., Cayolla, R., Afonso, S., Castelo-Branco, M., 2020. Ventral Caudate and Anterior Insula Recruitment During Value Estimation of Passionate Rewarding Cues. *Frontiers in neuroscience* 14, 678. <https://doi.org/10.3389/fnins.2020.00678>

Edmiston, E.K., Song, Y., Chang, M., Yin, Z., Zhou, Q., Zhou, Y., Jiang, X., Wei, S., Xu, K., Tang, Y., Wang, F., 2020. Hippocampal Resting State Functional Connectivity in Patients With Schizophrenia and Unaffected Family Members. *Frontiers in psychiatry* 11, 278. <https://doi.org/10.3389/fpsy.2020.00278>

Eggers, A.E., 2013. A serotonin hypothesis of schizophrenia. *Medical Hypotheses* 80(6), 791-794. <https://doi.org/https://doi.org/10.1016/j.mehy.2013.03.013>

Felleman, D.J., Van Essen, D.C., 1991. Distributed hierarchical processing in the primate cerebral cortex. *Cerebral cortex (New York, N.Y. : 1991)* 1(1), 1-47. <https://doi.org/10.1093/cercor/1.1.1-a>

Fornito, A., Bullmore, E.T., 2015. Reconciling abnormalities of brain network structure and function in schizophrenia. *Curr Opin Neurobiol* 30, 44-50. <https://doi.org/10.1016/j.conb.2014.08.006>

Fornito, A., Harrison, B.J., Goodby, E., Dean, A., Ooi, C., Nathan, P.J., Lennox, B.R., Jones, P.B., Suckling, J., Bullmore, E.T., 2013. Functional dysconnectivity of corticostriatal circuitry as a risk phenotype for psychosis. *JAMA Psychiatry* 70(11), 1143-1151. <https://doi.org/10.1001/jamapsychiatry.2013.1976>

Fornito, A.Z., A; Bullmore ET, 2016. Chapter 1 - An Introduction to Brain Networks, in: Fornito, A., Zalesky, A., Bullmore, E.T. (Eds.), *Fundamentals of Brain Network Analysis*. Academic Press, San Diego, pp. 1-35.

Fuzik, J., Rehman, S., Girach, F., Miklosi, A.G., Korchynska, S., Arque, G., Romanov, R.A., Hanics, J., Wagner, L., Meletis, K., Yanagawa, Y., Kovacs, G.G., Alpár, A., Hökfelt, T.G.M., Harkany, T., 2019. Brain-wide genetic mapping identifies the indusium griseum as a prenatal target of pharmacologically unrelated psychostimulants. *Proceedings of the National Academy of Sciences of the United States of America* 116(51), 25958-25967. <https://doi.org/10.1073/pnas.1904006116>

Gass, N., Schwarz, A.J., Sartorius, A., Cleppien, D., Zheng, L., Schenker, E., Risterucci, C., Meyer-Lindenberg, A., Weber-Fahr, W., 2013. Haloperidol modulates midbrain-prefrontal

functional connectivity in the rat brain. *European neuropsychopharmacology : the journal of the European College of Neuropsychopharmacology* 23(10), 1310-1319. <https://doi.org/10.1016/j.euroneuro.2012.10.013>

Gilks, W.P., Allott, E.H., Donohoe, G., Cummings, E., Gill, M., Corvin, A.P., Morris, D.W., 2010. Replicated genetic evidence supports a role for HOMER2 in schizophrenia. *Neuroscience letters* 468(3), 229-233. <https://doi.org/10.1016/j.neulet.2009.11.003>

Gogolla, N., Takesian, A.E., Feng, G., Fagiolini, M., Hensch, T.K., 2014. Sensory integration in mouse insular cortex reflects GABA circuit maturation. *Neuron* 83(4), 894-905. <https://doi.org/10.1016/j.neuron.2014.06.033>

Gold, M.G., 2012. A frontier in the understanding of synaptic plasticity: Solving the structure of the postsynaptic density. 34(7), 599-608. <https://doi.org/https://doi.org/10.1002/bies.201200009>

Grabrucker, A.M., Schmeisser, M.J., Schoen, M., Boeckers, T.M., 2011. Postsynaptic ProSAP/Shank scaffolds in the cross-hair of synaptopathies. *Trends in cell biology* 21(10), 594-603. <https://doi.org/10.1016/j.tcb.2011.07.003>

Hadley, J.A., Kraguljac, N.V., White, D.M., Ver Hoef, L., Tabora, J., Lahti, A.C., 2016. Change in brain network topology as a function of treatment response in schizophrenia: a longitudinal resting-state fMRI study using graph theory. *NPJ schizophrenia* 2, 16014. <https://doi.org/10.1038/npjischz.2016.14>

Hadley, J.A., Nenert, R., Kraguljac, N.V., Bolding, M.S., White, D.M., Skidmore, F.M., Visscher, K.M., Lahti, A.C., 2014. Ventral tegmental area/midbrain functional connectivity and response to antipsychotic medication in schizophrenia. *Neuropsychopharmacology : official publication of the American College of Neuropsychopharmacology* 39(4), 1020-1030. <https://doi.org/10.1038/npp.2013.305>

Hall, H., Sedvall, G., Magnusson, O., Kopp, J., Halldin, C., Farde, L., 1994. Distribution of D1- and D2-dopamine receptors, and dopamine and its metabolites in the human brain. *Neuropsychopharmacology : official publication of the American College of Neuropsychopharmacology* 11(4), 245-256. <https://doi.org/10.1038/sj.npp.1380111>

Harrison, P.J., 2004. The hippocampus in schizophrenia: a review of the neuropathological evidence and its pathophysiological implications. *Psychopharmacology* 174(1), 151-162. <https://doi.org/10.1007/s00213-003-1761-y>

Hu, B., 2018. *The SAGE Encyclopedia of Educational Research, Measurement, and Evaluation*. SAGE Publications, Inc., Thousand Oaks  
Thousand Oaks,, California.

Iasevoli, F., Buonaguro, E.F., Avagliano, C., Barone, A., Eramo, A., Vellucci, L., de Bartolomeis, A., 2020. The Effects of Antipsychotics on the Synaptic Plasticity Gene Homer1a Depend on a Combination of Their Receptor Profile, Dose, Duration of Treatment, and Brain Regions Targeted. *International journal of molecular sciences* 21(15). <https://doi.org/10.3390/ijms21155555>

Iasevoli, F., Buonaguro, E.F., Sarappa, C., Marmo, F., Latte, G., Rossi, R., Eramo, A., Tomasetti, C., de Bartolomeis, A., 2014. Regulation of postsynaptic plasticity genes' expression and topography by sustained dopamine perturbation and modulation by acute memantine: relevance to schizophrenia. *Progress in neuro-psychopharmacology & biological psychiatry* 54, 299-314. <https://doi.org/10.1016/j.pnpbp.2014.07.003>

Iasevoli, F., Fiore, G., Cicale, M., Muscettola, G., de Bartolomeis, A., 2010a. Haloperidol induces higher Homer1a expression than risperidone, olanzapine and sulpiride in striatal sub-regions. *Psychiatry research* 177(1-2), 255-260. <https://doi.org/10.1016/j.psychres.2010.02.009>

Iasevoli, F., Polese, D., Ambesi-Impiombato, A., Muscettola, G., de Bartolomeis, A., 2007. Ketamine-related expression of glutamatergic postsynaptic density genes: Possible implications in psychosis. *Neuroscience letters* 416(1), 1-5. <https://doi.org/https://doi.org/10.1016/j.neulet.2007.01.041>

Iasevoli, F., Tomasetti, C., Ambesi-Impiombato, A., Muscettola, G., de Bartolomeis, A., 2009. Dopamine receptor subtypes contribution to Homer1a induction: insights into antipsychotic molecular action. *Progress in neuro-psychopharmacology & biological psychiatry* 33(5), 813-821. <https://doi.org/10.1016/j.pnpbp.2009.02.009>

Iasevoli, F., Tomasetti, C., Marmo, F., Bravi, D., Arnt, J., de Bartolomeis, A., 2010b. Divergent acute and chronic modulation of glutamatergic postsynaptic density genes expression by the antipsychotics haloperidol and sertindole. *Psychopharmacology* 212(3), 329-344. <https://doi.org/10.1007/s00213-010-1954-0>

Inoue, Y., Udo, H., Inokuchi, K., Sugiyama, H., 2007. Homer1a regulates the activity-induced remodeling of synaptic structures in cultured hippocampal neurons. *Neuroscience* 150(4), 841-852. <https://doi.org/10.1016/j.neuroscience.2007.09.081>

Irons, T.D., Kelly, P.E., Hunter, D.L., Macphail, R.C., Padilla, S., 2013. Acute administration of dopaminergic drugs has differential effects on locomotion in larval zebrafish. *Pharmacology, biochemistry, and behavior* 103(4), 792-813. <https://doi.org/10.1016/j.pbb.2012.12.010>

Jiang, Y., Yao, D., Zhou, J., Tan, Y., Huang, H., Wang, M., Chang, X., Duan, M., Luo, C., 2022. Characteristics of disrupted topological organization in white matter functional connectome in schizophrenia. *Psychological Medicine* 52(7), 1333-1343. <https://doi.org/10.1017/S0033291720003141>

Joyce, K.E., Laurienti, P.J., Burdette, J.H., Hayasaka, S., 2010. A New Measure of Centrality for Brain Networks. *PLOS ONE* 5(8), e12200. <https://doi.org/10.1371/journal.pone.0012200>

Kapur, S., Agid, O., Mizrahi, R., Li, M., 2006. How antipsychotics work-from receptors to reality. *NeuroRx : the journal of the American Society for Experimental NeuroTherapeutics* 3(1), 10-21. <https://doi.org/10.1016/j.nurx.2005.12.003>

Kapur, S., Arenovich, T., Agid, O., Zipursky, R., Lindborg, S., Jones, B., 2005. Evidence for Onset of Antipsychotic Effects Within the First 24 Hours of Treatment. *American Journal of Psychiatry* 162(5), 939-946. <https://doi.org/10.1176/appi.ajp.162.5.939>

Kennedy, M.B., 2000. Signal-processing machines at the postsynaptic density. *Science (New York, N.Y.)* 290(5492), 750-754. <https://doi.org/10.1126/science.290.5492.750>

Kokkinou, M., Ashok, A.H., Howes, O.D., 2018. The effects of ketamine on dopaminergic function: meta-analysis and review of the implications for neuropsychiatric disorders. *Molecular psychiatry* 23(1), 59-69. <https://doi.org/10.1038/mp.2017.190>

Konradi, C., Heckers, S., 2001. Antipsychotic drugs and neuroplasticity: insights into the treatment and neurobiology of schizophrenia. *Biological psychiatry* 50(10), 729-742. [https://doi.org/10.1016/s0006-3223\(01\)01267-7](https://doi.org/10.1016/s0006-3223(01)01267-7)

Krystal, J.H., Karper, L.P., Seibyl, J.P., Freeman, G.K., Delaney, R., Bremner, J.D., Heninger, G.R., Bowers, M.B., Jr., Charney, D.S., 1994. Subanesthetic Effects of the Noncompetitive NMDA Antagonist, Ketamine, in Humans: Psychotomimetic, Perceptual, Cognitive, and Neuroendocrine Responses. *Archives of General Psychiatry* 51(3), 199-214. <https://doi.org/10.1001/archpsyc.1994.03950030035004>

Kusumi, I., Boku, S., Takahashi, Y., 2015. Psychopharmacology of atypical antipsychotic drugs: From the receptor binding profile to neuroprotection and neurogenesis. 69(5), 243-258. <https://doi.org/https://doi.org/10.1111/pcn.12242>

Laplante, F., Mnie-Filali, O., Sullivan, R.M., 2013. A neuroanatomical and neurochemical study of the indusium griseum and anterior hippocampal continuation: comparison with dentate gyrus. *Journal of chemical neuroanatomy* 50-51, 39-47. <https://doi.org/10.1016/j.jchemneu.2013.03.004>

Levitt, J.J., Nestor, P.G., Kubicki, M., Lyall, A.E., Zhang, F., Riklin-Raviv, T., LJ, O.D., McCarley, R.W., Shenton, M.E., Rathi, Y., 2020. Miswiring of Frontostriatal Projections in Schizophrenia. *Schizophrenia bulletin* 46(4), 990-998. <https://doi.org/10.1093/schbul/sbz129>

Livet, J., Weissman, T.A., Kang, H., Draft, R.W., Lu, J., Bennis, R.A., Sanes, J.R., Lichtman, J.W., 2007. Transgenic strategies for combinatorial expression of fluorescent proteins in the nervous system. *Nature* 450(7166), 56-62. <https://doi.org/10.1038/nature06293>

Lo, C.Y., Su, T.W., Huang, C.C., Hung, C.C., Chen, W.L., Lan, T.H., Lin, C.P., Bullmore, E.T., 2015. Randomization and resilience of brain functional networks as systems-level endophenotypes of schizophrenia. *Proceedings of the National Academy of Sciences of the United States of America* 112(29), 9123-9128. <https://doi.org/10.1073/pnas.1502052112>

Lynall, M.E., Bassett, D.S., Kerwin, R., McKenna, P.J., Kitzbichler, M., Muller, U., Bullmore, E., 2010. Functional connectivity and brain networks in schizophrenia. *The Journal of neuroscience : the official journal of the Society for Neuroscience* 30(28), 9477-9487. <https://doi.org/10.1523/jneurosci.0333-10.2010>

Majercikova, Z., Kiss, A., 2016. Stress alters asenapine-induced Fos expression in the Meynert's nucleus: response of adjacent hypocretin and melanin-concentrating hormone neurons in rat. *Neurological research* 38(1), 32-39. <https://doi.org/10.1080/01616412.2015.1105585>

Margulies, D.S., Kelly, A.M.C., Uddin, L.Q., Biswal, B.B., Castellanos, F.X., Milham, M.P., 2007. Mapping the functional connectivity of anterior cingulate cortex. *NeuroImage* 37(2), 579-588. <https://doi.org/https://doi.org/10.1016/j.neuroimage.2007.05.019>

McCutcheon, R.A., Abi-Dargham, A., Howes, O.D., 2019. Schizophrenia, Dopamine and the Striatum: From Biology to Symptoms. *Trends in neurosciences* 42(3), 205-220. <https://doi.org/https://doi.org/10.1016/j.tins.2018.12.004>

McHugh, M.L., 2012. Interrater reliability: the kappa statistic. *Biochemia medica* 22(3), 276-282.

Menon, V., Uddin, L.Q., 2010. Saliency, switching, attention and control: a network model of insula function. *Brain structure & function* 214(5-6), 655-667. <https://doi.org/10.1007/s00429-010-0262-0>

Murakoshi, H., Yasuda, R., 2012. Postsynaptic signaling during plasticity of dendritic spines. *Trends in neurosciences* 35(2), 135-143. <https://doi.org/10.1016/j.tins.2011.12.002>

Narr, K.L., Leaver, A.M., 2015. Connectome and schizophrenia. *Current opinion in psychiatry* 28(3), 229-235. <https://doi.org/10.1097/ycp.0000000000000157>

Neill, J.C., Barnes, S., Cook, S., Grayson, B., Idris, N.F., McLean, S.L., Snigdha, S., Rajagopal, L., Harte, M.K., 2010. Animal models of cognitive dysfunction and negative symptoms of schizophrenia: focus on NMDA receptor antagonism. *Pharmacology & therapeutics* 128(3), 419-432. <https://doi.org/10.1016/j.pharmthera.2010.07.004>

Ohyama, M., Kondo, M., Yamauchi, M., Imanishi, T., Koyama, T., 2016. Asenapine reduces anxiety-related behaviours in rat conditioned fear stress model. *Acta neuropsychiatrica* 28(6), 327-336. <https://doi.org/10.1017/neu.2016.17>

Park, D.K., Petshow, S., Anisimova, M., Barragan, E.V., Gray, J.A., Stein, I.S., Zito, K., 2022. Reduced d-serine levels drive enhanced non-ionotropic NMDA receptor signaling and destabilization of dendritic spines in a mouse model for studying schizophrenia. *Neurobiology of disease* 170, 105772. <https://doi.org/10.1016/j.nbd.2022.105772>

Park, S.H., Song, Y.S., Moon, B.S., Lee, B.C., Park, H.S., Kim, S.E., 2019. Combination of In Vivo [(123)I]FP-CIT SPECT and Microdialysis Reveals an Antipsychotic Drug Haloperidol-induced Synaptic Dopamine Availability in the Rat Midbrain and Striatum. *Experimental neurobiology* 28(5), 602-611. <https://doi.org/10.5607/en.2019.28.5.602>

Park, S.W., Seo, M.K., McIntyre, R.S., Mansur, R.B., Lee, Y., Lee, J.H., Park, S.C., Huh, L., Lee, J.G., 2018. Effects of olanzapine and haloperidol on mTORC1 signaling, dendritic outgrowth, and synaptic proteins in rat primary hippocampal neurons under toxic conditions. *Neuroscience letters* 686, 59-66. <https://doi.org/10.1016/j.neulet.2018.08.031>

Paxinos, G., Watson, C.R., Emson, P.C.J.J.o.n.m., 1980. AChE-stained horizontal sections of the rat brain in stereotaxic coordinates. 3(2), 129-149.

Power, J.D., Schlaggar, B.L., Lessov-Schlaggar, C.N., Petersen, S.E., 2013. Evidence for hubs in human functional brain networks. *Neuron* 79(4), 798-813. <https://doi.org/10.1016/j.neuron.2013.07.035>

Rubinov, M., Bullmore, E., 2013. Schizophrenia and abnormal brain network hubs. *Dialogues in clinical neuroscience* 15(3), 339-349. <https://doi.org/10.31887/DCNS.2013.15.3/mrubinov>

Sakaori, F., 2002. Permutation test for equality of correlation coefficients in two populations. *Communications in Statistics-simulation and Computation - COMMUN STATIST-SIMULAT COMPUT* 31, 641-651. <https://doi.org/10.1081/SAC-120004317>

Sapienza, J., Bosia, M., Spangaro, M., Martini, F., Agostoni, G., Cuoco, F., Cocchi, F., Cavallaro, R., 2022. Schizophrenia and psychedelic state: Dysconnection versus hyperconnection. A perspective on two different models of psychosis stemming from dysfunctional integration processes. *Molecular psychiatry*. <https://doi.org/10.1038/s41380-022-01721-5>

Scardoni, G., Laudanna, C.J.N.f.i.g.t., 2012. Centralities based analysis of complex networks. 323-348.

Schwarz, A.J., McGonigle, J., 2011. Negative edges and soft thresholding in complex network analysis of resting state functional connectivity data. *NeuroImage* 55(3), 1132-1146. <https://doi.org/10.1016/j.neuroimage.2010.12.047>

Seeley, W.W., Menon, V., Schatzberg, A.F., Keller, J., Glover, G.H., Kenna, H., Reiss, A.L., Greicius, M.D., 2007. Dissociable intrinsic connectivity networks for salience processing and executive control. *The Journal of neuroscience : the official journal of the Society for Neuroscience* 27(9), 2349-2356. <https://doi.org/10.1523/jneurosci.5587-06.2007>

Shahid, M., Walker, G.B., Zorn, S.H., Wong, E.H., 2009. Asenapine: a novel psychopharmacologic agent with a unique human receptor signature. *Journal of psychopharmacology (Oxford, England)* 23(1), 65-73. <https://doi.org/10.1177/0269881107082944>

Shiraishi-Yamaguchi, Y., Furuichi, T., 2007. The Homer family proteins. *Genome Biology* 8(2), 206. <https://doi.org/10.1186/gb-2007-8-2-206>

Smith, J.B., Alloway, K.D., Hof, P.R., Orman, R., Reser, D.H., Watakabe, A., Watson, G.D.R., 2019. The relationship between the claustrum and endopiriform nucleus: A perspective towards consensus on cross-species homology. *The Journal of comparative neurology* 527(2), 476-499. <https://doi.org/10.1002/cne.24537>

Spellmann, I., Rujescu, D., Musil, R., Mayr, A., Giegling, I., Genius, J., Zill, P., Dehning, S., Opgen-Rhein, M., Ceroveck, A., Hartmann, A.M., Schäfer, M., Bondy, B., Müller, N., Möller, H.J., Riedel, M., 2011. Homer-1 polymorphisms are associated with psychopathology and response to treatment in schizophrenic patients. *Journal of psychiatric research* 45(2), 234-241. <https://doi.org/10.1016/j.jpsychires.2010.06.004>

Sporns, O., Tononi, G., Kötter, R., 2005. The human connectome: A structural description of the human brain. *PLoS computational biology* 1(4), e42. <https://doi.org/10.1371/journal.pcbi.0010042>

Stahl, S.M., 2018. Beyond the dopamine hypothesis of schizophrenia to three neural networks of psychosis: dopamine, serotonin, and glutamate. *CNS spectrums* 23(3), 187-191. <https://doi.org/10.1017/s1092852918001013>

Stanley, M.L., Simpson, S.L., Dagenbach, D., Lyday, R.G., Burdette, J.H., Laurienti, P.J., 2015. Changes in brain network efficiency and working memory performance in aging. *PLoS One* 10(4), e0123950. <https://doi.org/10.1371/journal.pone.0123950>

Stephan, K.E., Baldeweg, T., Friston, K.J., 2006. Synaptic plasticity and dysconnection in schizophrenia. *Biological psychiatry* 59(10), 929-939. <https://doi.org/10.1016/j.biopsych.2005.10.005>

Stephan, K.E., Friston, K.J., Frith, C.D., 2009. Dysconnection in schizophrenia: from abnormal synaptic plasticity to failures of self-monitoring. *Schizophrenia bulletin* 35(3), 509-527. <https://doi.org/10.1093/schbul/sbn176>

Szumliński, K.K., Kalivas, P.W., Worley, P.F., 2006. Homer proteins: implications for neuropsychiatric disorders. *Current Opinion in Neurobiology* 16(3), 251-257. <https://doi.org/https://doi.org/10.1016/j.conb.2006.05.002>

Tarazi, F.I., Moran-Gates, T., Wong, E.H., Henry, B., Shahid, M., 2010. Asenapine induces differential regional effects on serotonin receptor subtypes. *Journal of psychopharmacology (Oxford, England)* 24(3), 341-348. <https://doi.org/10.1177/0269881108095704>

Tomasetti, C., Dell'Aversano, C., Iasevoli, F., de Bartolomeis, A., 2007. Homer splice variants modulation within cortico-subcortical regions by dopamine D2 antagonists, a partial agonist, and an indirect agonist: implication for glutamatergic postsynaptic density in antipsychotics action. *Neuroscience* 150(1), 144-158. <https://doi.org/10.1016/j.neuroscience.2007.08.022>

Tomasetti, C., Dell'Aversano, C., Iasevoli, F., Marmo, F., de Bartolomeis, A., 2011. The acute and chronic effects of combined antipsychotic-mood stabilizing treatment on the expression of cortical and striatal postsynaptic density genes. *Progress in neuro-psychopharmacology & biological psychiatry* 35(1), 184-197. <https://doi.org/10.1016/j.pnpbp.2010.10.025>

Tomasetti, C., Iasevoli, F., Buonaguro, E.F., De Berardis, D., Fornaro, M., Fiengo, A.L., Martinotti, G., Orsolini, L., Valchera, A., Di Giannantonio, M., de Bartolomeis, A., 2017. Treating the Synapse in Major Psychiatric Disorders: The Role of Postsynaptic Density Network in Dopamine-Glutamate Interplay and Psychopharmacologic Drugs Molecular Actions. *International journal of molecular sciences* 18(1). <https://doi.org/10.3390/ijms18010135>

Tsai, P.J., Keeley, R.J., Carmack, S.A., Vendruscolo, J.C.M., Lu, H., Gu, H., Vendruscolo, L.F., Koob, G.F., Lin, C.P., Stein, E.A., Yang, Y., 2020. Converging Structural and Functional Evidence for a Rat Salience Network. *Biological psychiatry* 88(11), 867-878. <https://doi.org/10.1016/j.biopsych.2020.06.023>

van den Heuvel, M.P., Mandl, R.C., Stam, C.J., Kahn, R.S., Hulshoff Pol, H.E., 2010. Aberrant frontal and temporal complex network structure in schizophrenia: a graph theoretical analysis. *The Journal of neuroscience : the official journal of the Society for Neuroscience* 30(47), 15915-15926. <https://doi.org/10.1523/jneurosci.2874-10.2010>

van den Heuvel, M.P., Mandl, R.C.W., Stam, C.J., Kahn, R.S., Hulshoff Pol, H.E., 2010. Aberrant Frontal and Temporal Complex Network Structure in Schizophrenia: A Graph Theoretical Analysis. *The Journal of Neuroscience* 30(47), 15915. <https://doi.org/10.1523/JNEUROSCI.2874-10.2010>

van den Heuvel, M.P., Sporns, O., Collin, G., Scheewe, T., Mandl, R.C., Cahn, W., Goñi, J., Hulshoff Pol, H.E., Kahn, R.S., 2013. Abnormal rich club organization and functional brain dynamics in schizophrenia. *JAMA Psychiatry* 70(8), 783-792. <https://doi.org/10.1001/jamapsychiatry.2013.1328>

van den Heuvel, M.P., Stam, C.J., Boersma, M., Hulshoff Pol, H.E., 2008. Small-world and scale-free organization of voxel-based resting-state functional connectivity in the human brain. *NeuroImage* 43(3), 528-539. <https://doi.org/10.1016/j.neuroimage.2008.08.010>

Wang, Q., Su, T.-P., Zhou, Y., Chou, K.-H., Chen, I.Y., Jiang, T., Lin, C.-P., 2012. Anatomical insights into disrupted small-world networks in schizophrenia. *NeuroImage* 59(2), 1085-1093. <https://doi.org/https://doi.org/10.1016/j.neuroimage.2011.09.035>

Wheeler, A.L., Creed, M.C., Voineskos, A.N., Nobrega, J.N., 2014. Changes in brain functional connectivity after chronic haloperidol in rats: a network analysis. *The international journal of neuropsychopharmacology* 17(8), 1129-1138. <https://doi.org/10.1017/s1461145714000042>

White, J.G., Southgate, E., Thomson, J.N., Brenner, S., 1986. The structure of the nervous system of the nematode *Caenorhabditis elegans*. *Philosophical transactions of the Royal Society of London. Series B, Biological sciences* 314(1165), 1-340. <https://doi.org/10.1098/rstb.1986.0056>

- Wiedemann, D.J., Garris, P.A., Near, J.A., Wightman, R.M., 1992. Effect of chronic haloperidol treatment on stimulated synaptic overflow of dopamine in the rat striatum. *The Journal of pharmacology and experimental therapeutics* 261(2), 574-579.
- Wiley, J.L., 2008. Antipsychotic-induced suppression of locomotion in juvenile, adolescent and adult rats. *European journal of pharmacology* 578(2-3), 216-221. <https://doi.org/10.1016/j.ejphar.2007.09.010>
- Wirkner, K., Krause, T., Köles, L., Thümmler, S., Al-Khrasani, M., Illes, P., 2004. D1 but not D2 dopamine receptors or adrenoceptors mediate dopamine-induced potentiation of N-methyl-D-aspartate currents in the rat prefrontal cortex. *Neuroscience letters* 372(1-2), 89-93. <https://doi.org/10.1016/j.neulet.2004.09.015>
- Wylie, K.P., Tregellas, J.R., 2010. The role of the insula in schizophrenia. *Schizophrenia research* 123(2-3), 93-104. <https://doi.org/10.1016/j.schres.2010.08.027>
- Yuen, E.Y., Jiang, Q., Chen, P., Feng, J., Yan, Z., 2008. Activation of 5-HT<sub>2A/C</sub> receptors counteracts 5-HT<sub>1A</sub> regulation of n-methyl-D-aspartate receptor channels in pyramidal neurons of prefrontal cortex. *The Journal of biological chemistry* 283(25), 17194-17204. <https://doi.org/10.1074/jbc.M801713200>
- Zhan, L., Jenkins, L.M., Wolfson, O.E., GadElkarim, J.J., Nocito, K., Thompson, P.M., Ajilore, O.A., Chung, M.K., Leow, A.D., 2017. The significance of negative correlations in brain connectivity. *The Journal of comparative neurology* 525(15), 3251-3265. <https://doi.org/10.1002/cne.24274>
- Zhang, J., Xu, T.X., Hallett, P.J., Watanabe, M., Grant, S.G., Isacson, O., Yao, W.D., 2009. PSD-95 uncouples dopamine-glutamate interaction in the D1/PSD-95/NMDA receptor complex. *The Journal of neuroscience : the official journal of the Society for Neuroscience* 29(9), 2948-2960. <https://doi.org/10.1523/jneurosci.4424-08.2009>

## 8. Acknowledgements

I would like to thank my PhD and residency tutors, Professors Andrea de Bartolomeis and Felice Iasevoli, as well as the people who helped make this project possible, Dr. Giuseppe De Simone, Dr. Mariateresa Ciccarelli, and Dr. Licia Vellucci, which are colleagues and life mates. I also thank my family and my friends who have supported me over these years. Finally, I feel so grateful for the amazing time spent in the Rione Sanità, that gave me birth for the second time, for the immense and unexpected love I found here.

## 9. Supplementary material

ROI	ROI	Pearson's <i>r</i>	p-value	ROI	ROI	Pearson's <i>r</i>	p-value
lg	cg2	0.884	<b>0.047</b>	cg2	GI	0.869	0.056
lg	cg1	0.921	<b>0.026</b>	cg1	GI	0.798	0.106
cg2	cg1	0.983	<b>0.003</b>	M2	GI	0.725	0.166
lg	M2	0.842	0.074	M1	GI	0.700	0.188
cg2	M2	0.915	<b>0.029</b>	S1FL	GI	0.663	0.223
cg1	M2	0.964	<b>0.008</b>	S1j	GI	0.847	0.070
lg	M1	0.756	0.139	S1JO	GI	0.213	0.731
cg2	M1	0.831	0.081	S1DZ	GI	0.953	<b>0.012</b>
cg1	M1	0.898	<b>0.039</b>	S1ULp	GI	0.993	<b>0.001</b>
M2	M1	0.974	<b>0.005</b>	lg	DI	0.732	0.160
lg	S1FL	0.590	0.295	cg2	DI	0.962	<b>0.009</b>
cg2	S1FL	0.750	0.144	cg1	DI	0.905	<b>0.035</b>
cg1	S1FL	0.811	0.096	M2	DI	0.827	0.084
M2	S1FL	0.928	<b>0.023</b>	M1	DI	0.751	0.143
M1	S1FL	0.968	<b>0.007</b>	S1FL	DI	0.710	0.179
lg	S1j	0.811	0.096	S1j	DI	0.907	<b>0.034</b>
cg2	S1j	0.948	<b>0.014</b>	S1JO	DI	0.434	0.466
cg1	S1j	0.967	<b>0.007</b>	S1DZ	DI	0.979	<b>0.004</b>
M2	S1j	0.980	<b>0.003</b>	S1ULp	DI	0.961	<b>0.009</b>
M1	S1j	0.959	<b>0.010</b>	GI	DI	0.954	<b>0.012</b>
S1FL	S1j	0.916	<b>0.029</b>	lg	AID	0.518	0.371
lg	S1JO	0.167	0.788	cg2	AID	0.823	0.087
cg2	S1JO	0.396	0.509	cg1	AID	0.805	0.101
cg1	S1JO	0.344	0.571	M2	AID	0.848	0.069
M2	S1JO	0.313	0.608	M1	AID	0.857	0.063
M1	S1JO	0.148	0.812	S1FL	AID	0.903	<b>0.036</b>
S1FL	S1JO	0.252	0.683	S1j	AID	0.915	<b>0.029</b>
S1j	S1JO	0.290	0.636	S1JO	AID	0.361	0.550
lg	S1DZ	0.797	0.106	S1DZ	AID	0.893	<b>0.041</b>
cg2	S1DZ	0.973	<b>0.005</b>	S1ULp	AID	0.838	0.076
cg1	S1DZ	0.943	<b>0.016</b>	GI	AID	0.883	0.047
M2	S1DZ	0.887	<b>0.045</b>	DI	AID	0.884	<b>0.046</b>
M1	S1DZ	0.843	0.073	lg	AIV	0.723	0.168
S1FL	S1DZ	0.778	0.121	cg2	AIV	0.843	0.073
S1j	S1DZ	0.956	<b>0.011</b>	cg1	AIV	0.885	<b>0.046</b>
S1JO	S1DZ	0.279	0.649	M2	AIV	0.933	<b>0.021</b>
lg	S1ULp	0.614	0.271	M1	AIV	0.864	0.059
cg2	S1ULp	0.873	0.053	S1FL	AIV	0.875	0.052
cg1	S1ULp	0.788	0.113	S1j	AIV	0.886	<b>0.045</b>
M2	S1ULp	0.687	0.200	S1JO	AIV	0.611	0.274
M1	S1ULp	0.639	0.246	S1DZ	AIV	0.770	0.128

S1FL	S1ULp	0.591	0.294
S1j	S1ULp	0.812	0.095
S1JO	S1ULp	0.261	0.671
S1DZ	S1ULp	0.942	<b>0.017</b>
Ig	GI	0.604	0.281
cg1	CI	0.773	0.125
M2	CI	0.893	<b>0.041</b>
M1	CI	0.877	0.051
S1FL	CI	0.929	<b>0.023</b>
S1j	CI	0.828	0.084
S1JO	CI	0.505	0.385
S1DZ	CI	0.649	0.236
S1ULp	CI	0.416	0.486
GI	CI	0.469	0.426
DI	CI	0.617	0.267
AID	CI	0.780	0.120
AIV	CI	0.959	<b>0.010</b>
Ig	Pir	0.522	0.367
cg2	Pir	0.399	0.506
cg1	Pir	0.551	0.336
M2	Pir	0.715	0.174
M1	Pir	0.746	0.148
S1FL	Pir	0.745	0.149
S1j	Pir	0.574	0.311
S1JO	Pir	0.146	0.814
S1DZ	Pir	0.315	0.606
S1ULp	Pir	-0.011	0.986
GI	Pir	0.058	0.926
DI	Pir	0.208	0.737
AID	Pir	0.398	0.507
AIV	Pir	0.729	0.162
CI	Pir	0.841	0.074
Ig	Den	0.531	0.357
cg2	Den	0.724	0.167
cg1	Den	0.780	0.120
M2	Den	0.903	<b>0.036</b>
M1	Den	0.926	<b>0.024</b>
S1FL	Den	0.987	<b>0.002</b>
S1j	Den	0.884	<b>0.047</b>
S1JO	Den	0.384	0.523
S1DZ	Den	0.737	0.155
S1ULp	Den	0.554	0.333
GI	Den	0.620	0.264
DI	Den	0.695	0.193
AID	Den	0.899	<b>0.038</b>
AIV	Den	0.907	<b>0.033</b>

S1ULp	AIV	0.567	0.318
GI	AIV	0.590	0.295
DI	AIV	0.766	0.131
AID	AIV	0.798	0.105
Ig	CI	0.579	0.307
M1	LSS	0.835	0.078
S1FL	LSS	0.940	<b>0.017</b>
S1j	LSS	0.811	0.095
S1JO	LSS	0.499	0.392
S1DZ	LSS	0.674	0.213
S1ULp	LSS	0.527	0.362
GI	LSS	0.589	0.297
DI	LSS	0.665	0.221
AID	LSS	0.895	<b>0.040</b>
AIV	LSS	0.880	<b>0.049</b>
CI	LSS	0.941	<b>0.017</b>
Pir	LSS	0.661	0.225
Den	LSS	0.980	<b>0.003</b>
Ig	CPDM	0.475	0.418
cg2	CPDM	0.606	0.279
cg1	CPDM	0.689	0.198
M2	CPDM	0.839	0.075
M1	CPDM	0.847	0.070
S1FL	CPDM	0.923	<b>0.025</b>
S1j	CPDM	0.770	0.128
S1JO	CPDM	0.467	0.428
S1DZ	CPDM	0.570	0.316
S1ULp	CPDM	0.336	0.580
GI	CPDM	0.401	0.504
DI	CPDM	0.533	0.355
AID	CPDM	0.754	0.141
AIV	CPDM	0.913	<b>0.031</b>
CI	CPDM	0.991	<b>0.001</b>
Pir	CPDM	0.855	0.065
Den	CPDM	0.961	<b>0.009</b>
LSS	CPDM	0.950	<b>0.013</b>
Ig	CPDL	0.612	0.273
cg2	CPDL	0.759	0.137
cg1	CPDL	0.823	0.087
M2	CPDL	0.933	<b>0.021</b>
M1	CPDL	0.931	<b>0.021</b>
S1FL	CPDL	0.973	<b>0.005</b>
S1j	CPDL	0.893	<b>0.041</b>
S1JO	CPDL	0.435	0.464
S1DZ	CPDL	0.739	0.154
S1ULp	CPDL	0.528	0.360

Cl	Den	0.962	<b>0.009</b>
Pir	Den	0.744	0.149
Ig	LSS	0.394	0.512
cg2	LSS	0.655	0.230
cg1	LSS	0.691	0.196
M2	LSS	0.821	0.089
Den	CPDL	0.989	<b>0.001</b>
LSS	CPDL	0.958	<b>0.010</b>
CPDM	CPDL	0.974	<b>0.005</b>
Ig	CPVL	0.695	0.192
cg2	CPVL	0.802	0.103
cg1	CPVL	0.870	0.055
M2	CPVL	0.965	<b>0.008</b>
M1	CPVL	0.959	<b>0.010</b>
S1FL	CPVL	0.971	<b>0.006</b>
S1j	CPVL	0.922	<b>0.026</b>
S1JO	CPVL	0.386	0.521
S1DZ	CPVL	0.774	0.124
S1ULp	CPVL	0.551	0.336
GI	CPVL	0.605	0.280
DI	CPVL	0.720	0.170
AID	CPVL	0.845	0.072
AIV	CPVL	0.958	<b>0.010</b>
Cl	CPVL	0.976	<b>0.004</b>
Pir	CPVL	0.811	0.096
Den	CPVL	0.973	<b>0.005</b>
LSS	CPVL	0.921	<b>0.027</b>
CPDM	CPVL	0.952	<b>0.012</b>
CPDL	CPVL	0.993	<b>0.001</b>
Ig	CPVM	0.605	0.280
cg2	CPVM	0.675	0.211
cg1	CPVM	0.771	0.127
M2	CPVM	0.909	<b>0.033</b>
M1	CPVM	0.930	<b>0.022</b>
S1FL	CPVM	0.958	<b>0.010</b>
S1j	CPVM	0.841	0.074
S1JO	CPVM	0.314	0.607
S1DZ	CPVM	0.646	0.239
S1ULp	CPVM	0.392	0.514
GI	CPVM	0.461	0.435
DI	CPVM	0.574	0.312
AID	CPVM	0.765	0.132
AIV	CPVM	0.909	<b>0.033</b>
Cl	CPVM	0.978	<b>0.004</b>
Pir	CPVM	0.894	<b>0.041</b>
Den	CPVM	0.962	<b>0.009</b>

GI	CPDL	0.585	0.300
DI	CPDL	0.698	0.190
AID	CPDL	0.859	0.062
AIV	CPDL	0.953	<b>0.012</b>
Cl	CPDL	0.988	<b>0.002</b>
Pir	CPDL	0.796	0.107
M2	AcCo	0.761	0.135
M1	AcCo	0.782	0.118
S1FL	AcCo	0.892	<b>0.042</b>
S1j	AcCo	0.695	0.193
S1JO	AcCo	0.479	0.415
S1DZ	AcCo	0.487	0.405
S1ULp	AcCo	0.273	0.657
GI	AcCo	0.342	0.573
DI	AcCo	0.462	0.434
AID	AcCo	0.731	0.161
AIV	AcCo	0.859	0.062
Cl	AcCo	0.963	<b>0.008</b>
Pir	AcCo	0.817	0.092
Den	AcCo	0.942	<b>0.017</b>
LSS	AcCo	0.955	<b>0.011</b>
CPDM	AcCo	0.989	<b>0.001</b>
CPDL	AcCo	0.942	<b>0.017</b>
CPVL	AcCo	0.904	<b>0.035</b>
CPVM	AcCo	0.941	<b>0.017</b>
Ig	AcSh	0.452	0.444
cg2	AcSh	0.627	0.257
cg1	AcSh	0.695	0.193
M2	AcSh	0.838	0.076
M1	AcSh	0.842	0.073
S1FL	AcSh	0.930	<b>0.022</b>
S1j	AcSh	0.785	0.116
S1JO	AcSh	0.507	0.383
S1DZ	AcSh	0.604	0.281
S1ULp	AcSh	0.396	0.509
GI	AcSh	0.458	0.438
DI	AcSh	0.581	0.304
AID	AcSh	0.801	0.103
AIV	AcSh	0.917	<b>0.028</b>
Cl	AcSh	0.987	<b>0.002</b>
Pir	AcSh	0.798	0.105
Den	AcSh	0.973	<b>0.005</b>
LSS	AcSh	0.975	<b>0.005</b>
CPDM	AcSh	0.995	<b>&lt;0.001</b>
CPDL	AcSh	0.978	<b>0.004</b>
CPVL	AcSh	0.949	<b>0.014</b>

LSS	CPVM	0.909	<b>0.032</b>
CPDM	CPVM	0.976	<b>0.005</b>
CPDL	CPVM	0.980	<b>0.003</b>
CPVL	CPVM	0.981	<b>0.003</b>
lg	AcCo	0.343	0.572
cg2	AcCo	0.509	0.381
cg1	AcCo	0.589	0.296
S1FL	LSD	0.218	0.724
S1j	LSD	0.420	0.482
S1JO	LSD	0.571	0.314
S1DZ	LSD	0.389	0.518
S1ULp	LSD	0.213	0.730
GI	LSD	0.153	0.805
DI	LSD	0.421	0.480
AID	LSD	0.130	0.835
AIV	LSD	0.625	0.260
CI	LSD	0.450	0.448
Pir	LSD	0.420	0.481
Den	LSD	0.250	0.685
LSS	LSD	0.191	0.759
CPDM	LSD	0.348	0.565
CPDL	LSD	0.384	0.523
CPVL	LSD	0.439	0.459
CPVM	LSD	0.369	0.542
AcCo	LSD	0.246	0.690
AcSh	LSD	0.319	0.601
lg	LSI	0.842	0.074
cg2	LSI	0.786	0.115
cg1	LSI	0.778	0.121
M2	LSI	0.650	0.235
M1	LSI	0.468	0.426
S1FL	LSI	0.353	0.560
S1j	LSI	0.607	0.278
S1JO	LSI	0.599	0.285
S1DZ	LSI	0.628	0.257
S1ULp	LSI	0.499	0.392
GI	LSI	0.441	0.458
DI	LSI	0.668	0.217
AID	LSI	0.363	0.548
AIV	LSI	0.715	0.175
CI	LSI	0.507	0.383
Pir	LSI	0.340	0.575
Den	LSI	0.372	0.538
LSS	LSI	0.316	0.605
CPDM	LSI	0.391	0.515
CPDL	LSI	0.483	0.410

CPVM	AcSh	0.961	<b>0.009</b>
AcCo	AcSh	0.990	<b>0.001</b>
lg	LSD	0.750	0.144
cg2	LSD	0.591	0.293
cg1	LSD	0.618	0.267
M2	LSD	0.516	0.374
M1	LSD	0.332	0.585
M2	LSV	0.699	0.189
M1	LSV	0.548	0.339
S1FL	LSV	0.520	0.369
S1j	LSV	0.600	0.285
S1JO	LSV	0.740	0.153
S1DZ	LSV	0.499	0.392
S1ULp	LSV	0.288	0.638
GI	LSV	0.262	0.670
DI	LSV	0.536	0.352
AID	LSV	0.410	0.493
AIV	LSV	0.859	0.062
CI	LSV	0.754	0.141
Pir	LSV	0.630	0.255
Den	LSV	0.581	0.304
LSS	LSV	0.559	0.327
CPDM	LSV	0.684	0.202
CPDL	LSV	0.687	0.200
CPVL	LSV	0.707	0.182
CPVM	LSV	0.659	0.227
AcCo	LSV	0.615	0.270
AcSh	LSV	0.668	0.218
LSD	LSV	0.908	<b>0.033</b>
LSI	LSV	0.889	<b>0.044</b>
lg	Shi	0.830	0.082
cg2	Shi	0.890	<b>0.043</b>
cg1	Shi	0.882	<b>0.048</b>
M2	Shi	0.803	0.102
M1	Shi	0.648	0.237
S1FL	Shi	0.586	0.299
S1j	Shi	0.776	0.123
S1JO	Shi	0.687	0.200
S1DZ	Shi	0.768	0.129
S1ULp	Shi	0.634	0.251
GI	Shi	0.599	0.286
DI	Shi	0.810	0.097
AID	Shi	0.611	0.274
AIV	Shi	0.877	0.051
CI	Shi	0.708	0.181
Pir	Shi	0.445	0.453

CPVL	LSI	0.538	0.349
CPVM	LSI	0.423	0.478
AcCo	LSI	0.282	0.646
AcSh	LSI	0.386	0.522
LSD	LSI	0.952	<b>0.012</b>
Ig	LSV	0.698	0.190
cg2	LSV	0.674	0.212
cg1	LSV	0.715	0.174
AcSh	Shi	0.619	0.265
LSD	Shi	0.856	0.064
LSI	Shi	0.953	<b>0.012</b>
LSV	Shi	0.916	<b>0.029</b>
Ig	MS	0.758	0.137
cg2	MS	0.824	0.087
cg1	MS	0.844	0.073
M2	MS	0.822	0.087
M1	MS	0.686	0.201
S1FL	MS	0.664	0.222
S1j	MS	0.765	0.132
S1JO	MS	0.740	0.153
S1DZ	MS	0.693	0.195
S1ULp	MS	0.513	0.377
GI	MS	0.496	0.396
DI	MS	0.728	0.163
AID	MS	0.621	0.264
AIV	MS	0.941	<b>0.017</b>
CI	MS	0.826	0.085
Pir	MS	0.598	0.287
Den	MS	0.713	0.176
LSS	MS	0.693	0.195
CPDM	MS	0.752	0.143
CPDL	MS	0.795	0.108
CPVL	MS	0.812	0.095
CPVM	MS	0.736	0.156
AcCo	MS	0.681	0.206
AcSh	MS	0.754	0.141
LSD	MS	0.832	0.081
LSI	MS	0.890	<b>0.043</b>
LSV	MS	0.966	<b>0.007</b>
Shi	MS	0.971	<b>0.006</b>
Ig	VDB	0.237	0.701
cg2	VDB	0.381	0.527
cg1	VDB	0.456	0.441
M2	VDB	0.615	0.270
M1	VDB	0.592	0.293
S1FL	VDB	0.722	0.168

Den	Shi	0.616	0.269
LSS	Shi	0.581	0.304
CPDM	Shi	0.610	0.275
CPDL	Shi	0.699	0.189
CPVL	Shi	0.732	0.160
CPVM	Shi	0.619	0.265
AcCo	Shi	0.520	0.370
AcSh	Shi	0.619	0.265
Pir	VDB	0.770	0.128
Den	VDB	0.812	0.095
LSS	VDB	0.858	0.063
CPDM	VDB	0.928	<b>0.023</b>
CPDL	VDB	0.836	0.077
CPVL	VDB	0.787	0.114
CPVM	VDB	0.832	0.081
AcCo	VDB	0.950	<b>0.013</b>
AcSh	VDB	0.925	<b>0.025</b>
LSD	VDB	0.362	0.549
LSI	VDB	0.336	0.581
LSV	VDB	0.709	0.180
Shi	VDB	0.533	0.355
MS	VDB	0.714	0.176
Ig	Icj	0.785	0.116
cg2	Icj	0.930	<b>0.022</b>
cg1	Icj	0.885	<b>0.046</b>
M2	Icj	0.792	0.111
M1	Icj	0.752	0.143
S1FL	Icj	0.653	0.232
S1j	Icj	0.883	0.047
S1JO	Icj	0.134	0.830
S1DZ	Icj	0.976	<b>0.004</b>
S1ULp	Icj	0.960	<b>0.009</b>
GI	Icj	0.962	<b>0.009</b>
DI	Icj	0.947	<b>0.014</b>
AID	Icj	0.806	0.099
AIV	Icj	0.620	0.264
CI	Icj	0.475	0.419
Pir	Icj	0.162	0.795
Den	Icj	0.588	0.297
LSS	Icj	0.508	0.382
CPDM	Icj	0.387	0.520
CPDL	Icj	0.584	0.301
CPVL	Icj	0.633	0.251
CPVM	Icj	0.491	0.401
AcCo	Icj	0.295	0.630
AcSh	Icj	0.422	0.479

S1j	VDB	0.520	0.370
S1JO	VDB	0.655	0.230
S1DZ	VDB	0.306	0.617
S1ULp	VDB	0.095	0.880
GI	VDB	0.141	0.821
DI	VDB	0.323	0.596
AID	VDB	0.553	0.333
AIV	VDB	0.813	0.094
CI	VDB	0.902	<b>0.036</b>
M2	VP	0.609	0.276
M1	VP	0.719	0.171
S1FL	VP	0.824	0.086
S1j	VP	0.534	0.353
S1JO	VP	0.086	0.890
S1DZ	VP	0.287	0.640
S1ULp	VP	0.058	0.927
GI	VP	0.162	0.795
DI	VP	0.194	0.754
AID	VP	0.575	0.311
AIV	VP	0.617	0.268
CI	VP	0.813	0.094
Pir	VP	0.840	0.075
Den	VP	0.835	0.079
LSS	VP	0.816	0.092
CPDM	VP	0.878	<b>0.050</b>
CPDL	VP	0.806	0.100
CPVL	VP	0.772	0.126
CPVM	VP	0.869	0.056
AcCo	VP	0.905	<b>0.035</b>
AcSh	VP	0.858	0.063
LSD	VP	-0.057	0.927
LSI	VP	-0.061	0.922
LSV	VP	0.301	0.622
Shi	VP	0.169	0.785
MS	VP	0.353	0.560
VDB	VP	0.796	0.107
lcj	VP	0.124	0.843
lg	Tu	0.766	0.131
cg2	Tu	0.498	0.394
cg1	Tu	0.552	0.335
M2	Tu	0.456	0.440
M1	Tu	0.300	0.624
S1FL	Tu	0.144	0.817
S1j	Tu	0.341	0.574
S1JO	Tu	0.347	0.567
S1DZ	Tu	0.294	0.632

LSD	lcj	0.325	0.594
LSI	lcj	0.579	0.306
LSV	lcj	0.360	0.552
Shi	lcj	0.680	0.206
MS	lcj	0.561	0.325
VDB	lcj	0.092	0.883
lg	VP	0.172	0.781
cg2	VP	0.258	0.675
cg1	VP	0.378	0.531
CPDL	Tu	0.287	0.640
CPVL	Tu	0.362	0.550
CPVM	Tu	0.316	0.604
AcCo	Tu	0.138	0.825
AcSh	Tu	0.203	0.744
LSD	Tu	0.965	<b>0.008</b>
LSI	Tu	0.878	<b>0.050</b>
LSV	Tu	0.812	0.095
Shi	Tu	0.736	0.156
MS	Tu	0.706	0.182
VDB	Tu	0.234	0.705
lcj	Tu	0.258	0.676
VP	Tu	-0.077	0.902

S1ULp	Tu	0.088	0.888
GI	Tu	0.036	0.954
DI	Tu	0.283	0.645
AID	Tu	-0.014	0.982
AIV	Tu	0.506	0.385
CI	Tu	0.351	0.562
Pir	Tu	0.457	0.439
Den	Tu	0.145	0.816
LSS	Tu	0.046	0.941
CPDM	Tu	0.254	0.681

**Supplementary table 1.** Results of Pearson's r correlations in VEH/VEH rats. Correlation coefficients and p-values for all possible pairs. Significant values were given in bold.

ROI	ROI	Pearson's r	p-value
lg	cg2	0.482	0.411
lg	cg1	0.319	0.601
cg2	cg1	0.276	0.654
lg	M2	-0.394	0.512
cg2	M2	0.057	0.927
cg1	M2	0.514	0.376
lg	M1	-0.591	0.294
cg2	M1	0.371	0.539
cg1	M1	-0.195	0.753
M2	M1	0.534	0.354
lg	S1FL	-0.163	0.794
cg2	S1FL	0.270	0.661
cg1	S1FL	0.403	0.501
M2	S1FL	-0.025	0.968
M1	S1FL	0.122	0.845
lg	S1j	-0.513	0.377
cg2	S1j	-0.753	0.142
cg1	S1j	0.224	0.717
M2	S1j	0.126	0.840
M1	S1j	-0.296	0.628
S1FL	S1j	0.379	0.529
lg	S1JO	-0.383	0.524
cg2	S1JO	-0.925	<b>0.025</b>
cg1	S1JO	-0.386	0.521
M2	S1JO	-0.390	0.517
M1	S1JO	-0.481	0.412
S1FL	S1JO	-0.069	0.912
S1j	S1JO	0.740	0.153

ROI	ROI	Pearson's r	p-value
M1	GI	-0.923	<b>0.025</b>
S1FL	GI	0.227	0.714
S1j	GI	0.363	0.548
S1JO	GI	0.484	0.408
S1DZ	GI	0.938	<b>0.018</b>
S1ULp	GI	0.804	0.101
lg	DI	0.301	0.623
cg2	DI	-0.151	0.809
cg1	DI	-0.162	0.795
M2	DI	-0.872	0.054
M1	DI	-0.644	0.241
S1FL	DI	0.408	0.495
S1j	DI	0.267	0.664
S1JO	DI	0.498	0.393
S1DZ	DI	0.695	0.193
S1ULp	DI	0.773	0.125
GI	DI	0.865	0.058
lg	AID	-0.185	0.766
cg2	AID	0.390	0.517
cg1	AID	-0.446	0.452
M2	AID	-0.477	0.417
M1	AID	0.396	0.510
S1FL	AID	0.554	0.332
S1j	AID	-0.213	0.731
S1JO	AID	-0.092	0.882
S1DZ	AID	-0.216	0.727
S1ULp	AID	0.260	0.673
GI	AID	-0.057	0.927

lg	S1DZ	0.735	0.157
cg2	S1DZ	-0.030	0.962
cg1	S1DZ	0.420	0.481
M2	S1DZ	-0.510	0.380
M1	S1DZ	-0.917	<b>0.028</b>
S1FL	S1DZ	0.173	0.781
S1j	S1DZ	0.182	0.769
S1JO	S1DZ	0.199	0.748
lg	S1ULp	0.619	0.266
cg2	S1ULp	0.309	0.613
cg1	S1ULp	0.425	0.476
M2	S1ULp	-0.532	0.357
M1	S1ULp	-0.592	0.293
S1FL	S1ULp	0.603	0.282
S1j	S1ULp	0.089	0.887
S1JO	S1ULp	-0.031	0.961
S1DZ	S1ULp	0.846	0.071
lg	GI	0.518	0.371
cg2	GI	-0.256	0.678
cg1	GI	0.182	0.770
M2	GI	-0.672	0.214
S1JO	CI	0.762	0.134
S1DZ	CI	0.403	0.501
S1ULp	CI	0.119	0.848
GI	CI	0.609	0.275
DI	CI	0.634	0.250
AID	CI	-0.018	0.977
AIV	CI	0.269	0.661
lg	Pir	0.143	0.819
cg2	Pir	0.375	0.533
cg1	Pir	-0.630	0.254
M2	Pir	-0.756	0.139
M1	Pir	0.127	0.839
S1FL	Pir	0.192	0.757
S1j	Pir	-0.462	0.434
S1JO	Pir	-0.056	0.928
S1DZ	Pir	-0.025	0.968
S1ULp	Pir	0.288	0.639
GI	Pir	0.109	0.861
DI	Pir	0.538	0.349
AID	Pir	0.878	<b>0.050</b>
AIV	Pir	0.696	0.192
CI	Pir	0.311	0.611
lg	Den	0.427	0.474
cg2	Den	-0.029	0.963
cg1	Den	-0.419	0.482

DI	AID	0.432	0.467
lg	AIV	0.713	0.177
cg2	AIV	0.580	0.305
cg1	AIV	-0.342	0.573
M2	AIV	-0.619	0.266
M1	AIV	-0.143	0.819
S1FL	AIV	-0.285	0.642
S1j	AIV	-0.845	0.071
S1JO	AIV	-0.400	0.504
S1DZ	AIV	0.235	0.704
S1ULp	AIV	0.288	0.639
GI	AIV	0.146	0.814
DI	AIV	0.268	0.663
AID	AIV	0.335	0.581
lg	CI	0.152	0.807
cg2	CI	-0.604	0.281
cg1	CI	-0.595	0.290
M2	CI	-0.781	0.119
M1	CI	-0.665	0.221
S1FL	CI	-0.391	0.515
S1j	CI	0.173	0.780
AIV	LSS	0.619	0.266
CI	LSS	0.245	0.691
Pir	LSS	0.870	0.055
Den	LSS	0.825	0.085
lg	CPDM	-0.270	0.660
cg2	CPDM	-0.953	<b>0.012</b>
cg1	CPDM	-0.135	0.829
M2	CPDM	-0.218	0.724
M1	CPDM	-0.607	0.278
S1FL	CPDM	-0.136	0.827
S1j	CPDM	0.801	0.103
S1JO	CPDM	0.949	<b>0.014</b>
S1DZ	CPDM	0.323	0.596
S1ULp	CPDM	-0.012	0.985
GI	CPDM	0.532	0.356
DI	CPDM	0.384	0.523
AID	CPDM	-0.380	0.528
AIV	CPDM	-0.503	0.388
CI	CPDM	0.679	0.207
Pir	CPDM	-0.336	0.581
Den	CPDM	0.217	0.726
LSS	CPDM	-0.266	0.666
lg	CPDL	-0.125	0.841
cg2	CPDL	-0.768	0.129
cg1	CPDL	-0.087	0.890

M2	Den	-0.993	<b>0.001</b>
M1	Den	-0.572	0.314
S1FL	Den	0.117	0.851
S1j	Den	-0.080	0.898
S1JO	Den	0.375	0.534
S1DZ	Den	0.581	0.304
S1ULp	Den	0.624	0.261
GI	Den	0.732	0.160
DI	Den	0.916	<b>0.029</b>
AID	Den	0.479	0.414
AIV	Den	0.589	0.296
CI	Den	0.741	0.152
Pir	Den	0.733	0.159
Ig	LSS	0.383	0.525
cg2	LSS	0.442	0.456
cg1	LSS	-0.224	0.718
M2	LSS	-0.792	0.110
M1	LSS	-0.172	0.782
S1FL	LSS	0.494	0.398
S1j	LSS	-0.270	0.661
S1JO	LSS	-0.068	0.913
S1DZ	LSS	0.388	0.519
S1ULp	LSS	0.719	0.171
GI	LSS	0.467	0.428
DI	LSS	0.775	0.124
AID	LSS	0.796	0.107
GI	CPVL	0.943	<b>0.016</b>
DI	CPVL	0.855	0.065
AID	CPVL	-0.067	0.915
AIV	CPVL	0.129	0.836
CI	CPVL	0.830	0.082
Pir	CPVL	0.156	0.802
Den	CPVL	0.779	0.120
LSS	CPVL	0.382	0.526
CPDM	CPVL	0.705	0.184
CPDL	CPVL	0.863	0.059
Ig	CPVM	0.380	0.529
cg2	CPVM	-0.363	0.548
cg1	CPVM	-0.107	0.864
M2	CPVM	-0.819	0.090
M1	CPVM	-0.858	0.063
S1FL	CPVM	0.158	0.800
S1j	CPVM	0.352	0.562
S1JO	CPVM	0.631	0.253
S1DZ	CPVM	0.810	0.097
S1ULp	CPVM	0.689	0.198

M2	CPDL	-0.474	0.420
M1	CPDL	-0.697	0.191
S1FL	CPDL	0.185	0.765
S1j	CPDL	0.790	0.112
S1JO	CPDL	0.914	<b>0.030</b>
S1DZ	CPDL	0.535	0.353
S1ULp	CPDL	0.357	0.555
GI	CPDL	0.764	0.132
DI	CPDL	0.713	0.176
AID	CPDL	-0.080	0.898
AIV	CPDL	-0.353	0.560
CI	CPDL	0.697	0.191
Pir	CPDL	-0.063	0.920
Den	CPDL	0.504	0.387
LSS	CPDL	0.127	0.838
CPDM	CPDL	0.910	<b>0.032</b>
Ig	CPVL	0.357	0.556
cg2	CPVL	-0.488	0.404
cg1	CPVL	-0.105	0.867
M2	CPVL	-0.752	0.143
M1	CPVL	-0.910	<b>0.032</b>
S1FL	CPVL	0.021	0.973
S1j	CPVL	0.403	0.501
S1JO	CPVL	0.702	0.187
S1DZ	CPVL	0.801	0.104
S1ULp	CPVL	0.585	0.300
CPVL	AcCo	0.473	0.421
CPVM	AcCo	0.591	0.294
Ig	AcSh	0.644	0.241
cg2	AcSh	0.729	0.162
cg1	AcSh	-0.288	0.638
M2	AcSh	-0.498	0.393
M1	AcSh	0.049	0.937
S1FL	AcSh	-0.174	0.779
S1j	AcSh	-0.907	<b>0.033</b>
S1JO	AcSh	-0.559	0.327
S1DZ	AcSh	0.104	0.868
S1ULp	AcSh	0.256	0.678
GI	AcSh	-0.008	0.990
DI	AcSh	0.161	0.795
AID	AcSh	0.434	0.466
AIV	AcSh	0.975	<b>0.005</b>
CI	AcSh	0.068	0.913
Pir	AcSh	0.718	0.172
Den	AcSh	0.473	0.421
LSS	AcSh	0.629	0.255

GI	CPVM	0.956	<b>0.011</b>
DI	CPVM	0.934	<b>0.020</b>
AID	CPVM	0.097	0.876
AIV	CPVM	0.199	0.748
CI	CPVM	0.779	0.120
Pir	CPVM	0.292	0.633
Den	CPVM	0.855	0.065
LSS	CPVM	0.539	0.349
CPDM	CPVM	0.599	0.285
CPDL	CPVM	0.827	0.084
CPVL	CPVM	0.983	<b>0.003</b>
Ig	AcCo	0.308	0.614
cg2	AcCo	0.218	0.725
cg1	AcCo	-0.561	0.326
M2	AcCo	-0.928	<b>0.023</b>
M1	AcCo	-0.212	0.732
S1FL	AcCo	0.173	0.781
S1j	AcCo	-0.317	0.604
S1JO	AcCo	0.138	0.824
S1DZ	AcCo	0.281	0.647
S1ULp	AcCo	0.485	0.407
GI	AcCo	0.428	0.472
DI	AcCo	0.764	0.132
AID	AcCo	0.744	0.149
AIV	AcCo	0.703	0.185
CI	AcCo	0.538	0.350
Pir	AcCo	0.941	<b>0.017</b>
Den	AcCo	0.919	<b>0.027</b>
LSS	AcCo	0.917	<b>0.028</b>
CPDM	AcCo	-0.099	0.874
CPDL	AcCo	0.204	0.742
cg1	LSI	-0.594	0.291
M2	LSI	-0.266	0.665
M1	LSI	0.622	0.263
S1FL	LSI	0.406	0.498
S1j	LSI	-0.138	0.825
S1JO	LSI	-0.010	0.988
S1DZ	LSI	-0.539	0.349
S1ULp	LSI	-0.103	0.869
GI	LSI	-0.338	0.578
DI	LSI	0.177	0.776
AID	LSI	0.927	<b>0.023</b>
AIV	LSI	0.132	0.832
CI	LSI	-0.064	0.919
Pir	LSI	0.751	0.144
Den	LSI	0.240	0.698

CPDM	AcSh	-0.676	0.210
CPDL	AcSh	-0.512	0.378
CPVL	AcSh	-0.061	0.922
CPVM	AcSh	0.032	0.959
AcCo	AcSh	0.660	0.226
Ig	LSD	-0.467	0.428
cg2	LSD	0.161	0.795
cg1	LSD	-0.732	0.160
M2	LSD	-0.334	0.582
M1	LSD	0.592	0.292
S1FL	LSD	0.229	0.711
S1j	LSD	-0.225	0.716
S1JO	LSD	0.029	0.963
S1DZ	LSD	-0.566	0.320
S1ULp	LSD	-0.194	0.754
GI	LSD	-0.356	0.557
DI	LSD	0.158	0.799
AID	LSD	0.888	<b>0.044</b>
AIV	LSD	0.231	0.709
CI	LSD	0.059	0.924
Pir	LSD	0.792	0.110
Den	LSD	0.288	0.638
LSS	LSD	0.497	0.394
CPDM	LSD	-0.282	0.646
CPDL	LSD	-0.151	0.809
CPVL	LSD	-0.232	0.708
CPVM	LSD	-0.122	0.845
AcCo	LSD	0.594	0.291
AcSh	LSD	0.319	0.601
Ig	LSI	-0.500	0.392
cg2	LSI	0.211	0.734
cg1	Shi	-0.234	0.705
M2	Shi	-0.628	0.257
M1	Shi	0.016	0.979
S1FL	Shi	0.730	0.161
S1j	Shi	0.074	0.906
S1JO	Shi	0.128	0.838
S1DZ	Shi	0.180	0.772
S1ULp	Shi	0.597	0.288
GI	Shi	0.356	0.557
DI	Shi	0.744	0.149
AID	Shi	0.897	<b>0.039</b>
AIV	Shi	0.230	0.710
CI	Shi	0.143	0.818
Pir	Shi	0.777	0.122
Den	Shi	0.668	0.217

LSS	LSI	0.523	0.366
CPDM	LSI	-0.310	0.612
CPDL	LSI	-0.139	0.824
CPVL	LSI	-0.263	0.669
CPVM	LSI	-0.136	0.828
AcCo	LSI	0.547	0.340
AcSh	LSI	0.245	0.691
LSD	LSI	0.981	<b>0.003</b>
Ig	LSV	-0.125	0.841
cg2	LSV	0.156	0.802
cg1	LSV	-0.536	0.352
M2	LSV	-0.707	0.182
M1	LSV	0.109	0.861
S1FL	LSV	0.495	0.396
S1j	LSV	-0.057	0.928
S1JO	LSV	0.192	0.757
S1DZ	LSV	-0.003	0.996
S1ULp	LSV	0.370	0.539
GI	LSV	0.218	0.725
DI	LSV	0.677	0.210
AID	LSV	0.943	<b>0.016</b>
AIV	LSV	0.343	0.572
CI	LSV	0.293	0.632
Pir	LSV	0.902	<b>0.036</b>
Den	LSV	0.709	0.180
LSS	LSV	0.858	0.063
CPDM	LSV	-0.096	0.878
CPDL	LSV	0.221	0.721
CPVL	LSV	0.258	0.676
CPVM	LSV	0.402	0.502
AcCo	LSV	0.869	0.056
AcSh	LSV	0.371	0.538
LSD	LSV	0.820	0.089
LSI	LSV	0.837	0.077
Ig	Shi	-0.039	0.951
cg2	Shi	0.233	0.707
LSV	MS	0.793	0.110
Shi	MS	0.877	0.051
Ig	VDB	-0.173	0.781
cg2	VDB	-0.614	0.270
cg1	VDB	-0.840	0.075
M2	VDB	-0.708	0.181
M1	VDB	-0.322	0.597
S1FL	VDB	-0.362	0.549
S1j	VDB	0.149	0.812
S1JO	VDB	0.767	0.131

LSS	Shi	0.892	<b>0.042</b>
CPDM	Shi	-0.105	0.867
CPDL	Shi	0.278	0.651
CPVL	Shi	0.298	0.626
CPVM	Shi	0.459	0.437
AcCo	Shi	0.780	0.119
AcSh	Shi	0.273	0.656
LSD	Shi	0.648	0.237
LSI	Shi	0.721	0.169
LSV	Shi	0.945	<b>0.016</b>
Ig	MS	0.328	0.590
cg2	MS	0.646	0.239
cg1	MS	-0.037	0.953
M2	MS	-0.555	0.332
M1	MS	0.049	0.938
S1FL	MS	0.646	0.239
S1j	MS	-0.322	0.597
S1JO	MS	-0.313	0.608
S1DZ	MS	0.259	0.674
S1ULp	MS	0.696	0.191
GI	MS	0.276	0.653
DI	MS	0.590	0.295
AID	MS	0.832	0.081
AIV	MS	0.535	0.353
CI	MS	-0.079	0.899
Pir	MS	0.793	0.110
Den	MS	0.602	0.283
LSS	MS	0.947	<b>0.015</b>
CPDM	MS	-0.491	0.401
CPDL	MS	-0.092	0.883
CPVL	MS	0.118	0.851
CPVM	MS	0.297	0.628
AcCo	MS	0.765	0.132
AcSh	MS	0.613	0.271
LSD	MS	0.500	0.391
LSI	MS	0.569	0.317
CPVL	Icj	0.547	0.340
CPVM	Icj	0.605	0.280
AcCo	Icj	0.381	0.527
AcSh	Icj	-0.422	0.479
LSD	Icj	0.352	0.562
LSI	Icj	0.427	0.474
LSV	Icj	0.640	0.245
Shi	Icj	0.708	0.181
MS	Icj	0.307	0.615
VDB	Icj	0.448	0.449

S1DZ	VDB	0.036	0.954
S1ULp	VDB	-0.136	0.828
GI	VDB	0.315	0.606
DI	VDB	0.503	0.387
AID	VDB	0.208	0.737
AIV	VDB	0.197	0.751
CI	VDB	0.918	<b>0.028</b>
Pir	VDB	0.449	0.448
Den	VDB	0.642	0.243
LSS	VDB	0.227	0.713
CPDM	VDB	0.591	0.294
CPDL	VDB	0.580	0.305
CPVL	VDB	0.600	0.285
CPVM	VDB	0.566	0.320
AcCo	VDB	0.565	0.321
AcSh	VDB	0.044	0.944
LSD	VDB	0.399	0.506
LSI	VDB	0.271	0.659
LSV	VDB	0.460	0.436
Shi	VDB	0.235	0.703
MS	VDB	-0.065	0.917
Ig	Icj	-0.420	0.481
cg2	Icj	-0.477	0.416
cg1	Icj	-0.184	0.768
M2	Icj	-0.434	0.465
M1	Icj	-0.222	0.720
S1FL	Icj	0.619	0.265
S1j	Icj	0.727	0.164
S1JO	Icj	0.716	0.173
S1DZ	Icj	0.206	0.739
S1ULp	Icj	0.372	0.538
GI	Icj	0.493	0.399
DI	Icj	0.716	0.174
AID	Icj	0.463	0.432
AIV	Icj	-0.381	0.527
CI	Icj	0.379	0.530
Pir	Icj	0.269	0.662
Den	Icj	0.473	0.421
LSS	Icj	0.407	0.497
CPDM	Icj	0.573	0.312
CPDL	Icj	0.793	0.110
GI	Tu	0.276	0.654
DI	Tu	0.607	0.278
AID	Tu	0.840	0.075
AIV	Tu	0.137	0.826
CI	Tu	-0.149	0.811

Ig	VP	0.663	0.223
cg2	VP	0.837	0.077
cg1	VP	0.354	0.559
M2	VP	-0.325	0.594
M1	VP	-0.084	0.893
S1FL	VP	0.517	0.372
S1j	VP	-0.470	0.424
S1JO	VP	-0.608	0.277
S1DZ	VP	0.448	0.449
S1ULp	VP	0.774	0.125
GI	VP	0.293	0.632
DI	VP	0.379	0.530
AID	VP	0.465	0.431
AIV	VP	0.590	0.295
CI	VP	-0.287	0.639
Pir	VP	0.483	0.409
Den	VP	0.391	0.515
LSS	VP	0.753	0.142
CPDM	VP	-0.639	0.246
CPDL	VP	-0.295	0.630
CPVL	VP	0.030	0.962
CPVM	VP	0.177	0.775
AcCo	VP	0.489	0.404
AcSh	VP	0.668	0.218
LSD	VP	0.061	0.922
LSI	VP	0.139	0.824
LSV	VP	0.380	0.528
Shi	VP	0.543	0.345
MS	VP	0.862	0.060
VDB	VP	-0.424	0.477
Icj	VP	-0.077	0.903
Ig	Tu	-0.001	0.998
cg2	Tu	0.411	0.491
cg1	Tu	0.048	0.939
M2	Tu	-0.404	0.499
M1	Tu	0.110	0.861
S1FL	Tu	0.882	<b>0.048</b>
S1j	Tu	0.066	0.916
S1JO	Tu	-0.094	0.881
S1DZ	Tu	0.181	0.771
S1ULp	Tu	0.661	0.225

Pir	Tu	0.628	0.256
Den	Tu	0.469	0.425
LSS	Tu	0.827	0.084
CPDM	Tu	-0.271	0.660
CPDL	Tu	0.124	0.842
CPVL	Tu	0.124	0.843
CPVM	Tu	0.298	0.627
AcCo	Tu	0.600	0.285
AcSh	Tu	0.230	0.710
LSD	Tu	0.520	0.369
LSI	Tu	0.641	0.244
LSV	Tu	0.812	0.095
Shi	Tu	0.948	<b>0.014</b>
MS	Tu	0.906	<b>0.034</b>
VDB	Tu	-0.084	0.893
lcj	Tu	0.604	0.280
VP	Tu	0.678	0.209

**Supplementary table 2.** Results of Pearson's  $r$  correlations in VEH/ASE rats. Correlation coefficients and p-values for all possible pairs. Significant values were given in bold.

ROI	ROI	Pearson's $r$	p-value
lg	cg2	0.366	0.545
lg	cg1	0.056	0.929
cg2	cg1	0.910	<b>0.032</b>
lg	M2	0.359	0.553
cg2	M2	0.930	<b>0.022</b>
cg1	M2	0.854	0.066
lg	M1	0.657	0.228
cg2	M1	0.813	0.094
cg1	M1	0.648	0.237
M2	M1	0.924	<b>0.025</b>
lg	S1FL	0.338	0.578
cg2	S1FL	0.848	0.069
cg1	S1FL	0.708	0.181
M2	S1FL	0.960	<b>0.010</b>
M1	S1FL	0.897	<b>0.039</b>
lg	S1j	0.450	0.446
cg2	S1j	0.927	<b>0.023</b>
cg1	S1j	0.833	0.080
M2	S1j	0.994	<b>0.001</b>
M1	S1j	0.954	<b>0.012</b>
S1FL	S1j	0.943	<b>0.016</b>
lg	S1JO	0.871	0.055
cg2	S1JO	0.675	0.211

ROI	ROI	Pearson's $r$	p-value
lg	S1DZ	0.527	0.362
cg2	S1DZ	0.974	<b>0.005</b>
cg1	S1DZ	0.840	0.075
M2	S1DZ	0.959	<b>0.010</b>
M1	S1DZ	0.922	<b>0.026</b>
S1FL	S1DZ	0.891	<b>0.042</b>
S1j	S1DZ	0.973	<b>0.005</b>
S1JO	S1DZ	0.815	0.092
lg	S1ULp	0.576	0.309
cg2	S1ULp	0.931	<b>0.021</b>
cg1	S1ULp	0.758	0.138
M2	S1ULp	0.962	<b>0.009</b>
M1	S1ULp	0.961	<b>0.009</b>
S1FL	S1ULp	0.934	<b>0.020</b>
S1j	S1ULp	0.978	<b>0.004</b>
S1JO	S1ULp	0.844	0.072
S1DZ	S1ULp	0.986	<b>0.002</b>
lg	GI	0.603	0.281
cg2	GI	0.940	<b>0.018</b>
cg1	GI	0.734	0.158
M2	GI	0.927	<b>0.024</b>
M1	GI	0.925	<b>0.024</b>
S1FL	GI	0.903	<b>0.036</b>

cg1	S1JO	0.478	0.416
M2	S1JO	0.732	0.160
M1	S1JO	0.918	<b>0.028</b>
S1FL	S1JO	0.658	0.227
S1j	S1JO	0.800	0.104
cg2	DI	0.833	0.080
cg1	DI	0.573	0.313
M2	DI	0.840	0.075
M1	DI	0.939	<b>0.018</b>
S1FL	DI	0.823	0.087
S1j	DI	0.881	<b>0.048</b>
S1JO	DI	0.922	<b>0.026</b>
S1DZ	DI	0.924	<b>0.025</b>
S1ULp	DI	0.954	<b>0.012</b>
GI	DI	0.965	<b>0.008</b>
lg	AID	0.713	0.176
cg2	AID	0.899	<b>0.038</b>
cg1	AID	0.696	0.192
M2	AID	0.898	<b>0.039</b>
M1	AID	0.954	<b>0.012</b>
S1FL	AID	0.847	0.070
S1j	AID	0.934	<b>0.020</b>
S1JO	AID	0.916	<b>0.029</b>
S1DZ	AID	0.970	<b>0.006</b>
S1ULp	AID	0.979	<b>0.004</b>
GI	AID	0.981	<b>0.003</b>
DI	AID	0.986	<b>0.002</b>
lg	AIV	0.711	0.178
cg2	AIV	0.755	0.140
cg1	AIV	0.575	0.311
M2	AIV	0.880	<b>0.049</b>
M1	AIV	0.995	<b>&lt;0.001</b>
S1FL	AIV	0.858	0.063
S1j	AIV	0.919	<b>0.027</b>
S1JO	AIV	0.942	<b>0.017</b>
DI	Pir	0.691	0.196
AID	Pir	0.780	0.120
AIV	Pir	0.846	0.071
CI	Pir	0.798	0.106
lg	Den	0.462	0.434
cg2	Den	0.793	0.110
cg1	Den	0.807	0.098
M2	Den	0.879	<b>0.050</b>
M1	Den	0.889	<b>0.044</b>
S1FL	Den	0.740	0.153
S1j	Den	0.908	<b>0.033</b>
S1JO	Den	0.834	0.079
S1DZ	Den	0.862	0.060
S1ULp	Den	0.842	0.074

S1j	GI	0.944	<b>0.016</b>
S1JO	GI	0.825	0.086
S1DZ	GI	0.982	<b>0.003</b>
S1ULp	GI	0.990	<b>0.001</b>
lg	DI	0.787	0.114
S1DZ	AIV	0.883	<b>0.047</b>
S1ULp	AIV	0.932	<b>0.021</b>
GI	AIV	0.894	<b>0.041</b>
DI	AIV	0.935	<b>0.020</b>
AID	AIV	0.938	<b>0.018</b>
lg	CI	0.824	0.086
cg2	CI	0.619	0.265
cg1	CI	0.474	0.420
M2	CI	0.710	0.179
M1	CI	0.901	<b>0.037</b>
S1FL	CI	0.618	0.267
S1j	CI	0.780	0.120
S1JO	CI	0.987	<b>0.002</b>
S1DZ	CI	0.769	0.129
S1ULp	CI	0.795	0.108
GI	CI	0.757	0.139
DI	CI	0.858	0.063
AID	CI	0.865	0.058
AIV	CI	0.929	<b>0.022</b>
lg	Pir	0.331	0.586
cg2	Pir	0.771	0.127
cg1	Pir	0.820	0.089
M2	Pir	0.898	<b>0.038</b>
M1	Pir	0.869	0.056
S1FL	Pir	0.781	0.119
S1j	Pir	0.911	<b>0.031</b>
S1JO	Pir	0.752	0.143
S1DZ	Pir	0.832	0.081
S1ULp	Pir	0.820	0.089
GI	Pir	0.742	0.151
GI	LSS	0.432	0.468
DI	LSS	0.549	0.338
AID	LSS	0.582	0.304
AIV	LSS	0.532	0.356
CI	LSS	0.788	0.113
Pir	LSS	0.511	0.379
Den	LSS	0.650	0.236
lg	CPDM	0.661	0.224
cg2	CPDM	0.908	<b>0.033</b>
cg1	CPDM	0.782	0.118
M2	CPDM	0.889	<b>0.044</b>
M1	CPDM	0.924	<b>0.025</b>
S1FL	CPDM	0.778	0.122
S1j	CPDM	0.929	<b>0.023</b>

GI	Den	0.778	0.121
DI	Den	0.755	0.140
AID	Den	0.837	0.077
AIV	Den	0.872	0.054
CI	Den	0.871	0.055
Pir	Den	0.984	<b>0.002</b>
lg	LSS	0.727	0.164
cg2	LSS	0.403	0.501
cg1	LSS	0.360	0.552
M2	LSS	0.319	0.601
M1	LSS	0.501	0.390
S1FL	LSS	0.110	0.860
S1j	LSS	0.409	0.494
S1JO	LSS	0.764	0.132
S1DZ	LSS	0.489	0.403
S1ULp	LSS	0.433	0.466
S1FL	CPDL	0.553	0.334
S1j	CPDL	0.781	0.119
S1JO	CPDL	0.920	<b>0.027</b>
S1DZ	CPDL	0.841	0.075
S1ULp	CPDL	0.802	0.103
GI	CPDL	0.796	0.107
DI	CPDL	0.841	0.074
AID	CPDL	0.885	<b>0.046</b>
AIV	CPDL	0.814	0.093
CI	CPDL	0.911	<b>0.031</b>
Pir	CPDL	0.771	0.127
Den	CPDL	0.872	0.054
LSS	CPDL	0.883	<b>0.047</b>
CPDM	CPDL	0.951	<b>0.013</b>
lg	CPVL	0.904	<b>0.035</b>
cg2	CPVL	0.657	0.228
cg1	CPVL	0.456	0.440
M2	CPVL	0.650	0.235
M1	CPVL	0.843	0.073
S1FL	CPVL	0.549	0.338
S1j	CPVL	0.728	0.164
S1JO	CPVL	0.982	<b>0.003</b>
S1DZ	CPVL	0.782	0.118
S1ULp	CPVL	0.789	0.112
GI	CPVL	0.790	0.112
DI	CPVL	0.897	<b>0.039</b>
AID	CPVL	0.891	<b>0.043</b>
AIV	CPVL	0.867	0.057
CI	CPVL	0.959	<b>0.010</b>
Pir	CPVL	0.671	0.215
S1FL	AcCo	0.115	0.853
S1j	AcCo	0.313	0.608
S1JO	AcCo	0.816	0.092

S1JO	CPDM	0.912	<b>0.031</b>
S1DZ	CPDM	0.965	<b>0.008</b>
S1ULp	CPDM	0.944	<b>0.016</b>
GI	CPDM	0.935	<b>0.020</b>
DI	CPDM	0.930	<b>0.022</b>
AID	CPDM	0.974	<b>0.005</b>
AIV	CPDM	0.904	<b>0.035</b>
CI	CPDM	0.885	<b>0.046</b>
Pir	CPDM	0.849	0.069
Den	CPDM	0.912	<b>0.031</b>
LSS	CPDM	0.696	0.192
lg	CPDL	0.740	0.153
cg2	CPDL	0.769	0.129
cg1	CPDL	0.669	0.217
M2	CPDL	0.717	0.173
M1	CPDL	0.815	0.093
Den	CPVL	0.781	0.119
LSS	CPVL	0.848	0.069
CPDM	CPVL	0.903	<b>0.036</b>
CPDL	CPVL	0.951	<b>0.013</b>
lg	CPVM	0.927	<b>0.024</b>
cg2	CPVM	0.540	0.347
cg1	CPVM	0.347	0.567
M2	CPVM	0.542	0.346
M1	CPVM	0.776	0.123
S1FL	CPVM	0.434	0.465
S1j	CPVM	0.630	0.255
S1JO	CPVM	0.962	<b>0.009</b>
S1DZ	CPVM	0.682	0.205
S1ULp	CPVM	0.692	0.195
GI	CPVM	0.689	0.198
DI	CPVM	0.827	0.084
AID	CPVM	0.814	0.094
AIV	CPVM	0.813	0.094
CI	CPVM	0.951	<b>0.013</b>
Pir	CPVM	0.610	0.275
Den	CPVM	0.730	0.162
LSS	CPVM	0.887	<b>0.045</b>
CPDM	CPVM	0.834	0.079
CPDL	CPVM	0.922	<b>0.026</b>
CPVL	CPVM	0.989	<b>0.001</b>
lg	AcCo	0.937	<b>0.019</b>
cg2	AcCo	0.215	0.729
cg1	AcCo	0.012	0.985
M2	AcCo	0.209	0.736
M1	AcCo	0.526	0.363
AIV	AcSh	0.365	0.545
CI	AcSh	0.648	0.237
Pir	AcSh	0.118	0.850

S1DZ	AcCo	0.378	0.530
S1ULp	AcCo	0.400	0.504
GI	AcCo	0.408	0.496
DI	AcCo	0.612	0.272
AID	AcCo	0.565	0.321
AIV	AcCo	0.592	0.293
CI	AcCo	0.815	0.092
Pir	AcCo	0.330	0.588
Den	AcCo	0.472	0.422
LSS	AcCo	0.872	0.054
CPDM	AcCo	0.582	0.303
CPDL	AcCo	0.750	0.144
CPVL	AcCo	0.872	0.054
CPVM	AcCo	0.933	<b>0.021</b>
lg	AcSh	0.838	0.077
cg2	AcSh	-0.055	0.931
cg1	AcSh	-0.219	0.724
M2	AcSh	-0.062	0.922
M1	AcSh	0.284	0.643
S1FL	AcSh	-0.152	0.807
S1j	AcSh	0.047	0.940
S1JO	AcSh	0.631	0.253
S1DZ	AcSh	0.109	0.861
S1ULp	AcSh	0.131	0.834
GI	AcSh	0.139	0.824
DI	AcSh	0.372	0.537
AID	AcSh	0.314	0.607
CPVL	LSD	0.873	0.053
CPVM	LSD	0.930	<b>0.022</b>
AcCo	LSD	0.949	<b>0.014</b>
AcSh	LSD	0.900	<b>0.037</b>
lg	LSI	0.585	0.301
cg2	LSI	0.254	0.680
cg1	LSI	0.247	0.688
M2	LSI	0.077	0.902
M1	LSI	0.225	0.716
S1FL	LSI	-0.152	0.807
S1j	LSI	0.164	0.792
S1JO	LSI	0.537	0.350
S1DZ	LSI	0.289	0.637
S1ULp	LSI	0.201	0.746
GI	LSI	0.227	0.714
DI	LSI	0.333	0.584
AID	LSI	0.368	0.542
AIV	LSI	0.250	0.685
CI	LSI	0.552	0.335
Pir	LSI	0.265	0.667
Den	LSI	0.420	0.481
LSS	LSI	0.947	<b>0.015</b>

Den	AcSh	0.263	0.669
LSS	AcSh	0.809	0.097
CPDM	AcSh	0.343	0.572
CPDL	AcSh	0.567	0.319
CPVL	AcSh	0.704	0.184
CPVM	AcSh	0.800	0.104
AcCo	AcSh	0.961	<b>0.009</b>
lg	LSD	0.814	0.093
cg2	LSD	0.295	0.630
cg1	LSD	0.210	0.735
M2	LSD	0.297	0.627
M1	LSD	0.554	0.332
S1FL	LSD	0.135	0.829
S1j	LSD	0.395	0.510
S1JO	LSD	0.821	0.088
S1DZ	LSD	0.436	0.463
S1ULp	LSD	0.424	0.477
GI	LSD	0.405	0.499
DI	LSD	0.569	0.317
AID	LSD	0.572	0.313
AIV	LSD	0.606	0.278
CI	LSD	0.856	0.064
Pir	LSD	0.510	0.380
Den	LSD	0.638	0.247
LSS	LSD	0.961	<b>0.009</b>
CPDM	LSD	0.654	0.231
CPDL	LSD	0.836	0.077
cg2	LSV	0.598	0.287
cg1	LSV	0.353	0.561
M2	LSV	0.716	0.174
M1	LSV	0.927	<b>0.023</b>
S1FL	LSV	0.710	0.179
S1j	LSV	0.777	0.122
S1JO	LSV	0.969	<b>0.007</b>
S1DZ	LSV	0.764	0.133
S1ULp	LSV	0.831	0.081
GI	LSV	0.807	0.099
DI	LSV	0.918	<b>0.028</b>
AID	LSV	0.883	<b>0.047</b>
AIV	LSV	0.959	<b>0.010</b>
CI	LSV	0.949	<b>0.014</b>
Pir	LSV	0.693	0.194
Den	LSV	0.753	0.142
LSS	LSV	0.604	0.281
CPDM	LSV	0.831	0.081
CPDL	LSV	0.796	0.107
CPVL	LSV	0.917	<b>0.028</b>
CPVM	LSV	0.896	<b>0.040</b>
AcCo	LSV	0.762	0.134

CPDM	LSI	0.503	0.387
CPDL	LSI	0.737	0.155
CPVL	LSI	0.671	0.215
CPVM	LSI	0.723	0.168
AcCo	LSI	0.768	0.129
AcSh	LSI	0.761	0.135
LSD	LSI	0.853	0.066
lg	LSV	0.868	0.056
S1FL	Shi	-0.163	0.794
S1j	Shi	0.082	0.896
S1JO	Shi	0.629	0.256
S1DZ	Shi	0.127	0.839
S1ULp	Shi	0.127	0.839
GI	Shi	0.115	0.853
DI	Shi	0.327	0.591
AID	Shi	0.302	0.622
AIV	Shi	0.363	0.548
CI	Shi	0.673	0.214
Pir	Shi	0.228	0.713
Den	Shi	0.364	0.547
LSS	Shi	0.875	0.052
CPDM	Shi	0.376	0.533
CPDL	Shi	0.617	0.267
CPVL	Shi	0.701	0.188
CPVM	Shi	0.798	0.105
AcCo	Shi	0.936	<b>0.019</b>
AcSh	Shi	0.977	<b>0.004</b>
LSD	Shi	0.944	<b>0.016</b>
LSI	Shi	0.827	0.084
LSV	Shi	0.543	0.345
lg	MS	0.042	0.947
cg2	MS	0.540	0.348
cg1	MS	0.699	0.189
M2	MS	0.299	0.625
M1	MS	0.153	0.806
S1FL	MS	0.044	0.944
S1j	MS	0.316	0.605
S1JO	MS	0.237	0.702
GI	VDB	0.261	0.671
DI	VDB	0.453	0.443
AID	VDB	0.410	0.493
AIV	VDB	0.342	0.574
CI	VDB	0.615	0.269
Pir	VDB	0.102	0.871
Den	VDB	0.273	0.657
LSS	VDB	0.872	0.054
CPDM	VDB	0.450	0.447
CPDL	VDB	0.667	0.218
CPVL	VDB	0.752	0.143

AcSh	LSV	0.579	0.306
LSD	LSV	0.716	0.174
LSI	LSV	0.341	0.574
lg	Shi	0.758	0.138
cg2	Shi	-0.025	0.968
cg1	Shi	-0.108	0.863
M2	Shi	-0.024	0.969
M1	Shi	0.289	0.637
S1DZ	MS	0.429	0.471
S1ULp	MS	0.275	0.655
GI	MS	0.298	0.627
DI	MS	0.204	0.742
AID	MS	0.327	0.592
AIV	MS	0.102	0.870
CI	MS	0.243	0.694
Pir	MS	0.392	0.514
Den	MS	0.469	0.425
LSS	MS	0.616	0.268
CPDM	MS	0.500	0.391
CPDL	MS	0.598	0.286
CPVL	MS	0.347	0.567
CPVM	MS	0.314	0.606
AcCo	MS	0.176	0.777
AcSh	MS	0.095	0.879
LSD	MS	0.383	0.524
LSI	MS	0.713	0.176
LSV	MS	-0.005	0.994
Shi	MS	0.227	0.714
lg	VDB	0.845	0.072
cg2	VDB	0.127	0.838
cg1	VDB	-0.055	0.930
M2	VDB	0.002	0.997
M1	VDB	0.284	0.643
S1FL	VDB	-0.122	0.845
S1j	VDB	0.107	0.864
S1JO	VDB	0.635	0.249
S1DZ	VDB	0.236	0.703
S1ULp	VDB	0.217	0.726
DI	Icj	0.529	0.360
AID	Icj	0.490	0.402
AIV	Icj	0.566	0.320
CI	Icj	0.811	0.096
Pir	Icj	0.357	0.555
Den	Icj	0.485	0.407
LSS	Icj	0.866	0.057
CPDM	Icj	0.526	0.362
CPDL	Icj	0.710	0.179
CPVL	Icj	0.827	0.084
CPVM	Icj	0.902	<b>0.036</b>

CPVM	VDB	0.820	0.089
AcCo	VDB	0.937	<b>0.019</b>
AcSh	VDB	0.941	<b>0.017</b>
LSD	VDB	0.879	<b>0.050</b>
LSI	VDB	0.880	<b>0.049</b>
LSV	VDB	0.532	0.356
Shi	VDB	0.913	<b>0.030</b>
MS	VDB	0.335	0.582
lg	lcj	0.878	<b>0.050</b>
cg2	lcj	0.130	0.835
cg1	lcj	-0.023	0.971
M2	lcj	0.168	0.787
M1	lcj	0.494	0.398
S1FL	lcj	0.066	0.916
S1j	lcj	0.273	0.657
S1JO	lcj	0.785	0.116
S1DZ	lcj	0.306	0.617
S1ULp	lcj	0.331	0.586
GI	lcj	0.317	0.603
DI	VP	0.422	0.479
AID	VP	0.386	0.521
AIV	VP	0.557	0.329
CI	VP	0.784	0.117
Pir	VP	0.395	0.510
Den	VP	0.484	0.408
LSS	VP	0.748	0.146
CPDM	VP	0.421	0.480
CPDL	VP	0.589	0.296
CPVL	VP	0.720	0.170
CPVM	VP	0.807	0.099
AcCo	VP	0.899	<b>0.038</b>
AcSh	VP	0.904	<b>0.035</b>
LSD	VP	0.899	<b>0.038</b>
LSI	VP	0.588	0.297
LSV	VP	0.711	0.178
Shi	VP	0.921	<b>0.026</b>
MS	VP	-0.030	0.962
VDB	VP	0.742	0.151
lcj	VP	0.957	<b>0.011</b>
lg	Tu	0.980	<b>0.003</b>
cg2	Tu	0.320	0.600
cg1	Tu	0.057	0.927
M2	Tu	0.370	0.540
M1	Tu	0.684	0.202
S1FL	Tu	0.334	0.583
S1j	Tu	0.464	0.431
S1JO	Tu	0.897	<b>0.039</b>
S1DZ	Tu	0.503	0.388
S1ULp	Tu	0.558	0.328

AcCo	lcj	0.985	<b>0.002</b>
AcSh	lcj	0.969	<b>0.007</b>
LSD	lcj	0.964	<b>0.008</b>
LSI	lcj	0.750	0.144
LSV	lcj	0.733	0.159
Shi	lcj	0.968	<b>0.007</b>
MS	lcj	0.142	0.820
VDB	lcj	0.897	<b>0.039</b>
lg	VP	0.768	0.129
cg2	VP	0.005	0.994
cg1	VP	-0.097	0.877
M2	VP	0.144	0.817
M1	VP	0.477	0.417
S1FL	VP	0.066	0.915
S1j	VP	0.240	0.698
S1JO	VP	0.723	0.168
S1DZ	VP	0.206	0.739
S1ULp	VP	0.258	0.676
GI	VP	0.208	0.737
GI	Tu	0.559	0.327
DI	Tu	0.753	0.142
AID	Tu	0.690	0.197
AIV	Tu	0.746	0.147
CI	Tu	0.881	0.048
Pir	Tu	0.418	0.483
Den	Tu	0.536	0.352
LSS	Tu	0.761	0.135
CPDM	Tu	0.659	0.226
CPDL	Tu	0.752	0.143
CPVL	Tu	0.911	<b>0.031</b>
CPVM	Tu	0.947	<b>0.015</b>
AcCo	Tu	0.961	<b>0.009</b>
AcSh	Tu	0.873	0.053
LSD	Tu	0.875	<b>0.052</b>
LSI	Tu	0.590	0.295
LSV	Tu	0.896	<b>0.040</b>
Shi	Tu	0.821	0.088
MS	Tu	0.019	0.976
VDB	Tu	0.827	0.084
lcj	Tu	0.935	<b>0.020</b>
VP	Tu	0.161	0.797

**Supplementary table 3.** Results of Pearson's  $r$  correlations in KET/ASE group. Correlation coefficients and p-values for all possible pairs are reported, significant values were given in bold.

